Electrochemical Society

UNIV. OF MICHIGAN
JAN 15 1953
EAST ENGINEERING
LIBRARY

ELECTROCHEMICAL INDUSTRY

India

Electrolytic Aids to
THE MODERN TEXTILE INDUSTRY

Chlorine and caustic soda, products of the electrolytic industry are essential in turning natural and man-made fibres into modern textiles of all kinds.

Uniformly high quality **GLC Graphite Anodes** are doing their share to help the electrolytic industry meet the ever increasing civilian and defense demands for chlorine and caustic soda.

ELECTRODE DIVISION

Great Lakes Carbon Corporation

Niagara Falls, N. Y. GLC Morganton, N. C.

Courtesy The Dow Chemical Company and The Saran Yarn Company

Graphite Anodes, Electrodes and Specialties

Sales office: Niagara Falls, N. Y. **Other offices:** New York N. Y., Chicago, Ill., Pittsburgh, Pa.

Sales Agents: J. B. Hayes, Birmingham, Ala., George O'Hara, Long Beach, Cal., Great Northern Carbon & Chemical Co. Ltd., Montreal, Canada

EDITORIAL STAFF

R. M. Burns, *Chairman*
Norman Hackerman, *Technical Editor*
Cecil V. King, *Associate Editor*
U. B. Thomas, *News Editor*
Ruth G. Sterns, *Assistant Editor*
Mary F. Murray, *Assistant Editor*

DIVISIONAL EDITORS

M. A. Streicher, *Corrosion*
Abner Brenner, *Electrodeposition*
N. C. Cahoon, *Battery*
H. C. Froelich, *Electronics*
W. C. Gardiner, *Industrial Electrolytic*
S. J. Sindeband, *Electrothermic*
John J. Chapman, *Electric Insulation*
L. B. Rogers, *Theoretical*
Sherlock Swann, Jr., *Electro-Organic*

REGIONAL EDITORS

Joseph A. Schulein, *Pacific Northwest*
J. C. Schumacher, *Los Angeles*
O. W. Storey, *Chicago*
G. W. Heise, *Cleveland*
Paul S. Brallier, *Niagara Falls*
Oliver Osborn, *Houston*
Earl A. Gulbransen, *Pittsburgh*
J. W. Cuthbertson, *Great Britain*
T. L. Rama Char, *India*

ADVERTISING OFFICE

Jack Bain
Advertising Manager
545 Fifth Avenue
New York 17, N. Y.
PHONE—*Murray Hill 2-3345*

Journal of the
Electrochemical Society

JANUARY, 1953 VOL. 100 · NO. 1

CONTENTS

Regional Features

World-Wide Electrochemistry—Editorial. *R. M. Burns.* 3C
Electrochemical Industry: India. *T. L. Rama Char.* 7C

Technical Papers

Microsegregation in the Lead-Antimony Alloys. *A. C. Simon and E. L. Jones* 1
The Relation of the Anodic Corrosion of Lead and Lead-Antimony Alloys to Microstructure. *J. B. Burbank and A. C. Simon* 11
The Effect of Temperature on the Cathode Potential during Nickel Plating. *Dennis R. Turner* 15
Saturation and Voltage Effects in Cathodoluminescence. *P. H. Dowling and J. R. Sewell* 22
Electrical Measurements on Electroluminescent Lamps with Zinc Sulfide Phosphors. *C. W. Jerome and W. C. Gungle* 34
Influence of Impurities in the Electrolyte in Chlorine-Caustic Electrolysis by the Mercury Cell Process, III. Investigation of the Influence of Anions upon the Decomposition Rate of Sodium Amalgam. *Gösta Angel, Tage Lundén, and Rolf Brännland* 39
Some Properties of Tin-II Sulfate Solutions and Their Role in Electrodeposition of Tin, I. Solutions with only Tin-II Sulfate Present. *C. A. Discher* 45

Current Affairs

William Blum Awarded Honorary Membership 11C
Division News 14C
Section News 15C
New Members 17C
Personals 17C
Book Reviews 18C
Literature from Industry 20C

Published monthly by The Electrochemical Society, Inc., Mount Royal and Guilford Aves., Baltimore 2, Md., combining the JOURNAL and TRANSACTIONS OF THE ELECTROCHEMICAL SOCIETY. Editorial offices: 235 West 102nd Street, New York 25, N. Y. Statements and opinions given in articles and papers in the JOURNAL OF THE ELECTROCHEMICAL SOCIETY are those of the contributors, and The Electrochemical Society assumes no responsibility for them. Subscription $11.25 to members, $15.00 to nonmembers. Single copies $1.25 to members, $1.50 to nonmembers. Copyright 1953 by The Electrochemical Society, Inc. Entered as second-class matter November 15, 1947, at the Post Office at Baltimore, Md., under the act of August 24, 1912.

SARGENT SLOMIN

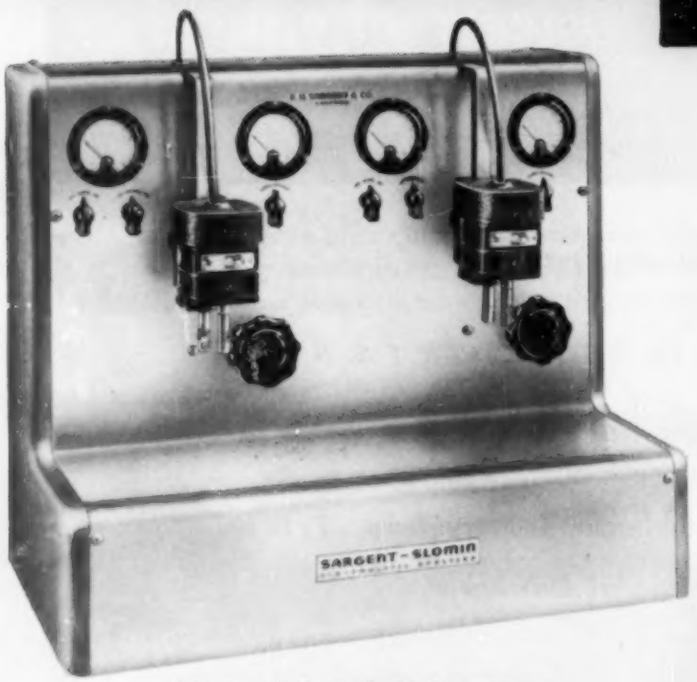

Motor-Stirred 5 Ampere

SARGENT HEAVY DUTY

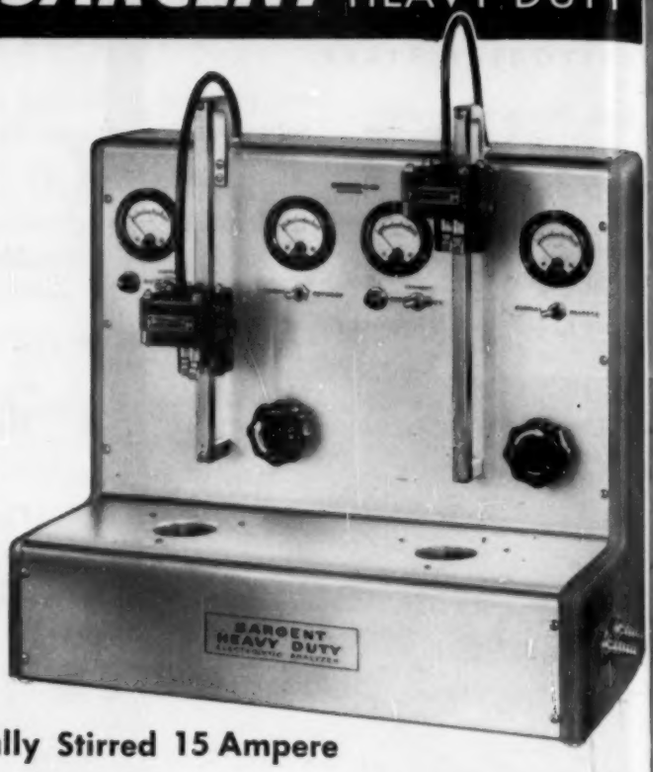

Magnetically Stirred 15 Ampere

Designed for continuous trouble-free performance, these electrolytic analyzers, manufactured by E. H. Sargent & Co., are durably constructed of the highest grade materials and component parts, including stainless steel front panel, cast aluminum end castings and stainless steel fittings.

Completely line operated, the Sargent analyzers employ self-contained rectifying and filter circuits. The deposition voltage between the electrodes is adjusted by means of auto-transformers, with meters indicating volts and amperes and controls on the panel. An easily replaceable fuse guards against circuit overload.

The Sargent-Slomin Analyzer stirs thorugh a rotating chuck operated from a capacitor type induction motor, motor having a fixed speed of 550 r.p.m. with 60 cycle A.C. current or 460 r.p.m. with 50 cycle A.C. current. Motors are sealed against corrosive fumes; are mounted on cast metal brackets, sliding on ½" square stainless steel rods, permitting vertical adjustment of electrode position over a distance of 4". Pre-lubricated ball-bearings support the rotating shaft.

The Sargent Heavy Duty Analyzer provides efficient stirring by the interaction between the cell current and the field established by a permanent magnet, tubular in shape and coaxial with the cell holder.

The Heavy Duty has recessed wells to hold the sample beakers, wells being 6¼" deep, designed to contain 250 ml electrolytic beakers. The wall of each well serves as an inner wall of the water jacket, for use in either heating or cooling. Two serrated nipples for rubber tubing connections for cooling or heating water are mounted on the right end casting. In plain copper analysis, 1 gram of copper may be deposited in 15 minutes with an accuracy of approximately 0.05% without the necessity of special techniques.

All electrolytic analyzers accommodate electrodes having shaft diameters no greater than 0.059 inch. Stainless steel spring tension chucks permit quick, easy insertion of the electrodes and maintain proper electrical contact. On the Heavy Duty Analyzer, the cathode chuck is eccentrically mounted, providing adjustability to accommodate electrodes up to 50 mm diameter. Special Sargent high efficiency electrodes are available for both analyzers.

Analyzers are complete with cord and plug for attachment to standard outlets. For operation from 115 volt, 50 or 60 cycle A.C. circuits.

	SARGENT-SLOMIN	HEAVY DUTY
Maximum D.C. current at each position	5 ampere	15 ampere
Maximum D.C. voltage at each position	10 volts	10 volts
Maximum power consumption	150* or 300 watts	400 watts
Height	18 inches	20¼ inches
Width	11¼* or 21 inches	21 inches
Depth	11¼ inches	11¼ inches
Net Weight	35* or 61 pounds	80 pounds
Shipping Weight	70* or 110 pounds	130 pounds

*One position unit

S-29459 ELECTROLYTIC ANALYZER — Motor Stirred, One Position, 5 Ampere, SARGENT-SLOMIN. (Not illustrated here) **$275.00**

S-29464 ELECTROLYTIC ANALYZER — Motor Stirred, Two Position, 5 Ampere, SARGENT-SLOMIN. (Illustrated above) **$425.00**

S-29480 ELECTROLYTIC ANALYZER — Heavy Duty, Magnetically Stirred, Two Position, 15 Ampere, Sargent. (Illustrated above) **$575.00**

(The Sargent-Slomin Analyzers are also available with integral, concealed heater unit.)

SARGENT

NEW SARGENT CATALOG — NOW AVAILABLE

SCIENTIFIC LABORATORY INSTRUMENTS • APPARATUS • SUPPLIES • CHEMICALS

E. H. SARGENT & COMPANY, 4647 W. FOSTER AVE., CHICAGO 30, ILLINOIS

MICHIGAN DIVISION, 1959 EAST JEFFERSON STREET, DETROIT 7, MICHIGAN

SOUTHWESTERN DIVISION, 5915 PEELER STREET, DALLAS 9, TEXAS

Microsegregation in the Lead-Antimony Alloys[1]

A. C. Simon and E. L. Jones

Naval Research Laboratory, Washington, D. C.

ABSTRACT

The freezing process occurring in lead and hypoeutectic lead-antimony alloys was studied in single crystals and polycrystalline aggregates by examination of the metallographic structure with microscopic, microradiographic, and chemical replica techniques. The formation of dendritic lead crystals was also observed in other systems. The microsegregation occurring in the lead-antimony alloys was found to be a result of the dendritic mode of growth. Production of a homogenous alloy was found to be impossible even when the amount of antimony was reduced to insignificant amounts. This was true whether the alloy was chill-cast or very slowly cooled. Segregation is shown to be caused both by the small concentration gradient and the large amounts of lead crystallizing in the first intervals of freezing. Alloys of higher concentration are shown to have a more uniform solid solution of antimony in lead but actual segregation of antimony or an antimony-rich phase is inevitable. The primary lead dendrites appear to grow by alternate dendritic extension and regular crystal growth, accounting for the structure observed in metallographic sections. The structure in these alloys, commonly referred to as eutectic, is not produced under eutectic conditions and is not representative of true eutectic structure. When chill cast, an alloy with 13 per cent antimony produces a normal eutectic crystallization. Normal eutectic crystallization could not be initiated in any slowly cooled alloy investigated. In general, the segregation that occurs in chill-cast alloys is much more uniformly distributed than that in slowly cooled alloys.

Introduction

The as-cast hypoeutectic lead-antimony alloys reveal a metallographic structure which consists of primary dendritic crystals of lead surrounded by segregated antimony. This boundary of antimony is not continuous but is made up of innumerable small particles of no definite shape that appear to be imbedded in a matrix of lead. The appearance of antimony would be expected in an alloy with more than 3.5 per cent by weight of this constituent, for this concentration corresponds to the maximum solid solubility in lead. Definite indication of segregation in an alloy with only 0.01 per cent of antimony, however, signifies a decided departure from equilibrium conditions.

Microsegregation defines the segregation that occurs on a microscopic scale within individual grains or in the constituent network. Usually microsegregation refers to the cored structure that results from the precipitation of successively richer alloy layers upon the dendrites that first solidify. Thus, if an alloy with the composition represented by the vertical line, *xy*, (Fig. 1) is allowed to cool slowly to the liquidus temperature, *a*, the first crystals will separate from solution with the composition represented by *c*. With continued temperature lowering the composition of the liquid solution will change along the liquidus curve, *ab*, and the composition of successive layers of material deposited on the original dendrites will change along the solidus curve, *cd*. Assuming equilibrium conditions, the ratio of diffusion in and between solid and liquid will be such as to insure that at the instant of final solidification the composition of any part will equal that represented by the line *xy*. If equilibrium is not attained, a cored solid structure will result.

That equilibrium conditions are not present in the usual casting process is generally realized, but the full extent of unbalance is not appreciated. The described investigations indicate that uniform solid solution is practically nonexistent in alloys of low antimony concentration under any casting conditions. The structure commonly referred to as cored is found to more nearly represent actual segregation rather than a gradual concentration gradient, and the structure usually referred to as eutectic is found to differ greatly from the true eutectic structure for this series of alloys, both in appearance and in mechanism of formation. The relation of microsegregation to corrosion resistance when these alloys are used in sulfuric acid electrolyte has been discussed elsewhere (1). The causes and extent of microsegregation will be discussed in the present paper.

Experimental Procedure

The experimental procedures have been described in detail elsewhere (2). Briefly, the following indirect

[1] Manuscript received June 4, 1952. This paper prepared for delivery before the Montreal Meeting, October 26 to 30, 1952.

methods were used to investigate the freezing process occurring in a melt:

(*a*) Observation of dendrites removed during the freezing process by centrifugal or gravity separation of melt and solid.

(*b*) Metallographic examination of an as-cast alloy series prepared by both slowly cooling and chill casting a number of the hypoeutectic alloys.

(*c*) Examination of thin cast specimens by the preparation of chemical replicas. This replica (2, 3) consisted of a thin, cohesive corrosion product of lead obtained by the chemical corrosion of thin lead alloy foils. Metallic antimony is unaffected by the corroding agent and remains in the translucent corrosion product in its original position. The resolution and degree of magnification are far superior to that which can be obtained by microradiography and

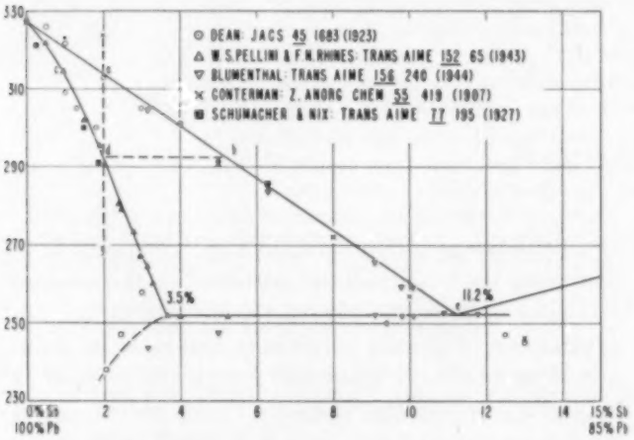

FIG. 1. Hypoeutectic portion of equilibrium phase diagram for the lead-antimony series of alloys.

the specimen can be studied by both vertical and transmitted illumination.

(*d*) Observation of the dendritic growth of lead crystals prepared by electrochemical reduction from solution.

DISCUSSION

Normal, inverse, and gravity segregation were all found to occur to a greater or lesser extent depending upon antimony concentration and other factors which will be discussed in a subsequent report. Microsegregation, however, was found to occur in every case examined regardless of antimony concentration or casting conditions and will be considered here.

Evidence of Microsegregation

The presence of pronounced segregation in very slowly cooled single crystals of nearly pure lead is particularly surprising since an approach to equilibrium is usually assumed under these conditions. The argument might be made that the alloy attained its maximum solubility at the eutectic temperature and with continued slow cooling and reduced solubility began to re-precipitate the dissolved antimony. If this were indeed the case, the antimony would be found in a finely divided and uniform dispersion throughout the dendritic structure and not segregated in large particles at the boundary. Other evidence for nonuniform structure and segregation is furnished by the following observations.

Pure lead when etched in glacial acetic acid containing a small amount of hydrogen peroxide is uniformly corroded and maintains a highly polished and brightly reflecting surface. For the same etch conditions, when the lead is alloyed with an extremely small amount of antimony, the surface is appreciably blackened and the reflectivity is dulled. Increased amounts of antimony alloyed with the lead increase the black coating until a concentration is reached where no further change can be detected in the film. This deposit cannot be removed by a vigorous water jet or by further etch action but is easily removed by rubbing or by certain chemical attacks.

This black deposit has been attributed to a finely dispersed deposit of antimony and, on the basis of x-ray analysis, this would appear to be correct. However, this effect cannot be produced upon pure lead when coupled with antimony in such a solution or by loading the solution with a high concentration of antimony ion. In addition, metallic antimony does not dissolve to an appreciable extent in such a solution. The phenomenon, therefore, does not appear to be caused by the usual process of electrochemical reduction from solution.

Whatever the mechanism, the alloys of low antimony concentration, when examined microscopically after this treatment, show unmistakable distribution of the deposit along dendritic boundaries (Fig. 2). The centers of the same dendrites show little or no black deposit. In comparatively short periods of time the black deposit can be converted to a white corrosion product in the acetic acid-peroxide solution, whereas metallic antimony in larger particles remains unchanged after several weeks.

When lead alloys with the low antimony concentrations are carefully polished and allowed to air-oxidize without etching, the first tarnish occurs in the same areas where the black deposit is found and the dendritic structure of the alloy is revealed. Several of the reagents used for etching have no visible effect on antimony but are effective in corroding lead. These give faster rates of corrosive attack in the same areas where the black deposit is formed than for the areas not so covered.

These factors indicate an increased activity for the areas surrounding each dendritic core which is

caused either by an increased concentration of antimony in the lattice at these areas, or by precipitation of very finely divided antimony from the structure. The important point is the evidence of extremely nonuniform distribution of antimony throughout the individual dendritic filaments.

Factors Controlling Microsegregation

The phase diagram predicts the compositions of solid and liquid that can exist in equilibrium at any temperature, but that crystals actually precipitate with the specified composition is unlikely. Antimony has a rhombohedral lattice while lead has the simple face-centered cubic type of structure. Reynolds and Tottle (4) have shown that nucleation cannot be

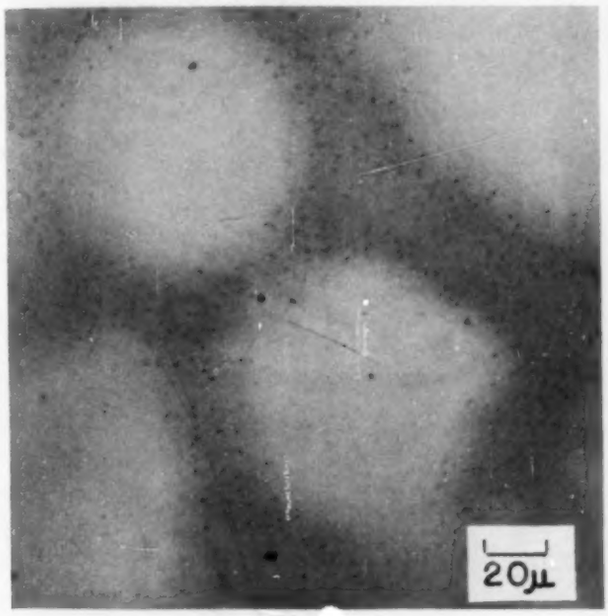

FIG. 2. Etched surface of a s rly cooled lead alloy with 0.01 per cent antimony, showing distribution of solid solution at dendritic boundaries (dark areas).

initiated by a second metal unless it has the same lattice structure as the first. This would indicate that there would be little tendency for two such metals as lead and antimony to form mixed crystals during growth.

Even with equilibrium conditions there is probably a statistical preference for the precipitating lead to form a lattice with all points occupied by lead atoms. This is offset by a constant diffusion of antimony atoms into the solid to maintain the equilibrium concentration. When conditions are far removed from equilibrium the first crystals to form are probably pure lead. The amount of antimony diffusing into such a structure will depend upon the following factors:

(*a*) The concentration gradient set up between solution and solid or within the solid. The rate of diffusion is directly proportional to the concentration gradient.

(*b*) The temperature. The rate of diffusion increases with the temperature.

(*c*) The time interval. Since the rate of diffusion increases with the temperature the longer the material is held at an elevated temperature the better will be the opportunity for diffusion.

The relative amounts of solid and liquid present and their corresponding average composition can be found at any temperature by means of the equilibrium phase diagram (5). If the amount of solid present at any instant is expressed as percentage of the total amount of alloy present and plotted against the temperature interval, the relative amount of solid present at any temperature during freezing can be readily determined (Fig. 3).

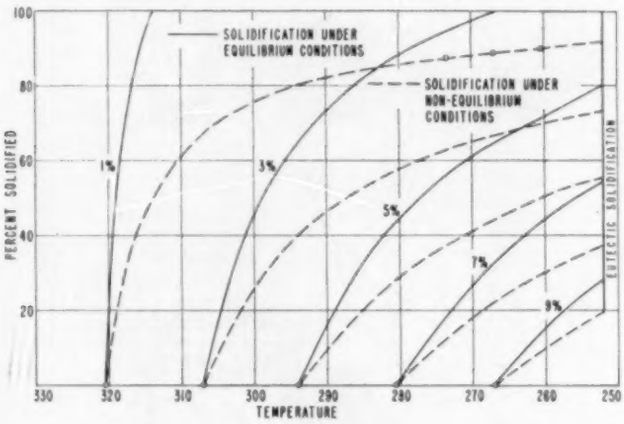

FIG. 3. Relation between solid formed and temperature increment.

For nonequilibrium conditions the same type of calculation can be used to determine the extreme condition of nonequilibrium that is likely to exist for any alloy and the relative amount of segregation that is possible. This calculation depends upon the assumption that pure lead is first precipitated and equilibrium then reached by diffusion of antimony into the solid. Even if this assumption should prove incorrect, the calculation is still approximately true.

At the freezing point, diffusion must take place much more rapidly in the disordered liquid state where solute atoms can be accommodated in all proportions than in the regulated structure of the solid where only a few solute atoms can be tolerated. The assumption can therefore be made that diffusion through the solid will be the rate-controlling step. For the purpose of calculating the limit of segregation that is possible under nonequilibrium conditions, a state may be assumed where the lead-antimony alloys would behave as if no solid solution were formed. In other words, the assumption is made that diffusion will take place at a rate sufficient to main-

tain a uniform composition in the liquid but insufficient to cause appreciable penetration into the solid. When the necessary calculations are made and the results graphically plotted they are compared with those obtained for equilibrium conditions (Fig. 3). An area is obtained between the curves for equilibrium and nonequilibrium conditions which represents all possible variations.

The concentration gradient can be calculated for equilibrium and also for nonequilibrium if the same conditions are assumed as outlined previously. The values thus obtained, when plotted against the percentage solidifying, yield additional information about the freezing process (Fig. 4). From a study of the two sets of curves the following information is obtained.

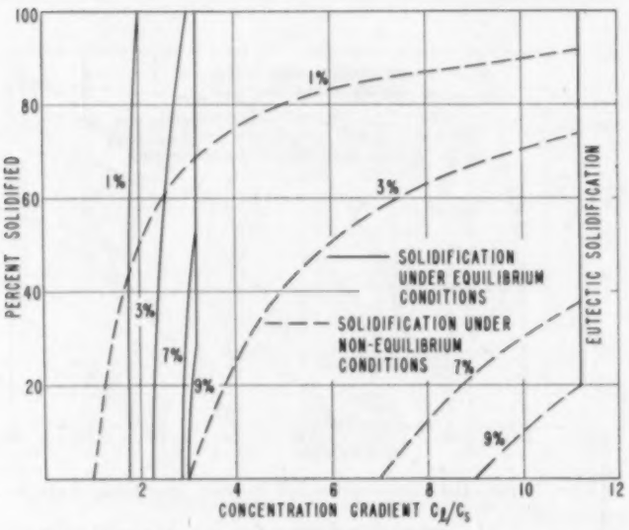

FIG. 4. Relation between solid formed and concentration gradient.

1. The possible variation from equilibrium conditions is much greater for the alloys containing small amounts of antimony than for those which approach eutectic composition.

2. The possible variation from equilibrium conditions for any given alloy composition becomes greater with increasing solidification but this variation is most evident for alloys of low antimony concentration.

3. The concentration gradient between liquid and solid, freezing under equilibrium conditions, varies but little either with increasing solidification for a given alloy or with variation in alloy composition.

4. The concentration gradient between liquid and solid, under nonequilibrium conditions, varies by a large amount. The gradient increases markedly with increasing solidification of a given alloy and reaches a maximum at the eutectic composition.

5. Under nonequilibrium conditions a small amount of supercooling can produce much more drastic supersaturation in the alloys of low antimony concentration than in those approaching eutectic composition.

6. Under nonequilibrium conditions the effective increase in the diffusion rate owing to the increased concentration gradient is offset to some extent by the reduced temperature under which freezing occurs.

Mechanism of Dendritic Growth

In the observation of dendritic crystals growing by electrochemical reduction, the development is found

FIG. 5. Drawing illustrating formation of regular crystalline plates on surface of original dendritic branches.

to occur by both regular and dendritic crystal growth. The first stage of growth takes place by the rapid extension of dendritic filaments which continue to elongate themselves without appreciable change in diameter until they approach one another or the container wall. The area of depleted nutrient surrounding the diameter of each filament is responsible for a return to conditions of regular crystal growth. A mosaic of tiny crystallites of regular crystal growth is observed to form upon the surface of each dendritic filament (Fig. 5) and the diameter of the filament is increased by the individual growth of

these mosaic crystallites in a regular manner. Occasionally one of these crystallites encounters favorable growth conditions so that it is able to outstrip its fellows and revert to dendritic growth. It is by this mechanism that secondary and tertiary branching occurred from the original dendritic filament. Depending upon growth conditions, the individual crystallites either remain fairly uniform and eventually grow together into a smooth surface or become all sizes and shapes and present extremely rough surfaces to the solution. By a combination of dendritic and regular crystal growth (Fig. 6) development proceeds until the original dendritic skeleton becomes a solid mass.

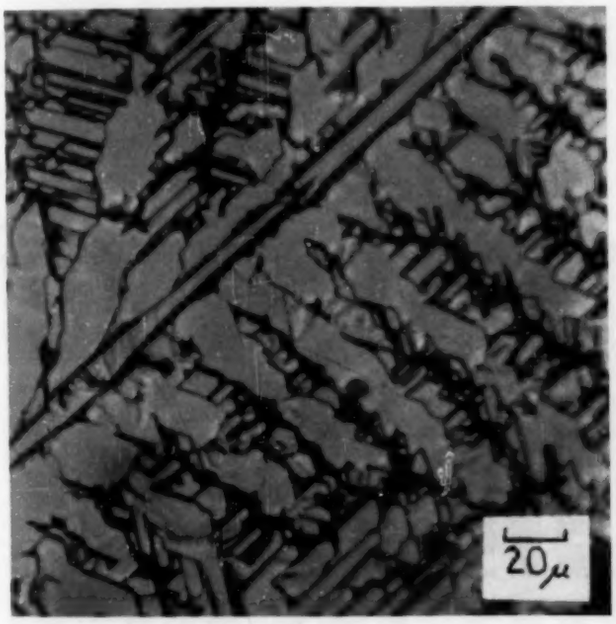

FIG. 6. Photomicrograph illustrating combined dendritic and regular mosaic crystal growth of actual lead crystal formed by electrochemical reduction.

The conclusion was reached (2) that the same process takes place in the case of lead and lead-antimony alloys freezing from the liquid state. Vogel (6) has shown that after a certain minimum cube size is reached, which is dependent upon heat conduction and the specific heat values for the system, further growth will occur most readily at the corners and least readily at the center so that a dendritic crystal is produced. Wherever conditions of supercooling occur the melt suddenly becomes labile. When this occurs at points where crystal apices jut into the labile liquid rapid deposition will take place and extension will occur in the direction of the outward thrusting point. The melt from which this material has been extracted is divided and pushed aside and this liquid contains the liberated heat of solution. The advancing dendritic filament is therefore surrounded by an envelope of metastable region in which only regular mosaic crystal growth can occur.

The term regular mosaic crystal growth in this report refers to growth of a host of crystallite extensions upon the original dendritic filaments. Individually these crystallites have regular crystal structure but collectively they exhibit the characteristics of dendritic growth since they must be regarded as dendritic extensions from a single crystal nucleus. In an alloy the tendency for regular mosaic crystal growth is increased by the high concentration of alloying element in the liquid surface immediately surrounding the dendrite (Fig. 7).

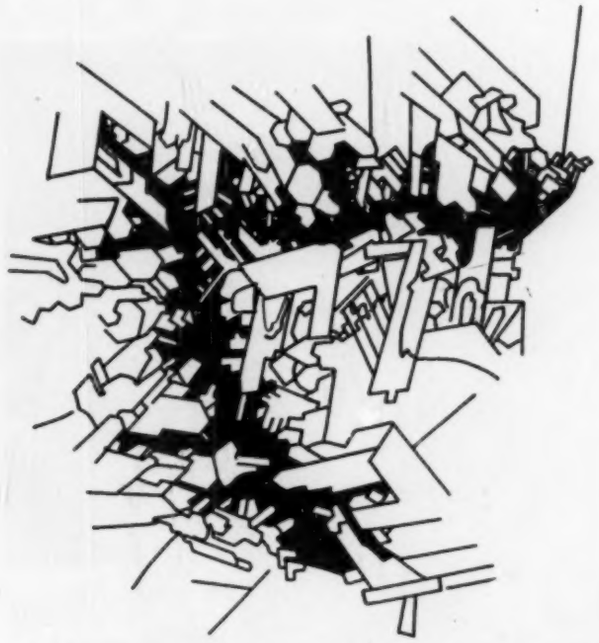

FIG. 7. Illustration of how regular mosaic crystal growth may occur in an alloy during freezing. Drawing represents primary lead dendritic branches enclosing pocket of near-eutectic composition into which extend numerous mosaic crystallites, lineages from the dendritic branches.

Segregation in the Solid Solution Range

The segregation and microstructure observed in the lead-antimony alloys may be explained by a consideration of the above factors. For lead alloyed with small amounts of antimony the observed segregation is large. The slowly cooled alloy with 0.01 per cent antimony, the lowest concentration prepared, gives definite evidence of microsegregation by the appearance of unequal rates of tarnish in the polished specimen and unequal deposition of antimony black on the etched specimens (Fig. 8). Chill-cast specimens of the same alloy do not exhibit these effects to the same extent but show a definite and sharply defined etch boundary for each dendrite. The possible digression of such alloys from equilibrium conditions may be quite large (Fig. 3).

A very large portion of the freezing will be accomplished with very little change in temperature so that there is the possibility of large supersaturation if very slight supercooling occurs. Such a condition is especially favorable for dendritic crystal growth and slowly cooled alloys are extremely likely to supercool. In such circumstances nucleation will be followed by immediate and rapid dendritic growth extending over relatively long distances (Fig. 8). Once the supersaturation is relieved, however, the temperature rises to normal with a return to metastable conditions and the dendritic skeleton grows in diameter by regular mosaic crystal growth. The metallographic structure is observed to consist of

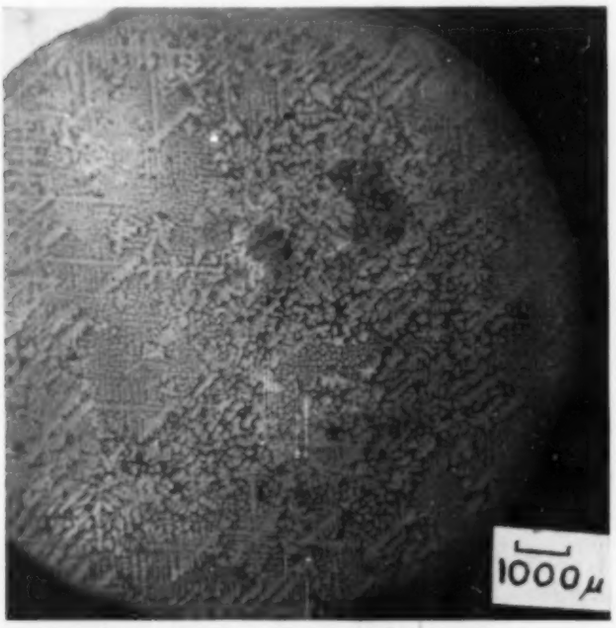

FIG. 8. Photomicrograph of slowly cooled crystal of lead alloyed with 0.01 per cent antimony, illustrating the extensive dendritic growth and the comparatively large diameter of individual filaments.

very extensive dendritic structure with individual dendritic filaments of large diameter but very little branching. As has been discussed previously, a large portion of the solid growth has taken place with only a very small concentration gradient existing between liquid and solid (Fig. 9). Diffusion is therefore a very slow process and the distances over which it must take place are long. Only in the outer fringes of the dendrite, in the small portions last to freeze, does a sufficiently high concentration gradient exist to insure anything like a uniform solid solution.

When a similar alloy is taken rapidly through the freezing interval a large number of nuclei are formed. In consequence the dendrites are much less individually extensive but far more numerous. They are observed to have much more numerous secondary and tertiary branches and the branches are of small diameter but uniformly spaced. They tend to enclose the entire crystal in a grid-like structure made up of individual dendritic branches (Fig. 10). They are, in addition, found to be severely distorted from a

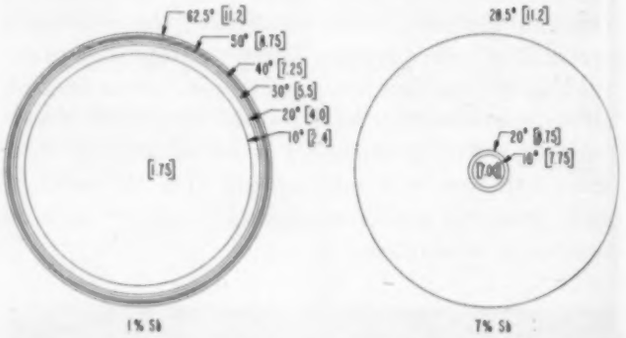

FIG. 9. Cross sections of two hypothetical crystal spheres of different alloy composition, grown under conditions of extreme nonequilibrium. The concentric rings indicate the relative amount of solid freezing in each 10°C increment. Figures enclosed in brackets represent concentration gradient present at temperature given.

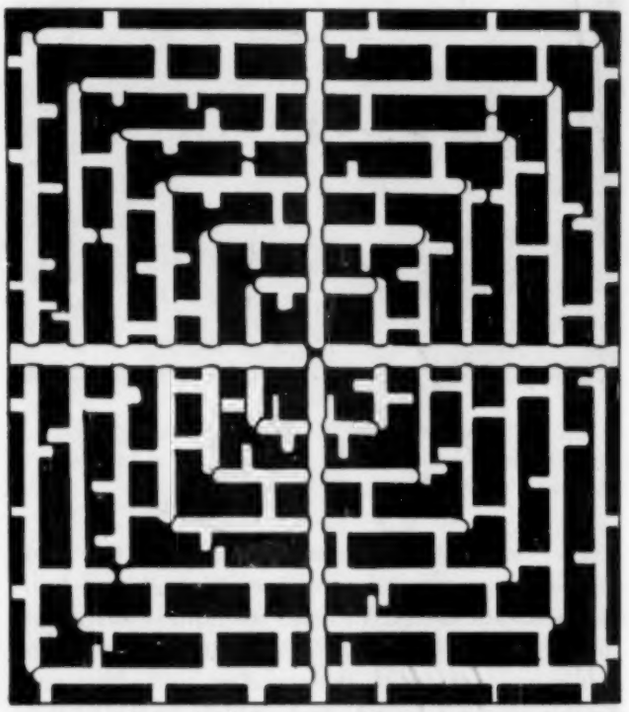

FIG. 10. Drawing illustrating the symmetrical and grid-like growth of dendritic metal crystals observed in chemical replicas prepared from thin cast alloy sections.

recognizable dendritic shape owing to strains produced in the sudden cooling and violent ebb and flow of the remaining liquid in the unequally shrinking mass (Fig. 11). The relative amounts of material solidifying in any temperature interval remain as before but the successive layers of solidification, being distributed over a much more extensive dendritic surface, are quite thin. The envelope of high

concentration gradient is tremendously increased in area and decreased proportionately in thickness. In such a zone the atomic distances are short and the concentration gradient large so that maximum solid solubility may be expected to occur during solidification. Etching should reveal a sharp and distinct demarcation between areas of low and high concentration, as is indeed the case (Fig. 11).

The inability of the antimony to diffuse rapidly from solution into the large amounts of lead first formed will cause a sharp change in concentration of the liquid toward the eutectic composition, with subsequent separation of metallic antimony in a recognizable form. Actual segregation of antimony

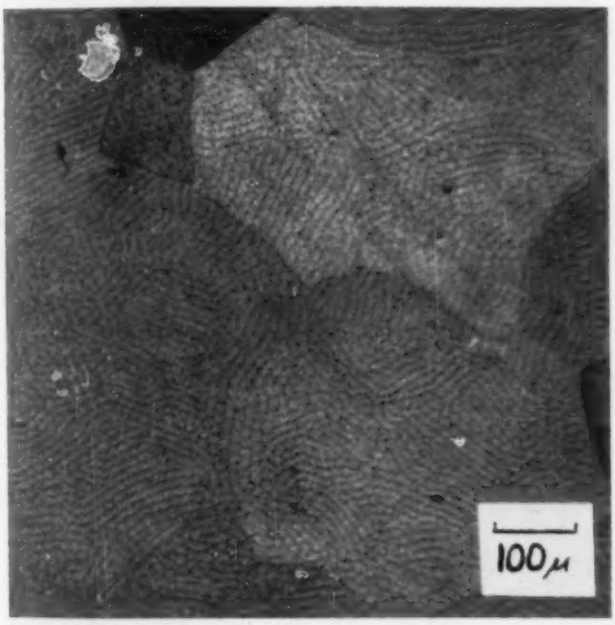

FIG. 11. Photomicrograph of chill-cast 0.01 per cent alloy of antimony with lead, showing uniform diameters of dendritic branches as well as the distortion caused by sudden cooling.

in particles large enough to recognize by their metallic luster was not detected in alloys containing less than 0.5 per cent antimony. In the lack of contrary evidence, the effects observed at lower concentrations than this must be attributed to a region of solid solution of high concentration around each dendritic branch. However, the appearance of the specimens does indicate that segregated particles of small size are present (Fig. 2).

Segregation in the Range of Eutectic Crystallization

The most noticeable segregation effects occur in the alloys containing less than 3.5 per cent antimony, because above this amount segregation of antimony will occur in any case, under equilibrium conditions or not. Comparison of equilibrium and nonequilibrium conditions (Fig. 3, 4) shows that the relative difference in microstructure in the two cases must become increasingly smaller as the eutectic composition is approached. The concentration gradient existing in such circumstances, together with increasing uniformity in the depth of deposited layers, appears to be sufficient to insure a uniform solid solution in both the primary dendritic structure and the lead deposited under eutectic conditions.

In these alloys of higher antimony concentration there is little opportunity for supersaturation when the alloy is slowly cooled since relatively large changes in temperature ordinarily produce but little additional solid. Therefore, individual dendritic crystals will not reach any great size before they revert to regular mosaic crystal growth. The growth of large single crystals therefore becomes increasingly difficult and the grain size becomes increasingly small as the eutectic composition is approached. The dendrites are observed to be short, with large diameter for individual filaments and very little branching. An extended structure of alternate lead and antimony is found surrounding the dendrites.

This extended structure is formed after the alloy reaches eutectic temperature but does not represent true eutectic configuration. Prior to reaching eutectic temperature the melt was freezing under conditions favorable for regular mosaic crystal growth. With true equilibrium conditions, the alloy will solidify isothermally when the eutectic temperature is reached. Both constituents precipitate simultaneously to maintain the eutectic composition in the solution. The eutectic solution contains approximately 11 per cent antimony and 89 per cent lead so that to maintain this composition unchanged requires a more rapid precipitation of lead than antimony.

With actual conditions of slow cooling the mechanism is found to be considerably different and cannot be considered representative of eutectic solidification. Blumenthal (7) has reported that the beginning of crystallization for the lead-antimony eutectic is accompanied by a special effect. His thermal analysis revealed that crystallization begins isothermally at the eutectic temperature but soon ceases. The melt then supercools to a considerable extent before crystallization begins again and this is then followed by a rise to eutectic temperature and isothermal freezing of the remainder of the melt. Blumenthal found that this effect was observed on both hypoeutectic and hypereutectic alloys and at all rates of cooling.

The nucleation of antimony does not appear to be initiated by the presence of lead. Blumenthal found that, although primary antimony crystallization is dependent upon the rate of cooling, considerable supercooling takes place even when the melt is vigor-

ously stirred. Reynolds and Tottle (4) have shown that a powdered metal may be used to nucleate the same metal in the liquid state (homogeneous nucleation) and that in some cases powders of a dissimilar metal are successful (heterogeneous nucleation). They found, however, that heterogeneous nucleation is successful only when the metals involved have the same lattice structure and do not vary more than 10 per cent in lattice spacing.

Turnbull (8) and Turnbull and Cech (9) have shown that the rate-determining step in the solidification of small particle aggregates is the rate of crystal nucleation rather than the rate of crystal growth. The interpretation they have placed on this result

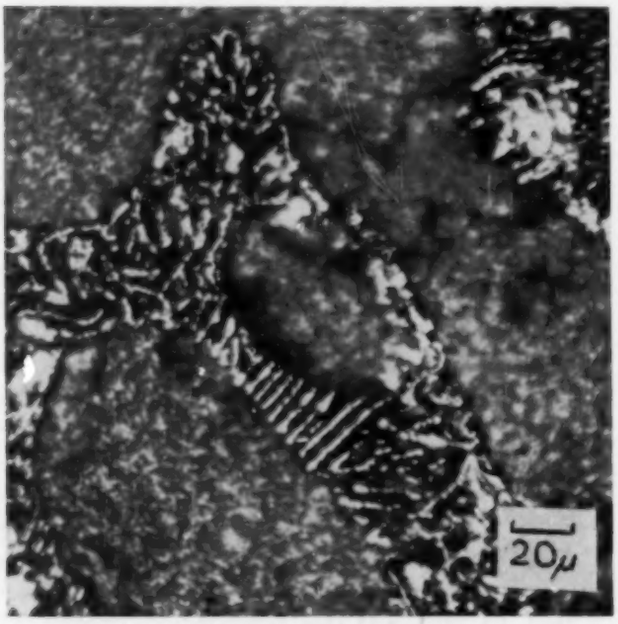

FIG. 12. Photomicrograph of slowly cooled alloy of lead with 7 per cent antimony, illustrating extensive dendritic growth of the antimony-rich phase during relief of supercooling.

is that the effective crystal nucleation catalyst usually present in large continuous masses is isolated on a small number of the resulting particles when the specimen is broken up. In their investigations they found that the maximum amount of supercooling for a large number of metals was about 0.18 times the absolute melting point. More specifically small droplets of lead could be supercooled as much as 67°C (121°F) while droplets of antimony were supercooled in some cases to 135°C (243°F) below the melting point.

Large masses of liquid metals that crystallize to close packed structure can rarely be supercooled more than 3 to 10 degrees while large masses that crystallize to a more complex structure can often be supercooled to a much greater extent. Turnbull points out that this may be explained on the basis that effective catalysts for the nucleation of close packed crystals (lead) occur much more frequently than those effective in the nucleation of more complex crystals (antimony).

When a slowly cooled hypoeutectic alloy reaches the eutectic temperature, the melt will have approximately the eutectic composition, whereas the solid will be unsaturated with respect to antimony. Conceivably there can be a brief crystallization of lead under isothermal conditions since the eutectic composition of the melt can be maintained by diffusion of antimony into the solid rather than by crystallization of antimony. When the concentration gradient becomes insufficient to maintain this process, further crystallization will cease and supercooling will take place until the nucleation of antimony is initiated. In the supercooled melt, crystallization of antimony will be dendritic, with extensive dendritic filaments and much branching, at least in alloys that approach eutectic composition. The initial isothermal crystallization of lead before supercooling begins will extend much further in the case of alloys well below the eutectic composition than for those very near to it. This is to be expected because of the greater degree of unsaturation in the solid, the much larger proportion of solid, and the much greater separation of the remaining melt into small masses, with consequent tendency for supercooling. The alloys near eutectic composition would therefore be expected to show large dendritic areas of primary antimony crystallization (Fig. 12) while those alloys with lower antimony concentration would tend to show isolated filaments of primary antimony crystallization surrounded by large areas of lead (Fig. 13). The observations made of actual specimens prepared for metallographic examination agree with these conclusions.

Mention should be made that after the supercooling of antimony has been relieved final crystallization of both constituents will be more or less simultaneous upon existing crystals since there will be no opportunity for supercooling of either component.

In the case of chill-cast alloys with compositions near the eutectic concentration the metallographic appearance is completely different. The structure is found to consist of a multitude of very small dendritic crystals having dendritic filaments of small diameter but considerable branching. The antimony is distributed as very finely divided particles in a network around these dendritic filaments. While the same mechanism operates as for the slowly cooled alloys, the portion crystallizing at the eutectic temperature is distributed over a much larger area and the extremely rapid cooling gives little opportunity for isothermal crystallization of lead. There would

also be less chance for pronounced supercooling and the final crystallization approaches closer to true eutectic crystallization.

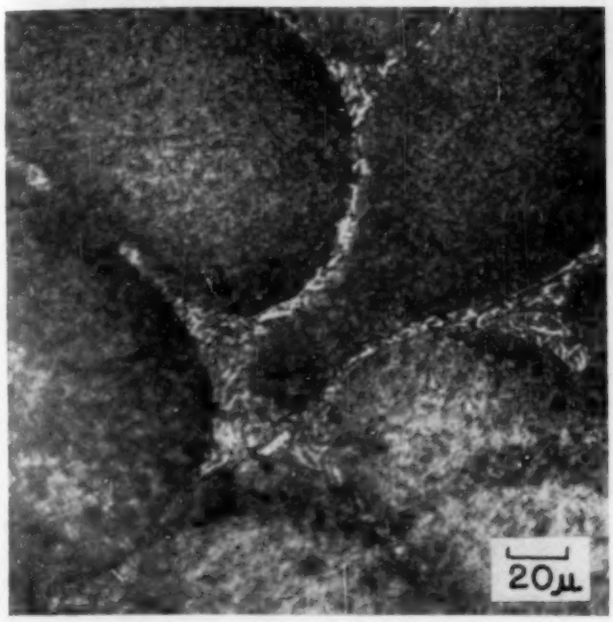

FIG. 13. Photomicrograph of slowly cooled 3 per cent alloy of antimony with lead, showing the small particle size and lack of extensive dendritic growth in the antimony-rich phase.

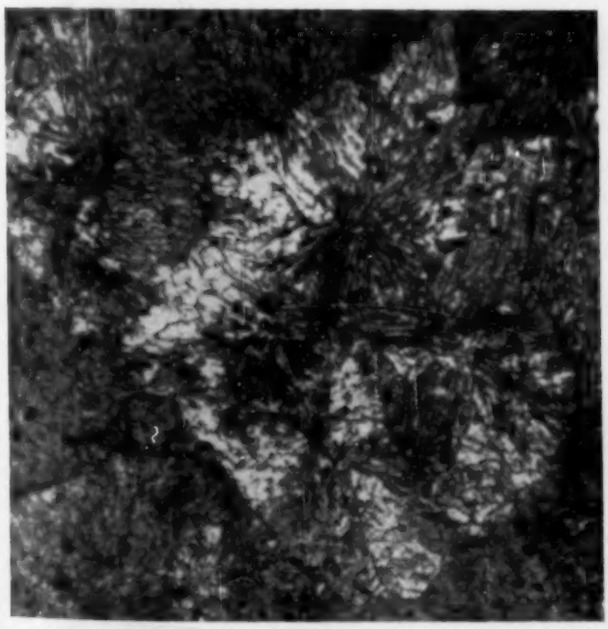

FIG. 14. Photomicrograph of the simultaneous eutectic crystallization of lead and antimony in a chill-cast alloy of 13 per cent antimony with lead.

True eutectic crystallization could not be produced experimentally in either slowly cooled or chill-cast alloys of eutectic composition. A chill-cast alloy containing 13 per cent antimony (Fig. 14) was the only alloy that apparently completely crystallized by the simultaneous precipitation of lead and antimony. This structure was experimentally reproducible at 13 per cent antimony and it appeared, mixed with primary crystals of one or the other constituent, in alloy compositions varying as much as 2 per cent to either side of this concentration.

This type of structure, which apparently represents true eutectic crystallization under nonequilibrium conditions, could not be reproduced in a slowly cooled alloy of any composition. Primary crystals of one or the other constituent invariably appeared and the crystallization apparently proceeded by the noneutectic freezing process previously described.

CONCLUSIONS

The results obtained appear to lead to the conclusion that a homogeneous alloy of uniform solid solution cannot be produced by any present casting process unless further heat treatment is employed. Slow cooling would appear to hinder rather than help the attainment of homogeneity in the solid solution. The possibility of a uniform solid solution increases with alloys of higher antimony concentration but, with increasing concentration of antimony, increasing amounts of melt will have eutectic composition when the eutectic temperature is reached.

From the standpoint of corrosion resistance it would appear that the more the antimony-rich phases could be distributed, the more uniform would be the corrosion attack. This is undoubtedly true for the hypoeutectic alloys that approach the eutectic composition. In these circumstances the lead will hold a uniform concentration of antimony in solid solution, causing uniform attack in the lead-rich phase. Very unequal attack is caused by large conglomerations of the antimony-rich phase.

For the hypoeutectic alloys with low antimony concentration, however, the situation is somewhat different. Because of the sharp demarcation between solid solution areas of high and low concentration, attack is more sharply pinpointed than in similar alloys slowly cooled and results in somewhat the same effect as a grain boundary attack. While the segregated areas in the slowly cooled alloys are somewhat more extensive and collectively fewer in number than in the chill-cast alloys, attack does not appear to be so destructively pinpointed. In general, however, the most desirable condition appears to be that which will produce the smallest dendrites with the most branching. The foregoing discussion has shown that the size and branching are inescapably dependent upon alloy composition. The greatest amount of branching will occur in the alloy with the composition nearest to pure lead, but the

smallest size will be exhibited in an alloy near eutectic composition. Chill casting produces large temperature gradients and increases the number of points where nucleation can begin, thus encouraging large numbers of dendritic crystals to form. Unfortunately the rates of cooling required in these experiments to produce extremely small and branched dendritic structure are not practical for large castings commercially produced. There are possibilities, however, of producing this structure in more slowly cooled alloys. Anything that can prevent supercooling of either lead or antimony will have a beneficial action. Thus, the work of Reynolds and Tottle (4), in which they coated the mold face with powdered metals which acted as nuclei for the crystallization of the melt, is important and suggestive. The work of Eberall (10) and Cibula (11) on the grain refinement of aluminum by nucleating agents that were not destroyed in the molten state of the alloy also offer suggestions for distributing the segregation in the lead-antimony alloys. And there are, of course, other means such as mechanical and ultrasonic vibration that tend to overcome supercooling in metals.

Any discussion of this paper will appear in a Discussion Section, to be published in the December 1953 issue of the JOURNAL.

REFERENCES

1. J. B. BURBANK AND A. C. SIMON, *J. Electrochem. Soc.*, **100**, 11 (1953).
2. A. C. SIMON AND J. B. BURBANK, Naval Research Laboratory Report No. 3941, March 11, 1952. Unclassified.
3. J. B. BURBANK AND A. C. SIMON, "A Replica Method for Study of the Structure of Lead-Antimony Alloys." To be published.
4. J. A. REYNOLDS AND C. R. TOTTLE, *J. Inst. Metals*, **80**, 93 (1951).
5. C. H. DESCH, "Metallography," p. 20, Longmans, Green and Co., New York (1944).
6. R. VOGEL, *Z. anorg. Chem.*, **116**, 21 (1921).
7. B. BLUMENTHAL, *Am. Inst. Mining and Met. Engrs.*, Tech. Pub. No. 1634, Metals Technology (1943).
8. D. TURNBULL, *J. Chem. Phys.*, **18**, 198 (1950).
9. D. TURNBULL AND R. E. CECH, *J. Applied Phys.*, **21**, 804 (1950).
10. M. D. EBERALL, *J. Inst. Metals*, **76**, 295 (1949).
11. A. CIBULA, *J. Inst. Metals*, **76**, 321 (1949).

The Relation of the Anodic Corrosion of Lead and Lead-Antimony Alloys to Microstructure[1]

J. B. Burbank and A. C. Simon

U. S. Naval Research Laboratory, Washington, D. C.

ABSTRACT

A technique is described for determining the relation of the microstructure of lead and its alloys to the anodic corrosion occurring in sulfuric acid. This method has been used to show the manner in which the corrosion of lead and of its hypoeutectic antimony alloys is related to their microstructures. It was found that pure lead and the lower alloys corrode by intercrystalline attack, and that the higher alloys corrode by penetration of the antimony-rich network.

Certain aspects of the corrosion taking place in the lead-acid storage battery are discussed.

Introduction

Among the factors limiting the life of the familiar lead-acid storage battery is the corrosion of the positive grid metal, which causes disintegration of the plate, loss of electrical contact, and ultimate failure of the cell. This study was undertaken to establish the manner in which corrosion takes place relative to the physical structures of the grid metals.

The factors influencing positive-grid life, including such considerations as tensile strength, creep resistance, and absolute corrosion rates of the metals under battery conditions, have been discussed previously by Lander (1) and others (2). Theoretically the anodic attack of the grid metal is not essential for the action of the cell, but practically this corrosion constitutes a limiting factor in cell life.

It is generally recognized that many corrosion processes are more destructive than is evident from weight-loss measurements (3). For example, grain boundary attack in aluminum alloys, dezincification of brass, and stress-corrosion cracking of steels all lead to premature failure in use, and have been understood and minimized only after the corrosion processes were related to the microstructures of these materials. In these instances weight-loss measurements alone are an inadequate indication of service durability. Thus for a complete understanding of the physical mechanism of the corrosion process taking place at the positive grid in the lead-acid storage battery, this study of the relation of the microstructure to corrosion was undertaken.

Experimental Procedure

These studies were carried out by assembling miniature storage cells with small positive-grid areas in which the conditions actually prevailing in the storage battery could be simulated. The cells used, shown in Fig. 1, were constructed of methacrylate plastic and had a positive-grid area of approximately 0.32 cm^2 (0.05 $in.^2$). The positive plate was a disk of the alloy under study, presenting one side to the cell action, and backed up with a brass plug to make electrical contact; the negative plate was hung in the neck of the cell. Polyethylene gaskets were used to seal all joints. The constant-current circuit used with these cells is shown in Fig. 2. The current density of 4.65 ma/cm^2 (30 ma/$in.^2$) was slightly less than that used for formation by battery manufacturers, but at higher current density gassing was evident. Since the portion of current going to gassing does not contribute to the corrosion process, it was considered most satisfactory to regulate the current density so that it was just insufficient to cause visible bubble formation. The positive plate potential was measured against a mercury-mercurous sulfate electrode with a Rubicon bench-type potentiometer, and followed the charging curves common to this system (4).

Preliminary experiments showed that it is not necessary to apply active material paste, nor to cycle the cells, nor to control closely the acid strength or temperature because the physical mechanism of the corrosion of lead and lead-antimony alloys is not affected by these factors. It must be emphasized, however, that the rate of attack is radically affected by variation in these factors as shown by the work of Lander (5).

Specimens were made using National Lead Company ingots of pure lead, of 4 and 9 per cent lead-antimony alloys, and of Baker's C. P. antimony metal. The specimens were cast in brass or aluminum molds and used in the as-cast state. The electrolyte was Baker's C. P. sulfuric acid, diluted with distilled water to a specific gravity of 1.21 at 15.56°C (60°F).

[1] Manuscript received April 19, 1952. This paper prepared for delivery before the Montreal Meeting, October 26 to 30, 1952.

Castings covering the range from pure lead to 12 per cent lead-antimony alloys were examined and the photomicrographs presented here are a few representative examples illustrating the types of corrosion observed.

After completion of a run in the microcell, the specimen was treated with saturated ammonium acetate solution to remove the corrosion products. After rinsing and drying, the specimen was examined under the microscope and the corrosion pattern related to the known microstructures (6) of these metals.

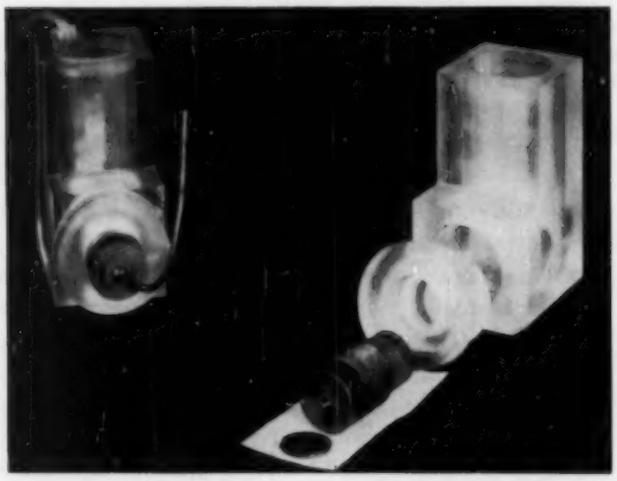

FIG. 1. Methacrylate plastic cell used for the anodic corrosion of the lead and lead-antimony alloys.

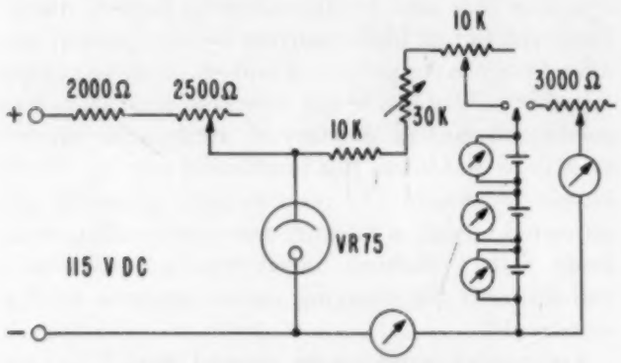

FIG. 2. Circuit used for the anodic corrosion studies

RESULTS AND DISCUSSION

Fig. 3 shows a photomicrograph of a pure lead specimen corroded anodically for 336 hours. The corrosion has been primarily intergranular and of the V-notch type. Portions of three grains are shown in this area and no striking effects are attributable to their varying orientations. The corrosion of lead containing low percentages of antimony (0.5% and under) takes place in the same manner as that of pure lead, i.e., by grain-boundary attack. This type of corrosion is particularly insidious because penetration takes place at isolated areas (the grain boundaries) and may cause structural weakening of the member and loss of conductivity of considerable amounts of material although the total amount of actual destruction remains relatively slight.

In alloys containing 1 per cent antimony the pattern formed during corrosion shows considerable subgrain attack, as illustrated in Fig. 4, a specimen corroded for 288 hours. Here a single grain boundary traversing the field has corroded more deeply than the channels traversing the grains. These subgrain paths are formed by preferential corrosion of the interdendritic network.

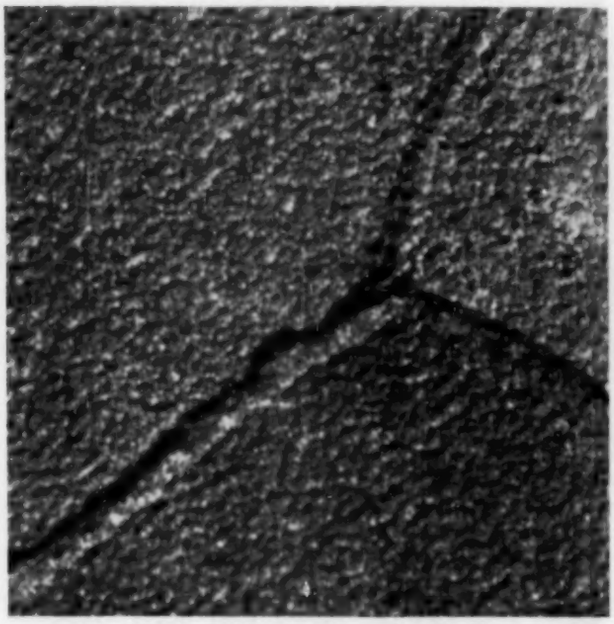

FIG. 3. Pure lead specimen corroded anodically for 336 hours showing grain boundary attack. 100×.

Fig. 5 shows the corrosion pattern formed in an alloy containing 9½ per cent antimony after 240 hours' attack. The grain boundaries are no longer being dissolved preferentially, and penetration is taking place more uniformly. Here again the destruction is along the interdendritic network of segregated antimony. This interdendritic penetration is characteristic of the hypoeutectic alloys and the corrosion is more uniformly distributed because it penetrates the eutectic network which is finer than the network of grain boundaries. The attack is distributed over a larger area, but less destructive corrosion occurs even though the total corrosion is greater from a weight-loss standpoint.

These results were observed on as-cast materials where the cast surface was presented to the cell action. If the metal is first deformed by compression, corrosion takes place in analogous manners. Thus a

pure lead specimen after deformation will corrode along the new, recrystallized grain boundaries. It has been shown that lead recrystallizes at room temperature (7), and the fact that it corrodes at the new grain boundaries indicates that boundary segregation of impurities is probably not the cause of this type of attack in lead. It seems more likely that the different orientation of adjacent grains accounts for the preferential attack in these regions (8). The alloys also corrode after deformation by the same mechanism as before cold working; the segregated antimony-rich phase is attacked as well as the new grain boundaries. If merely the surface of the casting is cold-worked by abrasion with emery,

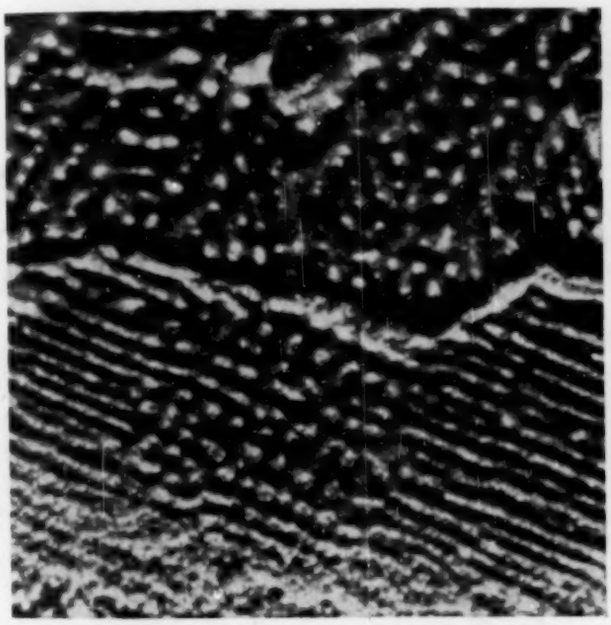

FIG. 4. Lead alloy containing 1 per cent antimony corroded anodically for 288 hours showing attack at the grain boundaries and in the interdendritic network. 100×.

anodic attack penetrates the distorted layer, and the as-cast structure beneath corrodes as before without any apparent influence from the layer of disturbed metal.

The findings reported here are in agreement with the conclusions of Bückel and Hannemann (9) who examined the corrosion in storage batteries by metallographic sectioning of grid members from commercial cells that had been in service for as much as two and one-half years. It is rather surprising that more attention has not been given to their paper which indicated so clearly the metallurgical relation of grid corrosion. The agreement of their conclusions with those reported here where corrosion was limited to a matter of hours shows that observations made with the microcell technique are indicative of actual service performance.

If the anodic corrosion process is followed by corroding the specimen continually for short periods of time (½ to 5 minutes) and the surface is examined microscopically, it will be found that the shiny cast surface typical of the lead-antimony alloys will become traced with a pattern of antimony crystallites as seen in hypereutectic alloys. This pattern is observed only in a thin layer of material on the as-cast surface, and will disappear in a short time under anodic conditions. The familiar dendritic structure of hypoeutectic alloys will then become visible, and clean channels will develop in the interdendritic space. Visible formation of the lead oxides does not take place until the antimony present in the surface

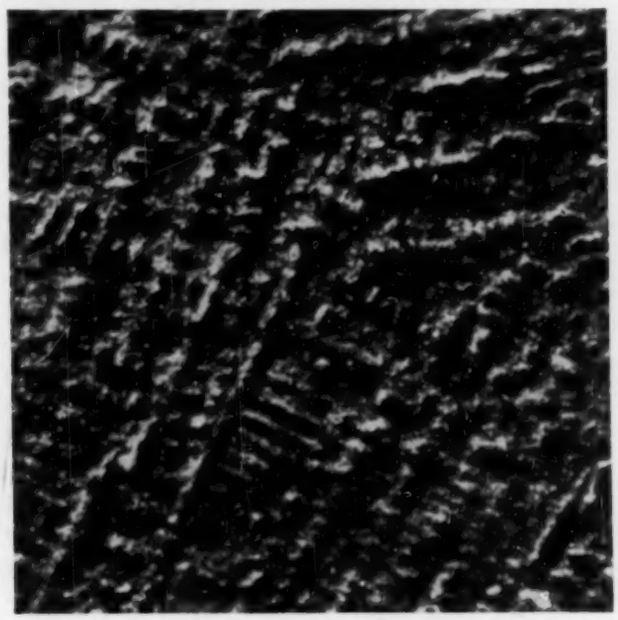

FIG. 5. Lead alloy containing 9½ per cent antimony corroded anodically for 240 hours showing attack in the interdendritic network. 100×.

of the casting has been largely leached out. This indication of high antimony content in the skin of the casting was verified by x-ray diffraction. In a practical way this high antimony concentration manifests itself in battery manufacture; the positive plates used in first quality cells are given the forming charge against dummy negatives. It has long been recognized by the practical man that batteries made in this way are less subject to self-discharge than those cells formed against their permanent negatives. It is now doubly clear why this practice is sound; the antimony dissolved from the positive plate is deposited on the dummy negatives and removed from the cell in final assembly, and, in addition, the amount of antimony leached from the positives is exceptionally large at the start of formation because of the high antimony content of the as-cast surface.

The electrochemical effect of the preferential leaching of the antimony from the alloys is reflected in the plate-potential measurements if these are recorded promptly and frequently at the beginning of the anodic treatment (10). The plate cannot attain the PbO_2 potential until the antimony content of the grid surface has been reduced. Future investigation is required to determine what actual surface concentration of antimony is tolerable at the time of lead oxide formation. It is probably low.

This leaching of the antimony from the grid metal is the physical mechanism of the anodic corrosion of these materials, and suggests that certain geometric considerations may be significant in determining the role of antimony in the storage cell. Thus, in effect, the removal of the antimony from the structure may provide space for the corrosion products of the lead. This would tend to relieve the stress applied to the metal by the oxide formations, and it may be that when the volume of metal leached from the surface is about equal to the volume of corrosion product, the destructive effect known as "growth" is minimized. It is known to be less in the case of antimonial grids than in pure lead grids.

Conclusions

It has been shown in these studies that the anodic corrosion of lead and lead-antimony alloys in sulfuric acid is related to the microstructure of these materials. Pure lead and alloys containing up to ½ per cent antimony corrode intergranularly. The alloys above this concentration corrode by a combination of intergranular and interdendritic penetration. In the range from ½ per cent to about 6 per cent antimony, the attack is preferentially intergranular. At higher antimony concentrations the corrosion is more evenly distributed between intergranular and interdendritic attack.

The surface of the castings containing 6 per cent or more antimony are richer in antimony than the bulk of the casting.

The technique used in making these observations is a satisfactory short-term test on a laboratory scale for demonstrating the structural relation of the corrosion processes occurring in storage batteries in actual use.

Any discussion of this paper will appear in a Discussion Section, to be published in the December 1953 issue of the Journal.

References

1. J. J. Lander, *J. Electrochem. Soc.*, **98**, 220 (1951).
2. W. H. Power, *et al.*, Naval Research Lab. Report # P-2908, January 9, 1947, unclassified; U. B. Thomas, F. T. Forster, and H. E. Haring, *Trans. Electrochem Soc.*, **92**, 313 (1947).
3. U. R. Evans, "Metallic Corrosion, Passivity and Protection," p. 421 ff, Longmans, Green and Co., New York (1946).
4. G. Vinal, "Storage Batteries," 3rd ed., p. 233 ff, John Wiley & Sons, Inc., New York (1940).
5. J. J. Lander, *J. Electrochem. Soc.*, **98**, 213 (1951).
6. R. S. Dean, L. Zickrick, and F. C. Nix, *Trans. Am. Inst. Mining Met. Engrs.*, **73**, 505 (1926).
7. P. A. Beck, *Trans. Am. Inst. Mining Met. Engrs.*, **137**, 222 (1940).
8. P. Lacombe and L. Beaujard, *J. Inst. Metals*, **74**, 1 (1948); G. Chaudron, *Helv. Chim. Acta*, **31**, 1553 (1948).
9. H. Bückel and H. Hannemann, *Z. Metallkunde*, **32**, 120 (1940).
10. H. E. Haring and U. B. Thomas, *Trans. Electrochem. Soc.*, **68**, 163 (1935).

The Effect of Temperature on the Cathode Potential during Nickel Plating[1]

DENNIS R. TURNER[2]

Westinghouse Research Laboratories, East Pittsburgh, Pennsylvania

ABSTRACT

The effect of temperature on the cathode potential during nickel plating was studied at current densities ranging from 0.4 to 100 ma/cm² and at temperatures from 20° to 90°C. The cathode potential-temperature relation is linear with a break in the slope at about −0.42 volt. The extrapolated E_c-T curves above −0.42 volt converge at about 0 volts and 165°C. An empirical equation was developed from the data: $E_c = 0.0034\ (4i^{1/2} + 1)\ (T - T^\circ)$. The observed change in cathode potential with current density is attributed to a hydrogen overvoltage which is controlled by the diffusion of hydrogen ions through a space-charged layer of nickel ions at the cathode surface. The equation does not apply at current densities below about 0.4 ma/cm². A hysteresis effect was observed in E_c-T curves using newly polished electrodes when the data were obtained first by decreasing and then increasing the temperature. Deviations from the empirical equation were attributed to hydrogen adsorption.

INTRODUCTION

The character of the deposit in metal electroplating processes is controlled primarily by the nature of the electrolyte immediately adjacent to the cathode surface. For optimum results with a particular plating process, it is usually necessary to adjust the concentration of the bath constituents, *p*H, current density, and temperature to some specific range. Each of these factors has some influence on the composition of the electrolyte at the metal-solution interface, and each affects the cathode potential. The effect of temperature on the cathode potential during plating has not been studied extensively.

In sulfuric acid solutions the temperature coefficient was found to be about 2 mv/°C for hydrogen ion discharge on several cathode materials (1, 2). Polarization studies by Salt (3) in a 0.5*M* nickel sulfate solution indicated the cathode polarization change with temperature to be an approximately linear function of the log of the current density. At 3 ma/cm², the change in polarization with temperature was a constant and apparently independent of the electrolyte and temperature.

The effect of temperature on the physical properties of electrodeposits has been the subject of several investigations. Frolich and Clark (4) studied deposits of nickel and concluded that high temperatures and low current densities gave the best development of structure. They found that hydrogen codeposition hindered the regular arrangement of the crystals. Graham (5) found that the increase of grain size obtained by a small temperature increase was greater than would be expected from the decrease in polarization. The stress in nickel deposits from sulfate solutions was shown by Macnaughtan and Hothersall (6) to decrease linearly with increasing temperature. The orientation of electrodeposited nickel crystallites in general was determined by Makar'eva (7) to be controlled by current density, i.e., rate of deposition. The effect of increasing the temperature was to make the orientation better defined.

The concentration of the metal ions at the electrode surface taking part in the cathode reaction tends to decrease during plating. This tendency is opposed by a renewal of ions to the cathode surface by diffusion, convection, and migration. An excellent discussion on the effect of concentration changes at electrodes on overvoltage has been given by Agar and Bowden (8).

The concentration gradient adjacent to the cathode surface is generally known as the diffusion layer since metal ions reach the cathode through the layer essentially by a process of diffusion. The thickness of the diffusion layer in unstirred aqueous solutions at room temperature has a fairly constant value of about 0.03 cm (9). It is appreciably decreased by an increase in temperature. Solution agitation is very effective in diminishing the diffusion layer thickness, but regardless of the method or extent of stirring, the limiting thickness appears to be about 0.001 cm. The diffusion coefficient of most substances in aqueous solutions increases by about 2.5 per cent/°C, due to a corresponding decrease in viscosity. Therefore, both increased temperature and

[1] Manuscript received March 25, 1952. This paper prepared for delivery before the Detroit Meeting, October 9 to 12, 1951.

[2] Present address: Bell Telephone Laboratories, Murray Hill, New Jersey.

agitation increase the rate of diffusion of metal ions to the cathode and permit higher plating rates.

The purpose of this investigation was to make a detailed study of the effect of temperature on the cathode potential during nickel plating over a wide range of temperatures and current densities.

Experimental Apparatus

The electrolytic cell used for this work is shown in Fig. 1. The 200-ml tall-form beaker in the center is the cathode chamber. This is thermostated by a water jacket which is formed by suspending the cathode chamber in a 600-ml beaker through a large stopper. Sections of 13-mm glass tubing, 1½ in. long, were added to the bottom and side of the outer vessel for the thermostating water inlet and exit,

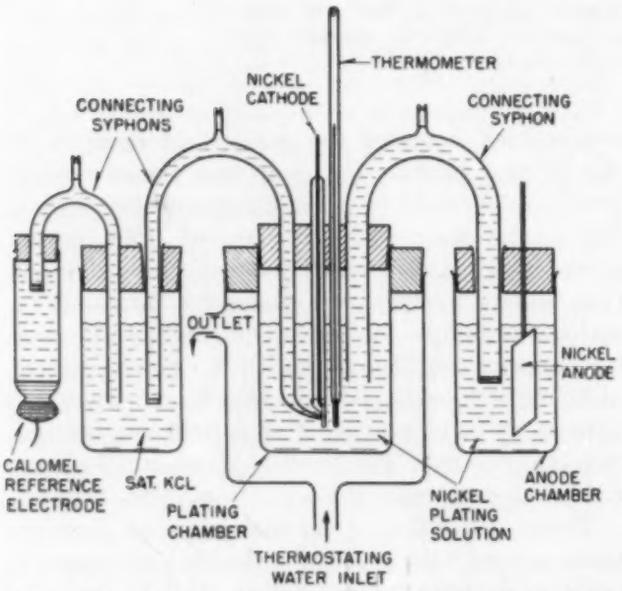

Fig. 1. Electrolytic cell with thermostated plating chamber

respectively. The water in a 5-gal reservoir was temperature controlled to ±0.02°C during potential measurements and was continuously pumped through the jacket around the cathode chamber.

The electrodes used as cathodes in this work were polished nickel disks, 1 cm² in front surface area; the back side was insulated with a solventless plastic stop-off material—Unichrome 218. Electrical connection to the electrode was made by inserting a heavy copper wire through a 5-mm glass tube and soldering the end to the back side prior to application of the stop-off material. Before each experiment, the nickel electrodes were polished mirror-bright using several grades of emery paper and finishing with 4-0. The anode was a sheet of nickel 4 cm by 5 cm placed in a 100-ml beaker shown at the right in Fig. 1 which connected to the cathode chamber through a syphon. A calomel electrode made with saturated KCl was the standard reference electrode used for potential measurements; its potential on the hydrogen scale was taken to be +0.246 volt. The calomel reference electrode was connected to the back side of the cathode in preference to the front side to eliminate the current shielding effect of the probe. Unfortunately all direct methods of measuring dynamic cell potentials have certain objections (10). The *IR* drop included in the potential measurement with the rear location of the probe was considered to be small since the Watts nickel bath has a resistivity of about 11 ohm-cm at 55°C (11). Another small error is involved in an unknown liquid junction potential between the reference electrode and the cathode due to the temperature differential. The importance of these errors of measurement was minimized by the fact that polarization voltages were recorded only to the nearest centivolt.

The Watts type of nickel plating solution used in these experiments was prepared from C. P. chemicals. The composition was as follows:

	g/l	mole/l
Nickel sulfate ($NiSO_4 \cdot 6H_2O$)	240	0.95
Nickel chloride ($NiCl_2 \cdot 6H_2O$)	38	.16
Boric acid (H_3BO_3)	38	.61

The solution was treated in the standard manner to remove organic and inorganic impurities; this included filtering at a *p*H of 5.0, treating with activated carbon, and electrolyzing 2 amp-hr/l of solution. The final *p*H adjustment was to 3.0.

Potential measurements were made on a Leeds and Northrup K-2 potentiometer. Plating currents were accurately measured with the aid of a 10-ohm standard resistor. A constant plating current was obtained using two 45-volt #2308 Burgess batteries connected in series and controlled by a variable high resistance.

Experimental Results

Prior to the determination of the effect of temperature on the cathode potential during nickel plating, it was necessary to know the influence of dissolved oxygen in the solution on the cathode potential. With the plating bath at room temperature, the cathode potential was measured at various current densities from 1.00 to 100 ma/cm², first in a nitrogen-saturated, oxygen-free solution and then in an oxygen-saturated solution. Tank gases were used, the nitrogen being purified of oxygen impurities by bubbling the gas through a solution of chromous chloride. Both gases were saturated with vapors of the plating solution before entering the plating cell. The results indicated that oxygen in the plating solution has no effect on the cathode potential during nickel plating. Therefore, no special effort was made to work in an oxygen-free solution. Generally the plating solution was air-saturated. Stirring un-

fortunately caused very erratic cathode potentials, and thus all measurements were made with an unstirred solution. The potential of the standard reference calomel electrode using saturated KCl was taken as +0.246 volt on the hydrogen scale. All potentials given in this paper were measured relative to the calomel electrode and are corrected to the hydrogen scale.

Temperature-cathode potential data

Temperature-cathode potential data were obtained in two ways: (*a*) at a constant temperature in intervals of 10°C, the cathode potential was measured at several current densities (Table I); and (*b*) at each constant current density, the cathode potential was measured with continually changing temperature. Within the limit of experimental reproducibility (±0.01 volt), the results were the same by either method. In obtaining data by the first method, the electrode potential was allowed to decay to its unpolarized value before a new current density was applied. This experimental technique is recommended by Bockris (12) and others in order to obtain more reproducible data. The potential was considered steady enough for measurement if the value did not change more than one millivolt in ten minutes.

TABLE I. *Effect of temperature on cathode potential during nickel plating*

Plating solution temperature °C	Plating current density							
	0.40 ma/cm²	1.0 ma/cm²	4.0 ma/cm²	10 ma/cm²	20 ma/cm²	30 ma/cm²	40 ma/cm²	100 ma/cm²
	Volts on hydrogen scale							
20	−0.52	−0.55	−0.62	−0.70	−0.79	−0.87	−0.93	−1.60
30	.48	.51	.58	.65	.72	.78	.85	−1.18
40	.44	.47	.53	.60	.67	.72	.78	−0.96
50	.41	.44	.49	.55	.62	.67	.71	.89
60	.38	.40	.45	.51	.57	.61	.65	.81
70	.35	.37	.41	.46	.52	.56	.59	.73
80	.32	.35	.38	.41	.46	.50	.54	.66
90	.29	.33	.36	.39	.42	.45	.48	.58

The data in Table I may be represented graphically two ways: (*a*) plot current density against cathode potential to obtain a curve at each temperature (Fig. 2*a*); and (*b*) plot temperature against cathode potential to obtain a curve at each current density (Fig. 2*b*). In order that better detail could be shown at the low current densities, the family of curves shown in Fig. 2*a* does not include the values at 100 ma/cm² current density. These curves are all about the same shape and are typical of current-potential curves in general. The temperature-cathode potential curves in Fig. 2*b* are straight lines over wide temperature ranges at all current densities. Deviations from the original straight line relation are observed at both ends of the curves. At the lower temperatures and high current densities, the deviations from the straight line were toward more negative potentials and coincided with the evolution of large quantities of hydrogen. The explanation is that in this region the diffusion and convection of nickel ions to the cathode surface is insufficient to maintain the major portion of the current, and hydrogen ions are discharged in greater quantities,

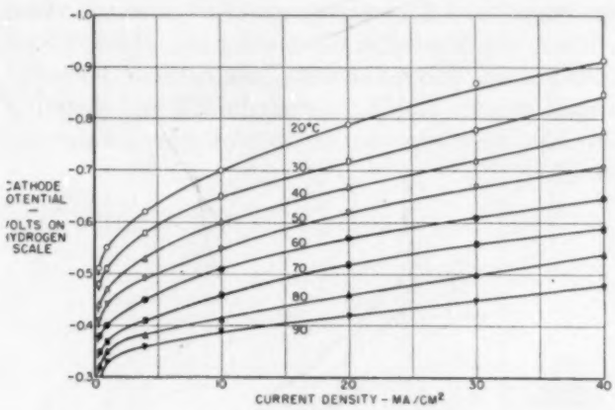

FIG. 2*a*. Effect of temperature on cathode potential during nickel plating. Plot of cathode potential vs. current density.

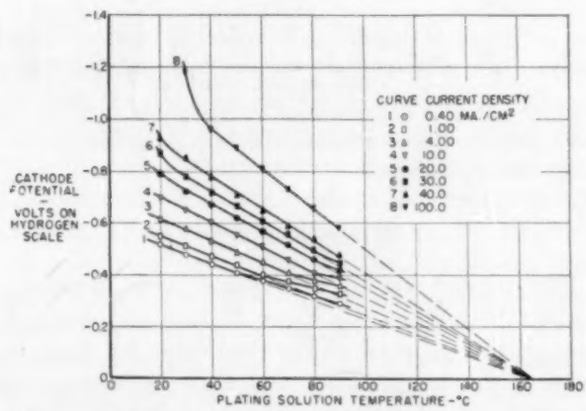

FIG. 2*b*. Effect of temperature on cathode potential during nickel plating. Plot of cathode potential vs. temperature.

this resulting in a more negative cathode potential. The deviations at the high temperature end appear to start at about −0.41 volt as the slope of the line changes abruptly to another straight line of lower slope. If the original straight lines are extrapolated, as shown in Fig. 2*b*, they all appear to converge at one point near zero volts and 165°C. Actually, the convergence point may not be exactly at these values, but it is certain that the lines appear to come together very near that point.

The cathode potential data obtained by the second method, i.e., at four constant current densities

with continually changing solution temperature, are shown in Fig. 3. In these experiments, the plating solution temperature was allowed to increase at the rate of about 10°C per hour. The change in slope below about −0.41 volt is shown in good detail, and it is clear that the break is sharp and not gradual. The change in the nickel electrode potential with temperature with no current flowing is shown as curve 1 in Fig. 3. An increase in temperature caused the potential to become more negative, changing about −0.1 volt from 20° to 80°C, which was just the opposite of the temperature effect observed when current was flowing in the plating cell. Below about 0.40 ma/cm current density, the cathode potential values became highly nonreproducible and therefore no data were recorded in the low current density range.

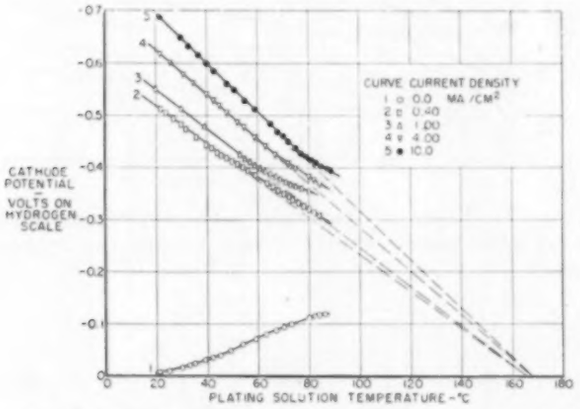

FIG. 3. Effect of temperature on cathode potential during nickel plating. (Data obtained with increasing temperature at a constant current.)

Hysteresis Effect

The data of Fig. 3 were taken with increasing temperature. When the E_c vs. T data are obtained, using newly polished nickel electrodes, by first decreasing the temperature and then increasing the temperature, a hysteresis effect is observed. This is shown in Fig. 4*a*. Curves 1 and 3 were obtained under conditions of decreasing temperature. The cathode potential-temperature curve deviated appreciably toward more negative potentials from the curve obtained when the temperature was increased instead of decreased. Curve 2 represents the data obtained with increasing temperature and was recorded soon after curve 1 was completed using the same electrode. The maximum deviation of curve 1 from curve 2 occurred at −0.43 volt. Following the maximum, the cathode potential changed to values approaching curve 2. No hydrogen gas bubbles were visible on the electrode in curve 1 until the maximum point was reached at A. In another experiment, curve 3 was recorded. It demonstrates that the position of the maximum relative to temperature is not reproducible although the potential at which it occurs is reasonably close, the two shown in Fig. 4*a* being 5 mv apart. The first visible sign of hydrogen on the electrode in curve 3 was far beyond the maximum point. When it did appear however, there was a slight break on the smooth curve at A.

If the cathode potential vs. temperature relation at decreasing temperatures is observed after a polished nickel electrode is nickel plated for a time with

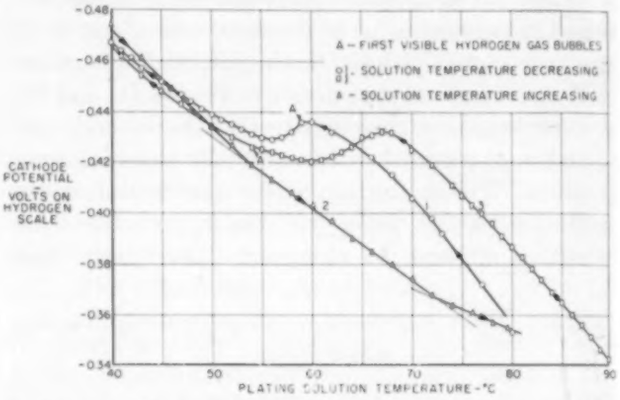
A - FIRST VISIBLE HYDROGEN GAS BUBBLES
○ - SOLUTION TEMPERATURE DECREASING
▲ - SOLUTION TEMPERATURE INCREASING
CATHODE POTENTIAL VOLTS ON HYDROGEN SCALE
PLATING SOLUTION TEMPERATURE - °C

FIG. 4*a*. Hysteresis effect of temperature on cathode potential during nickel plating; current density = 1.00 ma/cm². Temperature decreasing data obtained first.

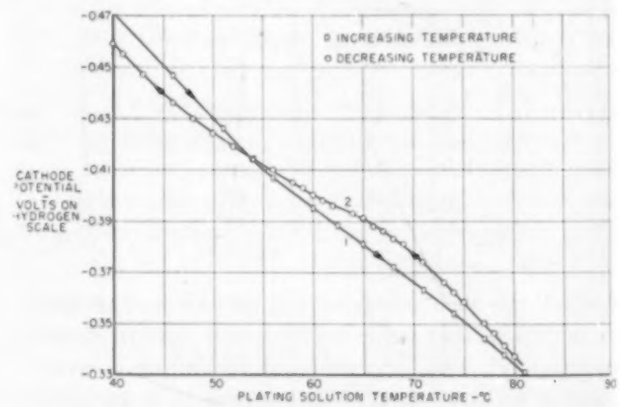
○ INCREASING TEMPERATURE
○ DECREASING TEMPERATURE
CATHODE POTENTIAL VOLTS ON HYDROGEN SCALE
PLATING SOLUTION TEMPERATURE - °C

FIG. 4*b*. Hysteresis effect of temperature on cathode potential during nickel plating; current density = 1.00 ma/cm². Temperature increasing data obtained first.

increasing temperature first, then there is no maximum point as in Fig. 4*a* although there is some deviation toward one initially. This is shown in Fig. 4*b*.

The maximum in the hysteresis effect and the sudden change in slope of the $E_c - T$ curves of Fig. 2*b* and 3 occur at very nearly the same potential, -0.42 ± 0.01 volt. It seems reasonable to assume that both phenomena are due to the same electrode process. During the experiments with increasing solution temperature, hydrogen gas bubbles were visible over the entire temperature range. On a freshly polished nickel electrode with the solution temperature decreasing, however, no hydrogen gas bubbles

were observed at the cathode surface until the maximum in the hysteresis effect was reached.

Discussion of Results

The most unusual feature of the data plotted in Fig. 2*b* and 3 is the apparent convergence of the extrapolated straight line portions to a common point which appears to be at or very near 0 volts and 165°C. The change in cathode potential with temperature, dEc/dT, was found to be proportional to the square root of the current density as shown in Fig. 5. From the slope and intercept of this line, it was possible to derive an empirical equation for

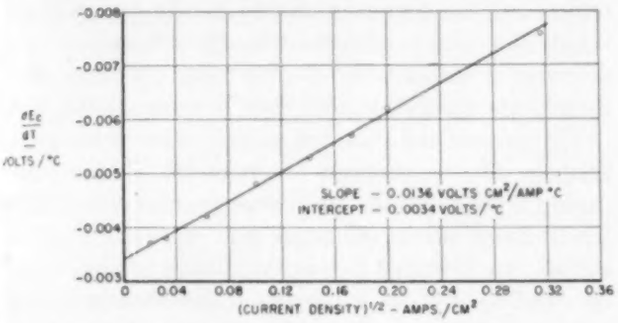

Fig. 5. Plot of cathode potential-temperature slope vs. the square root of current density.

much of the data. The equation for the straight line of Fig. 5 is as follows:

$$-\frac{dE_c}{dT} = (-0.0136i^{\frac{1}{2}} - 0.0034) \qquad \text{(I)}$$

where E_c is in volts, T is °C, and i is current density in amp/cm². On intergrating

$$E_c = (0.0136i^{\frac{1}{2}} + 0.0034)T + k \qquad \text{(II)}$$

where k is the integration constant. By rearranging and factoring

$$T = \frac{E_c}{0.0034(4i^{\frac{1}{2}} + 1)} - \frac{k}{0.0034(4i^{\frac{1}{2}} + 1)}. \qquad \text{(III)}$$

At $E_c = 0$, $T = 165$°C in Fig. 2*b*; therefore

$$T^\circ = \frac{-k}{0.0034(4i^{\frac{1}{2}} + 1)} = 165 \qquad \text{(IV)}$$

then

$$T = \frac{E_c}{0.0034(4i^{\frac{1}{2}} + 1)} + 165 \qquad \text{(V)}$$

or on rearranging again

$$E_c = 0.0034(4i^{\frac{1}{2}} + 1)\ (T - T^\circ) \qquad \text{where } T^\circ = 165^\circ\text{C}. \qquad \text{(VI)}$$

A plot of this equation and the experimental points of Table I above −0.42 volt in the straight line region are shown in Fig. 6. The empirical equation fits the experimental data fairly well since the observed deviations in most cases are no more than ±0.01 volt. The data at the lowest current density, 0.4 ma/cm², were all below the lines. As previously mentioned, no data were recorded below 0.4 ma/cm² current density because the reproducibility became poor. It is evident that even at 0.4 ma/cm² the results are beginning to feel the effect of the disturbing influence which causes poor reproducibility at lower current densities.

The cathode potential during electrolysis is generally considered to be proportional to the logarithm

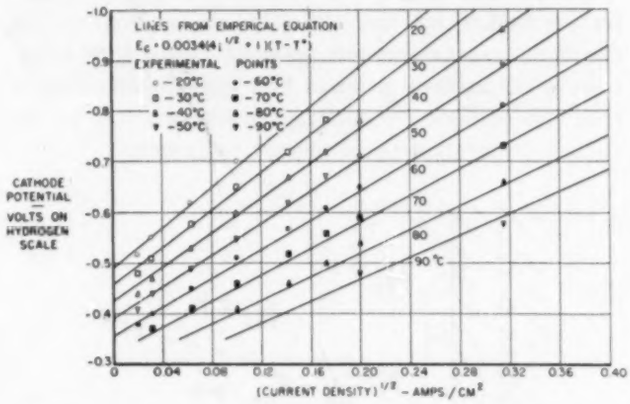
LINES FROM EMPERICAL EQUATION
EXPERIMENTAL POINTS
CATHODE POTENTIAL — VOLTS ON HYDROGEN SCALE
(CURRENT DENSITY)^1/2 - AMPS/CM²

Fig. 6. Comparison between empirical equation and experimental points.

of the current density. The empirical equation developed from the data of Table I, however, relates the cathode potential to the square root of the current density. Anodic overvoltages of a copper electrode in copper solutions have also been found to be proportional to the square root of the current density (13–15). These results are interpreted by Rubin as being due to a space-charge controlled diffusion process in a fixed layer of a cuprous salt on the electrode which has semiconducting properties or a similar process involving ions in a thin layer of solution containing cuprous ions next to the electrode.

Although concentration changes produce the most important form of polarization during metal deposition, there is evidence of an overvoltage due to other causes. This overvoltage is appreciable only for the deposition of nickel, cobalt, and iron. In plating these metals there is always a certain amount of hydrogen codeposition; thus the observed deposition overvoltage may be due entirely to a hydrogen gas overvoltage. Gardam (16) has shown that the cathode potential during nickel deposition is considerably more negative on mercury than on nickel. This is attributed to the larger hydrogen overvoltage on mercury than on nickel. If this is true, then it may be possible to explain the results of equation (VI) as a space-charge controlled diffusion process in a manner analogous to the mechanism proposed

by Rubin for copper anodes. The concentration of nickel in the plating solution is 1.1M, whereas at a pH of 3, the hydrogen ion concentration is 0.001M. The cathode surface layer during nickel plating may be pictured as one space charged with nickel ions (Fig. 7). All the ions are hydrated to some extent of course, but for purposes of simplicity this is not shown in the diagram. During nickel plating most of the current, usually about 95 per cent, is used to deposit nickel atoms; the remainder goes toward discharging hydrogen ions. If the cathode overvoltage can be attributed to a hydrogen overvoltage, then the actual rate of hydrogen ion deposition may be controlled by the diffusion of hydrogen ions through a space-charged layer of nickel ions adjacent to the cathode surface. This mechanism assumes that the cathode overvoltage is proportional to the surface concentration of atomic hydrogen.

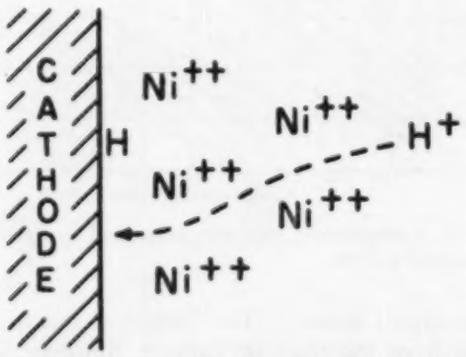

FIG. 7. Proposed mechanism for the linear cathode potential vs. square root of the current density relation.

The temperature coefficient of the cathode potential during nickel plating was positive in sign as indicated in equation (VI). In the static condition, that is, when the plating current is zero, the electrode potential becomes more negative with increasing temperature, −0.0017 volt/°C. This is slightly more than the value reported by Buffington (17). The slope of the potential-temperature curve is negative for most simple metal-metal ion electrodes.

The sudden change in the slope of the $E_c - T$ curves at about −0.42 volt and the hysteresis effect of Fig. 4a and 4b appear to be due to the same process involving hydrogen, that is, the adsorption of atomic hydrogen at the nickel cathode surface. The potential break at about −0.42 volt is interpreted as the point at which the available cathode surface energy equals that required to desorb hydrogen from nickel. An increase in surface atomic hydrogen due to adsorption should produce a change in the voltage toward more negative potentials. This is observed with the change in the slope of the $E_c - T$ curves. The total potential surface energy on polished amorphous metal surfaces is known to be greater than that on crystalline metal surfaces (18). Thus, a larger hydrogen adsorption capacity may be expected on a newly polished nickel cathode as compared to a surface having an appreciable nickel deposit already plated. This would explain the large deviation toward more negative potential on polished electrodes in the region of hydrogen adsorption. Although the experiment was not performed, it is expected that if a newly polished nickel cathode were nickel plated at a constant temperature—about 70°C—and at a constant plating current, the cathode potential would first slowly change toward more negative values due to hydrogen adsorption. After the surface adsorption centers become saturated with hydrogen, the potential should slowly become less negative as the plating thickness increases due to a decrease in the number of adsorption positions. Hydrogen gas bubbles should then become visible.

The present data are not sufficient for a complete analysis of the reaction energies at the cathode during nickel plating. Additional experiments of this kind, using other solutions and depositing other metals, are required before conclusive evidence can be cited to support a particular mechanism as the source of cathode polarizations during plating.

SUMMARY

The effect of temperature on the cathode potential during nickel plating from a Watts bath was studied at current densities ranging from 0.4 to 100 ma/cm² and at temperatures from 20° to 90°C. The cathode potential-temperature relation is linear with a sharp change in slope occurring at about −0.42 volt. The $E_c - T$ straight lines above −0.42 volt, when extrapolated toward higher temperatures, converge at about 0 volts and 165°C. Although the convergence to a common point seems significant, particularly at 0 volts, there was no obvious explanation. An empirical equation was developed from the data in which the cathode potential is proportional to the square root of the current density:

$$E_c = 0.0034\ (4i^{1/2} + 1)\ (T - T^\circ).$$

The observed change in cathode potential with current density is attributed to a hydrogen overvoltage which is controlled by the diffusion of hydrogen ions through a space-charged layer of nickel ions at the cathode surface. The equation does not apply at current densities below about 0.4 ma/cm².

The temperature coefficient of a nickel plated electrode in the nickel plating solution when no current flows is −0.0017 volt/°C.

The sudden change in slope of the $E_c - T$ curves at about −0.42 volt and the hysteresis effect observed are attributed to the adsorption of atomic

hydrogen at the nickel cathode, the potential of −0.42 volt corresponding to an energy of desorption.

Any discussion of this paper will appear in a Discussion Section, to be published in the December 1953 issue of the JOURNAL.

REFERENCES

1. M. KNOBLE AND D. B. JOY, *Trans. Electrochem. Soc.*, **44**, 443 (1923).
2. L. J. BIRCHER AND W. D. HARKINS, *J. Am. Chem. Soc.*, **45**, 2897 (1923).
3. F. W. SALT, *Disc. Faraday Soc.*, **1**, 169 (1947).
4. P. K. FROLICH AND G. L. CLARK, *Z. Elektrochem.*, **31**, 655 (1925).
5. A. K. GRAHAM, *Trans. Am. Electrochem. Soc.*, **52**, 157 (1927).
6. D. J. MACNAUGHTAN AND A. W. HOTHERSALL, *Trans. Faraday Soc.*, **24**, 387 (1928).
7. S. P. MAKAR'EVA, *Bull. acad. sci. U.R.S.S. Classe sci. chim.*, 573 (1941).
8. J. N. AGAR AND F. P. BOWDEN, *Proc. Roy. Soc. (London)*, **169A**, 206 (1938).
9. A. HICKLING AND W. H. WILSON, *Nature*, **162**, 489 (1948).
10. S. BARNARTT, *J. Electrochem. Soc.*, **99**, 549 (1952).
11. W. A. WESLEY AND E. J. ROEHL, *Trans. Electrochem. Soc.*, **86**, 418 (1944).
12. J. O'M. BOCKRIS, *Trans. Faraday Soc.*, **43**, 417 (1947).
13. E. HEINERT, *Z. Elektrochem.*, **37**, 61 (1931).
14. R. PIONTELLI AND G. POLI, *Gazz. chim. ital.*, **79**, 538 (1949).
15. T. RUBIN, *J. Chem. Phys.*, **19**, 803 (1951).
16. G. E. GARDAM, *Disc. Faraday Soc.*, **1**, 182 (1947).
17. R. M. BUFFINGTON, *Corrosion*, **3**, 613 (1947).
18. C. H. DESCH, "Chemistry of Solids," p. 165, Cornell University Press, Ithaca, N. Y. (1934).

Saturation and Voltage Effects in Cathodoluminescence[1]

P. H. Dowling and J. R. Sewell

Philips Laboratories, Inc., Irvington-on-Hudson, New York

ABSTRACT

The present work is an attempt at a quantitative study of the major phenomena of cathodoluminescence. Efficiency, current saturation, and the relation of brightness to electron accelerating voltage are correlated with the stopping power of the phosphor crystal for electrons, the decay characteristics, and the activator concentration. So far, exponential decay phosphors only have been considered and experiments have been made principally on Zn_2SiO_4—Mn. Steady state excitation only is considered. The experiments confirm the theory fairly well and the following inferences can be drawn.

(*a*) The principal relationship between brightness and accelerating voltage is a linear one. (*b*) For the first few kilovolts, this relationship is distorted because of a dead layer on the crystal surface averaging some 150 Å in thickness. (*c*) The electron beam loses energy along its penetration path in an exponential-like manner. (d) Within the approximate range 1 kv to 10 kv, the range of the primary electron beam varies as the first power of the accelerating voltage. Evidence is presented that above about 10 kv there is a transition to a faster-than-linear increase of range with voltage. (*e*) The brightness increases in a logarithmic manner with increasing current density. As far as current saturation alone is concerned, there is thus no real maximum brightness, at least for infinitely thick phosphor samples. (*f*) The current density at which saturation effects are noticeable is a function of the accelerating voltage. In the approximate range 1 kv to 10 kv it is practically constant. Above about 10 kv, it increases with increasing voltage. (*g*) In Zn_2SiO_4—Mn, the percentage of Mn ions which are effective luminescent centers decreases with increasing Mn content, reaching the order of 0.03 per cent at 10 mole per cent total Mn content.

I. Fundamental Theoretical Considerations

Our picture of the complicated processes which result in the excitation of activator ions by a beam of electrons passing through a crystal lattice is a considerably simplified one. The primary beam gives its energy to secondary electrons along its path. The word "secondary" is meant to include all the electrons appearing in the conduction band of the host crystal as a result of the primary beam energy-loss. In the unactivated crystal, these secondary electrons in turn give up their energy to thermal motion in the lattice. Under favorable circumstances, foreign ions in the crystal are able to appropriate some of the original energy of the secondary electrons and convert it into radiation in and near the visible spectrum. Luminescence thus appears as an incidental phenomenon and its efficiency might be expected to be proportional to the concentration of unexcited effective activators. Specifically, we assume the following relationship:

$$C = Q(N - n)dE/dx \qquad \text{(I)}$$

where C is the number of activator excitations per second per cm³ of the volume of the electron beam, N is the total effective activator concentration per cm³, n is the concentration of excited centers, x is the distance along the electron beam path within the crystal, dE/dx is the power expended by the electron beam in electron volts/sec per cm³ of beam volume, and Q is a factor of proportionality. E, then, is the beam power per cm².

Actually, Q is the number of secondary electrons which (when the primary beam loses 1 ev/cm³) return to the valence band of the host crystal at a location favorable for the excitation of a given activator ion. It is determined by the number of secondary electrons produced by the primary beam per ev of energy-loss and by the relative probability of return of these electrons to the valence band at normal host ion sites and at (or near) activator sites. If, now, every activator were capable of functioning as a luminescent center, QN_{Chem} would give the number of excitations per ev (n being small), where N_{Chem} is the actual activator concentration. It is quite possible, however, that for one reason or another some activators will be incapable of being excited even when a secondary electron returns to the valence band in their vicinity or, if excited, will dissipate *all* their energy in radiationless transitions. For this reason N is to be taken as the concentration of effective activators. To be "effective" an activator must have a finite excitation probability and a finite

[1] Manuscript received April 15, 1952. Paper prepared for delivery before the Washington Meeting, April 8 to 12, 1951.

probability of emitting radiation. It may also have a high probability of radiationless transitions and still be classed as effective. QN relates to the luminescence excitation efficiency only and is but one of several factors in the over-all luminescence efficiency.

Q is also closely related to the saturation characteristics of the phosphor, since from equation (I) the time between excitations of a given activator is given roughly by $1/(Q\,dE/dx)$. When this time becomes of the same order as the time constant τ of the phosphor, saturation effects will become important under steady state excitation. The condition for the onset of saturation is thus given roughly by

$$\tau Q\,dE/dx = 1. \qquad \text{(II)}$$

Small values of the time constant, of Q, and of the power density in the beam path are thus conditions which make for a phosphor having low saturation under steady state excitation. It will be noted that the activator concentration does not appear explicitly in the condition for saturation. Since it does not seem likely that dE/dx will be greatly affected by the activator concentrations ordinarily encountered, any dependence of saturation on activator concentration must arise because of such a dependence of τ and/or Q.

In the development of our theory we have taken Q to have no explicit dependence on the beam energy and/or the distance along the beam path within the crystal. A dependence of Q on the beam energy implies that the energy abstracted from the primary beam, by the formation of a secondary electron within the crystal, is a function of the energy of the primary beam. It seems to us that this is unlikely, at least to any significant extent (1). We feel that it is also unlikely that $Q = f(x)$. In order to explain some of our results, we have suggested instead that $N = f(x)$, as will appear later.

For phosphors whose decay is exponential, the number of luminescent centers returning to the ground state per second is given by $B = n/\tau$. In the steady state, $B = C$ of equation (I) and we may write for an electron beam of unit cross section and length dx,

$$dB = \frac{h\nu bN}{1 + 1/(\tau Q\,dE/dx)}\,dx \text{ ev/sec cm}^2. \qquad \text{(III)}$$

This has been written for the general case where there are radiation transitions of probability b and radiationless transitions of probability γ. When the decay of luminescence is determined in the usual way, it is $\tau = 1/(b + \gamma)$ which is measured. $h\bar{\nu}$ is the average quantum of the emitted radiation in ev. For purposes of discussion, we shall assume that no radiation is lost within the sample and that all the radiation leaves from one side of the sample.

Equation (III) is of the type always arrived at for exponential decay phosphors when saturation is ascribed to depletion of centers (2). It clearly contains condition (II) for the saturation of light contributed by the element dx. For the behavior of the total light output, we need to know dE/dx as a function of x and of the initial beam energy. dB can then be integrated over the path length. A determination of this function on theoretical grounds is not a simple matter. Theoretical solutions have been obtained for the loss of energy of an electron along its actual path within the material (3) but this path, for most electrons, is not the same as our x, the distance along the beam path. Furthermore, the current density along the beam path is not constant; within each element of path, dx, a certain number of primary electrons are completely stopped. Stinchfield, as reported by Leverenz (4), has approached the problem of determining E as a function of x by combining the Thompson-Whiddington law, for the loss of energy of individual electrons, with the experimentally determined law for the change in current density along the beam path. While this approach has considerable attractiveness, it seems to us that it is open to some question since the Whiddington law, in this connection, strictly applies to undeflected electrons only, i.e., those for which the actual path is the same as the beam path. Furthermore, we believe we have evidence that the Thompson-Whiddington law does not hold at lower voltages (see section II). In the voltage range of most of our experiments, 1 to 10 kv, we have approached the problem entirely empirically and have inferred for this range, from experimental curves showing the relation between brightness and accelerating voltage, what seems to be a reasonable behavior of E as a function of x and the initial beam power.

II. General Form for the Relationship between E and X. Penetration Range vs. Accelerating Voltage

An experimental observation which seems to us to be of the greatest importance is that, over quite a range of voltages below 10 kv, the shape of the saturation curve (brightness plotted against current density at a constant accelerating voltage) is independent of the value of the accelerating voltage, V_o, at which the readings are taken (5). As an example of this, Fig. 1 shows our results for Zn_2SiO_4 — 1 mole per cent Mn in the range 1 to 10 kv.[2] Since, by our equation for dB, dE/dx is an important

[2] Our experimental work on saturation was for the most part confined to the range 1 to 10 kv. A discussion of what may occur outside this range is given in section VII-2.

factor in the condition for saturation and it may well be a function of V_o, this observation places some restrictions on the functional behavior of dE/dx. dE/dx equal to a constant will, of course, meet the requirements but this is more restrictive than necessary. B is the integral of dB along the beam path and, in order to have saturation independent of voltage, it is sufficient that, to each element in the path for a given voltage, there correspond another element in the path for a second voltage where dE/dx is the same. This condition is possible when

$$E = I_d V_o f(x/\delta) \qquad \text{(IV)}$$

where I_d is the incident current density and δ has the attributes of a range; i.e., when $x = \delta$, the beam

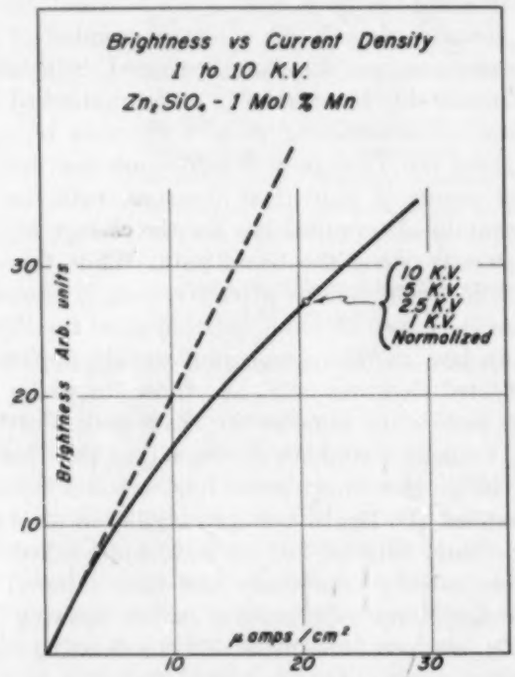

FIG. 1. The saturation is independent of accelerating voltage between 1 and 10 kv.

energy has dropped to some definite fraction of its initial value. $f(x/\delta)$ must, of course, have the characteristic that it reduces to unity when $x = 0$. If now we require that $\delta = KV_o$, we have from equation (IV),

$$dE/dx = \frac{I_d}{K} f'(x/KV_o). \qquad \text{(V)}$$

This expression has the desired properties. For example, if we double V_o, dE/dx in an element dx at depth x for the original voltage will have the same value as in an element $2dx$ at depth $2x$ for the doubled voltage. The two elements will thus saturate alike and since the argument holds for any two corresponding elements, the saturation for the entire path will be the same in the two cases.

The possibility of a range which varies with first power of the voltage (i.e., $\delta = KV_o$, see also section VIII-3) is not in agreement with the accepted relationship in which the range varies with the square, i.e., the Thompson-Whiddington law (6). However, we are speaking of voltages below 10 kv, whereas the square relationship has been derived theoretically and verified experimentally only for considerably higher voltages. We do not believe there is necessarily any conflict. A linear variation of range with voltage below 10 kv necessarily means that, below 10 kv, the range will be greater than predicted by extrapolation of higher voltage data by means of the square law. Supporting evidence for this viewpoint has been found by Diemer and Jonker (7). Others have also questioned the validity of the Thompson-Whiddington law at lower voltages (8–10). Other possibilities which might account for the independence of saturation and applied voltage have been considered by us, but the above seems to us to offer the best explanation of this as well as other cathodoluminescent phenomena below about 10 kv.

III. General Experimental Techniques

Measurements were made in a demountable tube, using ground glass joints sealed with Apiezon W. Phosphor samples about 1 in. in diameter could be moved successively before a fused silica window where they could be bombarded with electrons from an electrostatically focussed gun whose axis was at 45° to the surface of the samples. The gun was provided with a tantalum filament and allowed us to obtain sharply defined spots with uniform current density, so that actual current densities were easy to calculate. Direct light from the filament was never enough to interfere with the measurements. The second anode was divided into two parts insulated from one another. The first part, in the vicinity of the electron gun, was maintained 90 volts negative to the second part, which surrounded the phosphor sample. By dividing the second anode in this way, inclusion in the measurements of stray electrons directly from the gun was minimized. Preliminary measurements by means of a Faraday cage in place of the sample assured us that the current into the sample was actually equal to the current measured into the second part. The tube was evacuated by means of a high speed mercury diffusion pump with liquid nitrogen trap and vacuum connections of as low impedance as practicable. While measurements were being made, the ionization gauge immediately at the tube read about 10^{-6} mm. The whole tube could not, of course, be baked out. However, the gun was always outgassed before each run, by means of high frequency heating, and the samples themselves could be moved into a region of the tube where

they could be baked out. A number of experiments indicated that, for our purpose,[3] nothing was gained by the latter procedure. Care was always taken to see that results were not falsified by fatigue of the phosphors during a series of measurements.

Whenever the energy in the electron beam was to be low throughout a series of measurements, the samples consisted of loose powder packed in aluminum trays without binder. If the beam energy was to be high, the samples were settled in a thin layer of measured thickness on aluminum disks, using water-alcohol-ethyl silicate settling solution so as to obtain colloidal silica as a binding agent in a more or less standard way. Except for a slight shift in the intercept of the brightness-voltage curve (section IV), no effect of the binder could be detected. Considerable attention was paid to the possibility that heating effects from the electron bombardment were falsifying the results. In doubtful cases estimates of the surface temperature of the phosphor were made by substituting for it a phosphor whose decay or color changed with temperature in a predetermined manner. Occasionally measurements were made on settled powder samples or single crystals which had been aluminized in the standard way, the aluminum thickness being determined chemically. Light measurements in the case of nonaluminized samples were always made from the bombarded side. Except in a few instances, the effect of particle size was not investigated. Since for most of our experiments, the range of the electron beam in the phosphor was less than about 0.6 μ (accelerating voltages usually less than 10 kv, see section VIII-3) our particles were coarse enough to ensure that the beam did not completely penetrate the surface grains to any significant extent. A photomultiplier tube was used for light measurements, a single stage d-c amplifier being frequently used to give an improvement of about 300 in the sensitivity. Care was taken to ensure linearity of the combination.

We believe the conductivity of a powdered phosphor sample, held in a metal tray or settled on a metal disk connected to the second anode, is usually sufficient to maintain the screen potential within a few volts of the second anode potential, even when the latter is considerably above the "sticking potential." For a sample well-insulated from the second anode, the screen potential rapidly becomes negative with respect to the second anode as the sticking potential is exceeded. This is evidenced in Fig. 5, curve B. All our results on nonaluminized samples are consistent when interpreted on the basis of these ideas and fit together well with our results on aluminized powdered samples and aluminized single crystals where there is no possibility of surface charging. We, therefore, usually accepted the measured second anode potential as the actual screen potential.

[3] It should perhaps be emphasized that our primary purpose was to measure the cathodoluminescence characteristics of a material rather than its secondary emission characteristics. If the latter had been our purpose, vacuum conditions would have been much more important.

IV. Brightness vs. Accelerating Voltage. The Dead Layer

In view of the rather unsatisfactory state of the literature on the subject (11), we have spent considerable effort in experimental determination of the brightness-voltage relation. For a given set of observations, the current was fixed at a low value (1 μa/cm^2) in order to avoid saturation effects.

Except for obvious deviations due to secondary emission failure (Fig. 5, curve B), the experiments indicate that the brightness increases linearly with accelerating voltage. For a variety of phosphor powders (those tested included ZnS—Ag, Zn_2SiO_4—Mn, $CaMg(SiO_3)_2$—Ti, $CaWO_4$) the straight line so determined had an intercept on the voltage axis in the approximate range 1 to 2 kv. This intercept has been referred to as the "extrapolated dead voltage" (12). Our experiments show it to be independent of temperature between liquid nitrogen and room temperature and independent of current density. Single crystals of $CaWO_4$[4] and $CdWO_4$[4] give results similar to these on powders. Experiments on aluminized samples were carried to 35 kv and no reason was found for believing that, as long as the sample is thick enough, the relation between brightness and voltage is not essentially linear and that therefore, except for saturation effects, the cathodoluminescent process is essentially one in which the emitted radiant energy is directly proportional to the energy absorbed from the electron beam. This conclusion is consistent with the assumption that Q is independent of E and x. Fig. 2 shows the behavior of nonaluminized $CaMg(SiO_3)_2$—Ti up to 20 kv.

If the principal relationship between brightness and voltage is linear, then the "toe" of the actual B vs. V_0 curve must be due to special circumstances. The most obvious of these, and one that was suggested early in the history of the study of phosphors (13), is that the properties of the surfaces are different from those obtaining in the interior of the phosphor crystals with the result that there is an inactive surface layer. At first sight, it would seem reasonable to expect that a more or less continuous gradient of activator efficiency might exist through such a layer, thus accounting for the toe of the B vs. V_0 curve. However, measurements of the spectral distribution and decay characteristics at low

[4] Obtained from Linde Air Products Company.

voltages, within the toe, show no change from what is obtained at higher voltages. These characteristics might be expected to be rather sensitive to the surroundings in which an activator finds itself and it therefore seems that the activators responsible for the light in the toe must be in the same surroundings as those responsible for the light at higher voltages and that they are not located within the inactive layer. We are thus led to consider the inactive layer as a rather sharply defined dead layer within which the activator ions are completely nonluminescent.

If this picture is correct, the question arises as to how any light can be emitted at voltages below about 1 kv, the average energy which the dead layer is

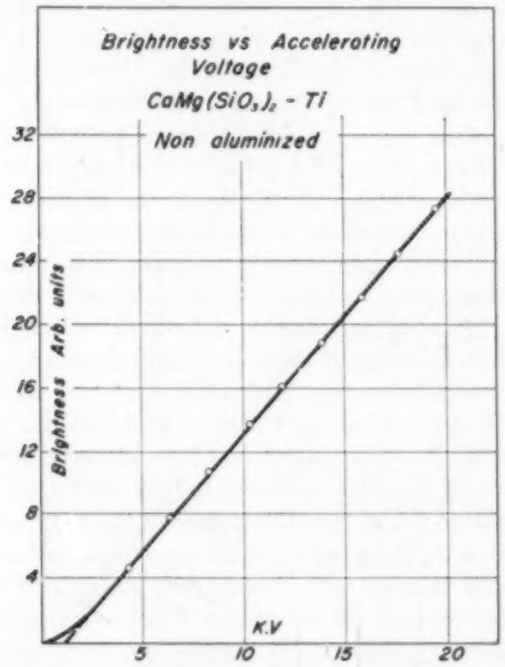

FIG. 2. The principal relationship between brightness and accelerating voltage is a linear one. Powder packed in metal tray.

able to absorb from, say, a 5 kv electron. Actually light has been observed when phosphors are bombarded with electrons whose energy is of the order of 10 volts (14). The answer to this question lies in the specific form of the E vs. x curve.

V. Specific Form for the Relationship between E and x

Using a step by step constructional method, it is possible to infer from the experimental curve for B vs. V_o, measured at a low current density where saturation is not appreciably involved,[1] an empirical curve showing the relation between E and x. The following assumptions are made:

1. E has the general form $E = I_d V_o f(x/\delta)$.

2. $\delta = KV_o$.

3. There is a sharply defined dead layer at the surface of the phosphor crystal which has negligible fluorescent efficiency but has the same energy absorbing characteristics for the primary electron beam as does the body of the crystal.

4. The emitted light is directly proportional to the power remaining in the electron beam after it has passed through the dead layer.

5. The activator concentration is uniform.

The construction of the E vs. x curve proceeds as follows. First, the experimental B vs. V_o curve is plotted as a B vs. E_o curve for a given current density, as in Fig. 3*a*, by multiplying each of the abscissas by the given current density. This B vs. E_o curve is for use in the construction only, and must not be taken to mean that B is a function of E_o alone. Now from assumptions 1 and 2 it will be seen that $(dE/dx)_o$, i.e., at the surface where $x = 0$, is independent of V_o. Hence for sufficiently high voltages, where the thickness of the dead layer is small compared to the total penetration, the energy lost in the dead layer does not vary with V_o. Together with assumption 4, this line of reasoning leads us to draw as a straight line the curve between brightness and the power remaining after the beam has penetrated the dead layer. This line passes through the origin and is parallel to the linear portion of the B vs. E_o curve (Fig. 3*a*). It is, of course, independent of the current density for which the B vs. E_o curve was drawn and along this line B is a function of beam power alone (I_d so low as to avoid saturation). As an example of the construction, three points are shown in Fig. 3*a* for the three incident voltages V_o', V_o'', and V_o'''. The corresponding beam powers after the beam has penetrated the dead layer are E', E'', and E'''.

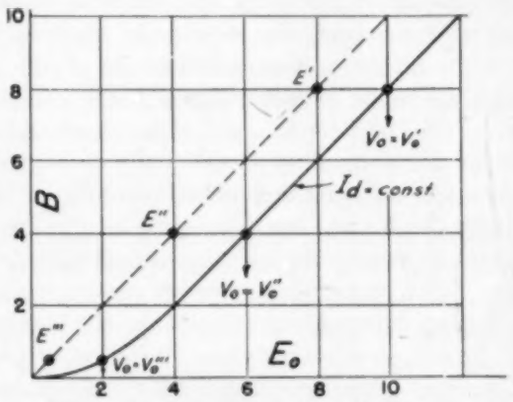

FIG. 3*a*. The method of constructing the E vs. x curves. Full line: measured brightness vs. incident beam energy for nonaluminized sample; dotted line: deduced variation of brightness with beam energy remaining after penetration of dead layer.

In Fig. 3*b* are shown three possible E vs. x curves for the three incident voltages of Fig. 3*a*. The dead

layer is arbitrarily taken as being of unit thickness. On these curves, the only points known at the start are the values of E at $x = 0$ and $x = 1$, as taken from Fig. 3*a*. However by assumptions 1 and 2, there is a one to one correspondence between the points of these curves such that, for example, the following relationships hold,

$$E_{(V_{O'},\,x)} = \frac{V_{O'}}{V_{O''}} \cdot E_{(V_{O''},\,x_d)}$$
$$x = \frac{V_{O'}}{V_{O''}} \cdot x_d \qquad \text{(VI)}$$

where x_d is the thickness of the dead layer,—unity in Fig. 3*b*. The coordinates of points 3 and 4, on the curve for $E_o = 10$, are computed from those of E'' and E''' by means of relations (VI). In a similar

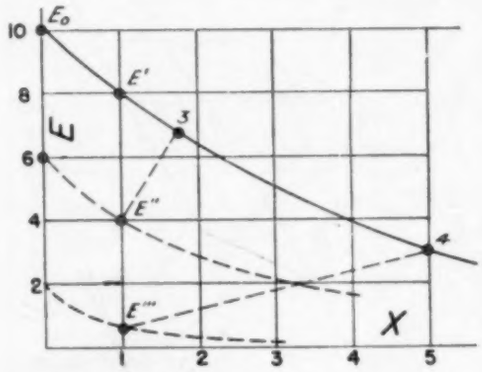

FIG. 3*b*. The method of constructing the E vs. x curves. Full line: the E vs. x curve under construction; dotted lines: representative E vs. x curves for voltages V_o'' and V_o''', respectively.

way the entire curve for $E_o = 10$ can be constructed. We have thus used the dead layer as a sort of thin film within which we have measured the loss of energy of the primary beam at various applied voltages.

It is evident from Fig. 3*b* that, as far as making the current saturation independent of voltage, assumption 3 is antagonistic to assumptions 1 and 2. Thus, for example, the luminescent segment of the beam path between the symbols E' and 3 corresponds to no luminescent segment in the uppermost dotted beam path. Therefore, unless the E vs. x relation is linear, the two paths cannot saturate alike. We are thus in the position of obtaining a clue to the E vs. x relation through the independence of saturation and voltage and then introducing a modifying factor in the shape of the dead layer. We may expect, then, to come out finally with an expression for the fluorescent brightness which makes the saturation a function of voltage but which may, in voltage ranges where E varies approximately linearly with x throughout a distance into the crystal somewhat greater than the dead layer, make the saturation substantially independent of voltage.

Fig. 4 shows the results of the construction for Zn_2SiO_4—Mn. The beam power falls off linearly for a short distance and then becomes exponential in x. In another case we have calculated, the linear portion is relatively longer than as shown here so that we cannot claim that the exponential law holds closely for all phosphors. However, the exponential-like character of the E vs. x curve has important consequences and in the following, we will proceed on the basis that E is actually the exponential

$$E = I_d V_o \, e^{-x/KV_o}. \qquad \text{(VII)}$$

Because of the method of its derivation, equation (VII) with K = constant really applies to the voltage range where saturation is substantially inde-

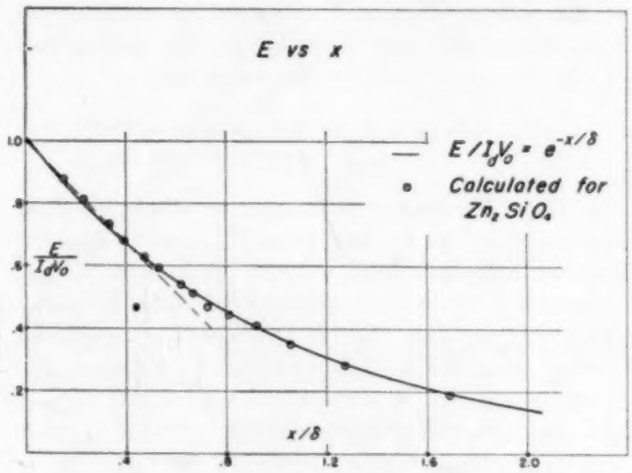

FIG. 4. The constructed E vs. x curve compared to an actual exponential.

pendent of voltage. It is likely, however, that the exponential-like character of the E vs. x curves extends to other voltage ranges and that in these other ranges, it is the dependence of K on V_o which changes, i.e., $K = F(V_o)$. Somewhere above 10 kv, K may be expected to increase linearly with V_o (Whiddington law). At very low voltages, of the order of 20 volts, Katz (8) has found exceptionally long electron ranges. Somewhere below 1 kv then, we may expect to find that K actually increases with decreasing voltage. These variations in the dependence of K on V_o must be associated with changes in the probability that a primary electron makes an "ionizing collision" with an atom of the host crystal (15).

VI. The Expression for B in Terms of I_d and V_o

When the exponential form for dE/dx is substituted in equation (III), the latter integrates rigor-

ously[5] over the luminescent path length, x_d to ∞ into the expression

$$B = h\bar{\nu}KV_oNb \log_e\left(1 + \frac{QI_d\tau}{K} e^{-x_d/KV_o}\right) \quad \text{(VIII)}$$

ev/sec cm^2.

If I_d is sufficiently small, so that saturation effects are not encountered, this reduces to

$$B = h\bar{\nu}QI_dV_oNb\tau e^{-x_d/KV_o}. \quad \text{(IX)}$$

In equation (IX), the factor $b\tau = b/(b + \gamma)$ merely represents the fractional number of centers which, in returning to the ground state, result in luminescence. The exponent containing x_d can also be written as $\Delta V/V_o$ where ΔV is the voltage intercept of the linear portion of B vs. V_o curve. (See section VIII-2).

Departures from these equations can be expected to the extent that the E vs. x curves depart from true exponentials and to the extent that our picture of the inactive layer is oversimplified.

VII. Discussion of Equations (VIII) and (IX)

1. $B - V_o$ curve.—A number of observers have found a single power law, $B \sim V_o^n$, for the relation between brightness and voltage up to 8 or 10 kv. Values of n have been reported for different phosphors ranging from 1 to 2.9. Agreement is sometimes lacking, even for the same phosphors, between different observers. When plotted on log-log paper, our own B vs. V_o curves usually can be divided into two voltage ranges within which they fit a power law fairly well, n being higher for the lower voltage range. They are quite similar to Fig. 15 of Ref. (5). Equation (IX) accounts for our experimental curves satisfactorily but will not very well approximate a single power law up to 10 kv. We have not been able entirely satisfactorily to explain the apparent discrepancies in the literature, either on experimental or theoretical grounds.[6] We suggest, however, that the concept of an essentially linear B vs. V_o curve with a variable toe, whose exact shape depends on the vagaries of an inactive surface layer, may offer at least a partial explanation.

[5] For this integration, we make the reasonable assumption that τ and Q are independent of x. τ and Q may be functions of the activator concentration, as long as it does not vary with x, without invalidating the integration.

[6] It is possible in a formal way to account for $B \sim V_o^2$ and current saturation independent of V_o by using equation (III) and assuming (*a*) the range $\sim V_o^2$, (*b*) dE/dx = const., (*c*) no inactive layer, and (*d*) $Q \sim V$ or $Q \sim \sqrt{x}$. Here V is the energy of an undeflected primary electron at point x in the beam path, on the basis of the Whiddington law. Difficulties are encountered in explaining values of n other than 2 in $B \sim V_o^n$, using this approach.

Equation (IX) explains satisfactorily the emission of light at voltages far below 1 kv. Because of the exponential-like tail of the E vs. x curve, even at 10 volts some electrons penetrate the dead layer into the luminescent part of the crystal. Equation (IX) also accounts for the effect of increasing the thickness of the dead layer. When x_d is increased, the intercept of the linear portion of the $B - V_o$ curve moves to higher voltages and the nonlinear part of the curve reaches to higher voltages and higher values of B. This is actually what happens when an artificial dead layer in the form of an aluminum coating is applied to the phosphor. (See Fig. 5.)

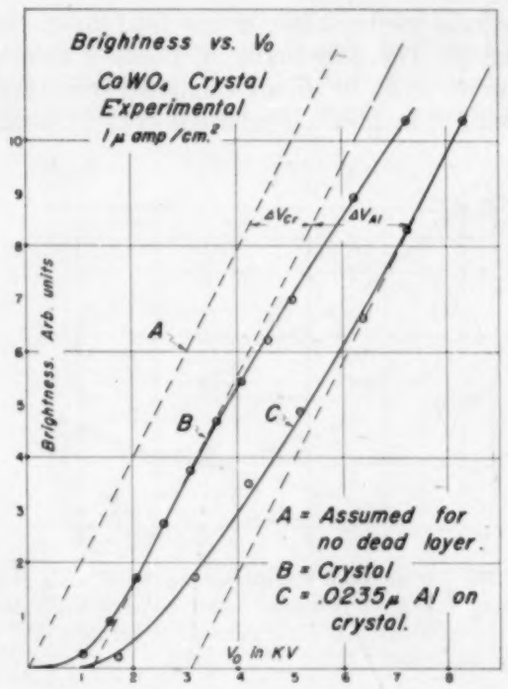

FIG. 5. The method for calculating the range constant, K, and the thickness of the dead layer. Note that the linear portion of the curve for the nonaluminized crystal has been extrapolated (dotted line) to allow for secondary emission failure. The slope for the linear portion of curve C was actually obtained by measurements carried to 30 kv.

2. Saturation as a function of voltage.—As predicted in section V, equation (VIII) contains V_o in the term controlling saturation. Decreasing V_o increases the value of I_d at which saturation effects become important. This is because of the dead layer; as the voltage decreases, an increasingly greater proportion of the light is excited by electrons in the tail of the E vs. x curve where dE/dx and, hence, saturation effects are small. As shown in Fig. 6*a*, drawn from equation (VIII) using values of the constants we have obtained for Zn_2SiO_4 — Mn, this effect is noticeable below 5 kv. This is not entirely in accord with our experiments on nonaluminized samples of Zn_2SiO_4 — 1 mole per cent Mn, where any effect of the dead layer on the constancy

of saturation is not noticeable above 1 kv. We believe this discrepancy arises from an oversimplification in our assumed activator distribution in the surface layers of the crystal and/or from a possible deviation from an exact exponential variation of E with x. Above 5 kv equation (VIII) makes the saturation independent of voltage as required by experiment up to at least 10 kv.

Our best experiments on the saturation of nonaluminized samples did not extend below 1 kv because of difficulties with the electron gun. However, such experiments as we have on nonaluminized samples of Zn_2SiO_4 — Mn at voltages below 1 kv do

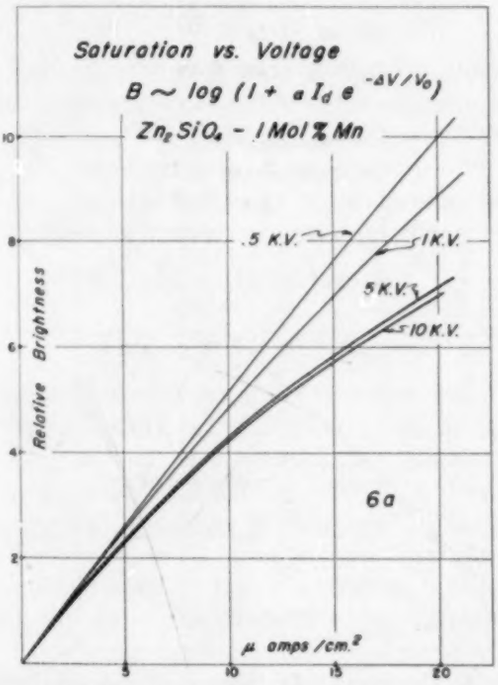

FIG. 6a. Theoretical saturation curves for various voltages for nonaluminized samples, from equation (VIII). The abscissas of both sets of curves are in actual units and the ordinates in arbitrary units, different for the two sets.

indeed show saturation decreasing with decreasing voltage. By aluminizing the sample, the electron gun could be operated at satisfactorily high voltages although the phosphor was energized approximately as it would be if the sample were nonaluminized and the voltage low. Saturation curves taken in this way are shown in Fig. 6*b* and exhibit quite definitely the effects predicted by equation (VIII). We have not worked out the correlation between the voltages of Fig. 6*a* and 6*b* except that at the lowest voltage, the phosphor is quite feebly energized in both cases.

Above 10 kv, of course, equation (VIII) makes saturation independent of voltage. However, the fact that there is so much evidence in the literature that the electron range increases faster than linearly with increasing voltage, somewhere above 10 kv, makes us believe the saturation should begin to decrease at higher voltages. Some of our experiments, not entirely satisfactory, on aluminized samples of normal thickness, indicated that the saturation does decrease with increasing voltage above 10

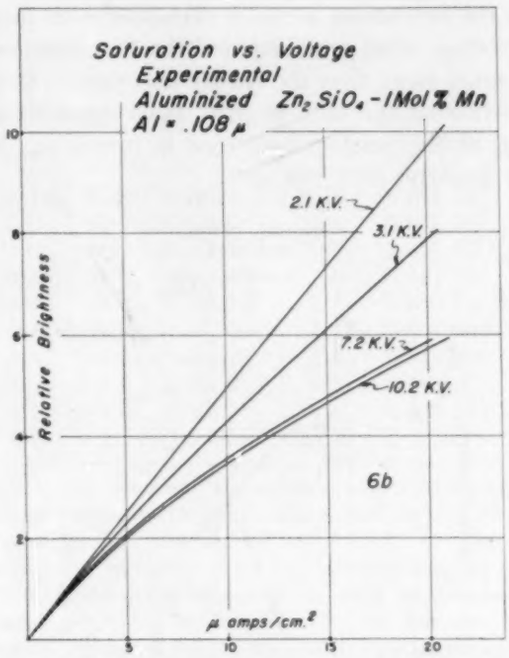

FIG. 6b. Experimental saturation curves for comparison with Fig. 6a. (See section VII-2 of text for the explanation as to why the experimental curves were not made on nonaluminized samples.)

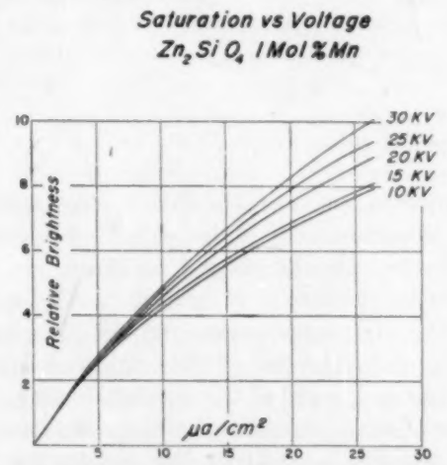

FIG. 7. Saturation as a function of voltage above 10 kv. Effects accentuated by use of a very fine-grained, thin screen; 1.3 mg of powder/in.² Screen settled on aluminum.

kv. The effect will be most pronounced in the case of a thin phosphor layer completely penetrated by the electron beam. This is because the portions of the beam paths corresponding roughly to excitation voltages of 10 kv and less (i.e., toward the ends of the beam paths), where saturation may be considered to be independent of the incident voltage, do not give rise to luminescence. Saturation curves,

taken on a very fine-grained and thin phosphor layer settled on an aluminum disk, are reproduced in Fig. 7 and show a very definite decrease of saturation with increasing voltage at the higher voltages.

Another manifestation of the transition to the square law, for the increase of range with voltage, is found in Fig. 8 (see section VIII-1*b*). The fact that the brightness actually decreases with increasing voltage after penetration of the thin luminescent film must mean that the energy absorbed in the film is decreasing and this, in turn, must mean that the range of the primary electrons is increasing faster than linearly with voltage.

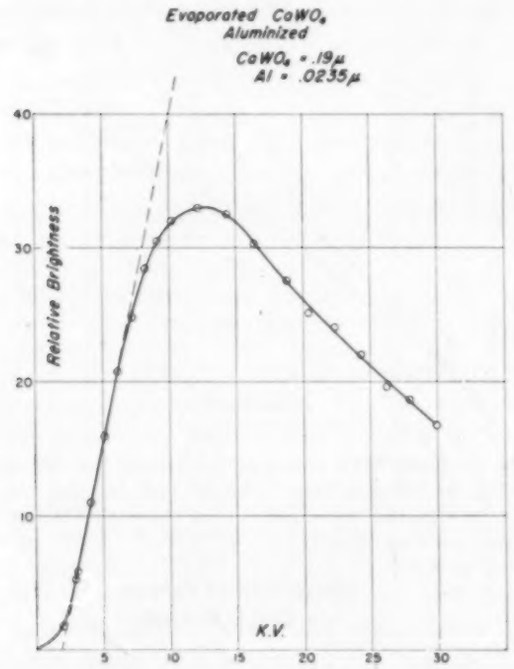

FIG. 8. Brightness vs. accelerating voltage for a very thin phosphor layer.

We hope to return in the future to a more satisfactory determination of the effect of voltage on saturation outside the range 1 to 10 kv.

3. Reciprocal plots of B against I_d.—It has been shown (2), and our experiments are in agreement, that when the reciprocal of the brightness is plotted against the reciprocal of the current density, for an exponential decay phosphor showing saturation when excited steadily, a straight line results for larger values of $1/I_d$. This line intersects the $1/B$ axis, indicating that there is a maximum brightness. However, equation (VIII) has no maximum, the brightness increasing continuously with current density. On the reciprocal plot, this should show up as a departure from linearity, the curve tending toward the origin at sufficiently small values of $1/I_d$.

We have carried measurements of saturation on Zn_2SiO_4 − 1 mole per cent Mn to current densities as high as 130 μa/cm². In order to minimize heating effects, a pulse technique was used in which the "on" period was 0.1 sec and the "off" period 0.9 sec. Since the time constant of this phosphor is about 0.01 sec, this excitation was essentially steady state. Fig. 9 displays experimental points plotted together with a curve showing values calculated from equation (VIII). The expected departure from linearity in the experimental points is not large but we believe it to be real.

VIII. Quantitative Considerations

1. The range constant, K.—In order to use equation (VIII) quantitatively, it is evident that we need a value for K. We have estimated the value of K from two experiments and obtained reasonably con-

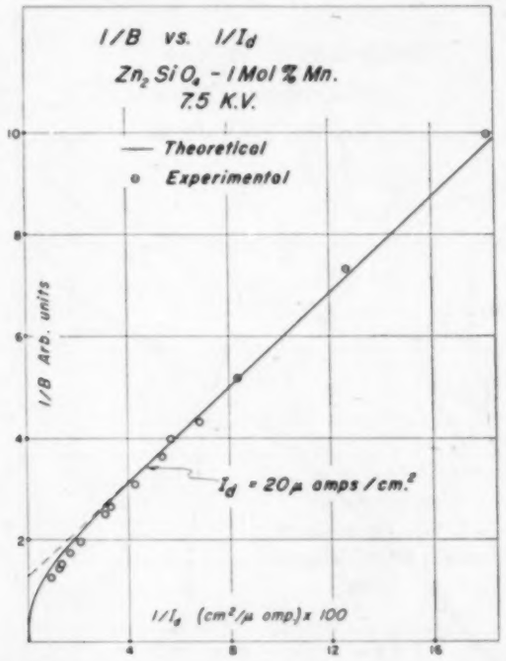

FIG. 9. Comparison of theoretical and experimental reciprocal brightness vs. current density curves. Ordinates are in arbitrary units, abscissas in actual units. The experimental points were normalized to the theoretical curve at an abscissa of 8.3. The arrow indicates the point corresponding to 20 μa/cm².

cordant results. Electron ranges calculated from this value agree reasonably well with published values for aluminum. The two experiments are as follows. (*a*) *The shift in the B vs. V_0 curve, at voltages where it is linear, caused by a thin coat of aluminum applied to the surface of a single crystal of* $CaWO_4$, (*Fig. 5*).—There is experimental evidence (16) that, for a sufficiently thin film, an electron beam maintains its current density; i.e., scattering has not developed to a point where any significant number of electrons are completely stopped within the film. The loss of energy of the beam is thus almost entirely due to ΔV, the average loss in potential of the electrons, nearly all of which completely penetrate the film. This is to say that, for voltages so high that a surface film is thin compared to the total range of the elec-

tron beam, we can write $(dE/dx)_o = I_d \Delta V/\Delta x$, where Δx is the thickness of the film. Now it has already been shown in section V that $(dE/dx)_o$ is independent of V_o. The above argument indicates that ΔV, for sufficiently high voltages, is also independent of V_o and that therefore the effect of any nonluminescent surface film will be to shift the linear portions of the B vs. V_o curve along the voltage axis by the constant amount ΔV. This is the reasoning which leads us to use the intercepts, on the voltage axis, of the curves of Fig. 5 as measuring the losses of potential, ΔV_{Cr} in the inactive layer of the crystal and ΔV_{Al} in the aluminum. Finally, from equation (VII)

$$K = I_d/(dE/dx)_o \cong 1/(\Delta V/\Delta x).$$

In the case of the $CaWO_4$ crystal, the thickness of the aluminum was determined chemically to be 235 Å, yielding the value $(\Delta V_{Al}/\Delta x) = 5.7 \times 10^8$ volts/cm. From results in the literature (6, 16), it seems reasonable to take $\Delta V/\Delta x$ to be proportional to the density, whence

$$K_{CaWO_4} = .79\ 10^{-9}\ \text{cm/volt}$$
$$K_{Zn_2SiO_4} = 1.2\ 10^{-9}\ \text{cm/volt}. \qquad \text{(X)}$$

(*b*) *Complete penetration of a thin evaporated film of luminescent* $CaWO_4$.—Fig. 9 shows[7] that as the accelerating voltage is increased, the brightness of such a film behaves initially exactly as it does for a thick sample. A voltage is soon reached, however, at which the $B - V_o$ curve departs from linearity. This voltage may be taken as that at which electrons just start to pass completely through the layer. In order to prevent distortion of the curve by secondary emission failure, we found it necessary to aluminize the $CaWO_4$ and hence this voltage had to be corrected, along the lines of the preceding section, for the voltage of the beam lost in the aluminum. Both the thickness of the aluminum and that of the $CaWO_4$ were determined chemically. Knowing the thickness of the $CaWO_4$, the voltage at which complete penetration becomes evident, and making the assumption that complete penetration actually becomes evident when the electron beam power has been reduced to about 1 per cent of its initial value; we have calculated from equation (VII) values of K which come out some 30 per cent higher than those shown in (X). Considering the nature of the calculations, we consider this a reasonable agreement. In the following sections, we have used the values of K shown in (X).

2. The thickness of the dead layer.—From the discussion of the preceding section, it is evident that the thickness of the dead layer is given by $K\Delta V$, where ΔV is the intercept on the voltage axis of the linear portion of the $B - V_o$ curve for the unaluminized phosphor. In this way we have found for Zn_2SiO_4 – Mn values ranging from 50 to 250 Å for the dead layer thickness. The thickness depends to some extent upon the activator concentration (see Table I where values of the voltage intercept

TABLE I

Mn mole %	Eff. %	τ sec	ΔV kv	B_8/B_2	Q exc. $\frac{\text{ev}}{\text{cm}^3} \times$ act.	N Mole %	N % of Chem.	$1/QN$ ev/exc.
0.01	0.74	13×10^{-3}	0.5	2.49	6.0×10^{-21}	0.004	41	215
0.05	1.7	13	0.5	2.63	4.6	0.012	24	98
0.1	3.0	13.5	1.1	2.82	3.7	0.027	27	52
0.4	6.3	12.5	1.2	3.11	2.5	0.084	21	25
0.5	6.3	13	1.2	3.14	2.3	0.090	18	26
1.0	6.3	13	1.1	3.16	2.1	0.096	9.6	26
2.0	5.6	10.5	1.2	3.19	2.6	0.074	3.7	28
3.0	5.7	8.0	1.3	3.27	2.9	0.066	2.2	28
5.0	4.7	3.3	1.4	3.51	4.4	0.035	0.70	34
10.0	1.7	0.7	1.9	3.58	20.0	0.0033	0.033	82

Col. 1, the chemical manganese concentration; col. 2, measured values of efficiency (100 × radiated power/electron beam power) at 2/μa/cm² and 4 kv, from which the corresponding values of B are readily calculable in ev/sec cm²; col. 3, measured values of the time constant; col. 4, measured intercepts of the $B - V_o$ curves; col. 5, the measured brightness ratio at 8 and 2/μa/cm² (in the absence of saturation, it would have a value of 4); col. 6, calculated values of the probability constant Q in excitations per ev/cm³ per activator; cols. 7 and 8, calculated values of effective activator concentration in actual mole per cent and in per cent of the chemical concentration; col. 9, calculated values of the fundamental excitation efficiency (in the absence of saturation and dead layer) in ev per excitation.

are given). For the $CaWO_4$ crystal, (Fig. 5), we found a dead layer thickness of 67 Å. These seem to be reasonable values to be accounted for on the basis that the nonuniform surroundings prevent activator ions incorporated in the crystal surface from being luminescent centers.

3. The range of the primary electrons.—As ordinarily used, the range of the primary electron beam refers to that distance at which it has lost all its energy. If the beam energy varies as shown by equation (VII), the range in this sense is infinite. In order to get some idea, however, of what might be measured in an actual experiment, we may arbitrarily say the range is that distance at which the primary beam is reduced to 1 per cent of its initial value. Equation (VII) then gives for the range, $r = 4.6\ KV_o$. Using the value of K from (X), this gives a value of 0.55 μ at 10 kv for Zn_2SiO_4. One might expect that this should agree fairly well with the values found experimentally for aluminum at higher voltages when they are corrected for density and figured to 10 kv by means of the square law. Using Terrill's

[7] Similar curves have been reported by Studer, *et al.* (17).

experimental values (6), a value of 0.6 μ is obtained in this way for the range in Zn_2SiO_4 at 10 kv, which is as good agreement as can be expected. This agreement may be considered as a check on our values of K.

4. Determination of Q and N.—Equation (VIII) contains two unknown parameters, Q and N. We include N as an unknown since there is always the possibility that not all the activator ions are incorporated at locations where they are effective luminescent centers. Q and N can be determined independently if B is measured for two values of the current density. For at least one of these, the brightness measurement must be in absolute amount, i.e., in ev/sec cm². In order to carry out the calculation, the following series of measurements have been made for each sample of Zn_2SiO_4 – Mn.

(*a*) *The brightness in ev/sec cm² at some one value of I_d and V_o.*—For this purpose, the sample was held in a thick layer in an aluminum tray so that by internal reflection within the layer, most of the generated light was emitted from the side bombarded by the electron beam. The light lost within the sample was estimated at 7 per cent by comparing the reflectivity of the sample with that of the standard reflectance which accompanies a MacBeth illuminator. Because of the thickness of the sample, it was necessary to keep the incident beam power low in order to avoid thermal effects. The beam current for this measurement was usually 2 μa/cm² and the voltage usually between 4 and 8 kv, enough to insure that we were working on the linear part of the $B - V_o$ curve. A Lambert distribution was assumed for the emitted light. For the brightness measurement, the relative spectral distribution was measured and calibrated at one wavelength by a lamp whose emission in ev/sec cm² was known for that wavelength. Planimetering the entire spectral distribution curve then gave the radiant output of the phosphor.

(*b*) *The current saturation curve at the same voltage used in* (*a*).—For this purpose, in order to avoid thermal effects, small settled "screens" were used as described in section III. To determine Q and N, it was not necessary to go above about 10 μa/cm².

(*c*) *The time constant, τ.*—The settled screens were used for this measurement. Although no effects which could be attributed to variations in incident current and voltage, as such, were found, the measurements were made at the current and voltage used in (*a*). Standard techniques were used; the electron beam was cut off with a thyratron and a photomultiplier tube with a d-c cathode ray oscilloscope was used in photographing a trace of the decay curve.

(*d*) *The dissipation constant, γ.*—Sufficient measurements of the sort described by Kröger and Hoogenstraaten (18) were made to satisfy ourselves that this constant had a negligible value within the range of our experiments. The calculations were thus made on the basis that $\tau = 1/b$.

(*e*) *The $B - V_o$ curve.*—This was taken on thick samples in aluminum trays at a low current density, usually 1 μa/cm². The purpose was to determine the thickness of the dead layer, $x_d = K \cdot \Delta V$.

(*f*) The value of K as given by (X) was used for the calculations and was taken to be independent of the activator concentration.

(*g*) The value of $h\bar{\nu}$ was obtained from the spectral distribution curve.

Having the preceding results, the calculations proceed as follows. The ratio, R, of the brightness at 8 μa/cm² and at 2 μa/cm² is given by equation (VIII) as

$$R = B_8/B_2 = \frac{\log(1 + 4\alpha)}{\log(1 + \alpha)} \qquad \text{(XI)}$$

where

$$\alpha = \frac{1.26 \cdot 10^{13} Q e^{-\Delta V/V_O}}{K}. \qquad \text{(XII)}$$

Here the numerical factor is the current density (2 μa/cm²) expressed in electrons per sec per cm². R is determined experimentally from the saturation curve (*b*) and the corresponding value of α is read from a plot of R against α as given by (XI). Q is then calculated from (XII).

N is now calculated from (VIII), using this value of Q and the experimental value of B found in (*a*),

$$N = B/h\bar{\nu}KV_o b \log(1 + \alpha). \qquad \text{(XIII)}$$

We have determined Q and N in this way for a number of different samples of Zn_2SiO_4 – Mn containing various amounts of manganese. The results are shown in Table I. Some difficulty was experienced in obtaining reproducible results, due principally to the saturation measurement. A small variation in the experimental value of R produces a large change in the calculated value of α, and great care must be taken in measuring the saturation. Thermal effects are particularly disturbing. Each row in Table I is the result of several determinations of each measured quantity and in most cases involves more than one sample of a given manganese content. Although some inconsistency is evident, Table I does show certain definite trends.

IX. Discussion of Table I

Our experimental results on efficiency and time constant are quite in accord with results already published. The results on the intercept of the $B - V_o$ curve and some of those on saturation may be new. The intercept is quite small for very low Mn concentration; at 0.1 mole per cent it becomes practically constant at a higher level until, at about 3 mole per cent, it starts to increase again. The saturation, as evidenced by column five, decreases steadily with increasing Mn content.

Q is undoubtedly rather strongly dependent on the

activator concentration, passing through a minimum at about 1 mole per cent. It is this dependence, together with the variation in the time constant, which determines the variation of saturation with activator concentration. The effective activator concentration varies in a way opposite to Q, passing through a maximum at about 1 mole per cent; adding manganese above this value actually results in a decrease in effective centers. Since Q and N vary in opposite ways, the excitation efficiency, which is determined by the product of the two, is not subject to such wide variations. The percentage of Mn ions actually present which form effective centers falls off with increasing total Mn content, rapidly at first and then more slowly. At 10 mole per cent, it is only 0.033 per cent. At the moment we have no certain explanation for the fact that the calculations show only 41 per cent of the activator ions to be effective at very low Mn concentrations. Values nearer 100 per cent would seem more reasonable.

The calculations for Q are capable of yielding estimates of activator collision cross sections and the loss in energy of the primary electrons per "ionization" of the ions of the host lattice. Those for N can be analyzed in terms of interacting activator ions, in the manner used by Johnson and Williams (19). These extensions are, however, beyond the scope of the present paper.

Acknowledgments

We should like to acknowledge very helpful discussions with Dr. O. S. Duffendack of this laboratory and with Dr. A. Bril of the Philips Laboratories in Eindhoven. We are also very much indebted to Dr. N. C. Jamison of this laboratory for developing the techniques involved in making luminescent films of $CaWO_4$ by evaporation and for preparing the actual samples.

Any discussion of this paper will appear in a Discussion Section, to be published in the December 1953 issue of the Journal.

References

1. W. Lang, *Optik*, **3**, 233 (1948); H. Geiger, *Handb. d. Phys.*, **22 Pt. 2**, 56 (1933).
2. R. B. Nelson, R. P. Johnson, and W. B. Nottingham, *J. Applied Phys.*, **10**, 335 (1939); A. Bril, *Physica*, **15**, 361 (1949).
3. H. A. Bethe, *Ann. Physik*, **5**, 325 (1930); N. Bohr, *Phil. Mag.*, **30**, 581 (1915).
4. H. W. Leverenz, "Luminescence of Solids," p. 156, John Wiley & Sons, Inc., New York (1950).
5. W. B. Nottingham, *J. Applied Phys.*, **8**, 762 (1937).
6. H. M. Terrill, *Phys. Rev.*, **22**, 101 (1923); **24**, 616 (1924).
7. G. Diemer and J. L. H. Jonker, *Philips Research Repts.*, **5**, 161 (1950).
8. H. Katz, *Z. tech. Physik*, **18**, 555 (1937).
9. J. W. Strange and S. T. Henderson, Ref. (11).
10. U. Fano, *Phys. Rev.*, **58**, 544 (1940).
11. P. Lenard, *Ann. Physik*, **12**, 449 (1903); I. G. Maloff and D. W. Epstein, "Electron Optics in Television," p. 219, McGraw-Hill Book Co., Inc., New York (1938); W. B. Nottingham, *J. Applied Phys.*, **10**, 73 (1939); S. T. Martin and L. B. Headrick, *J. Applied Phys.*, **10**, 116 (1939); J. W. Strange and S. T. Henderson, *Proc. Phys. Soc. (London)*, **58**, 383, 392 (1946); Ref. (4), p. 441 ff.
12. Ref. (4), p. 319.
13. P. Lenard, Ref. (11).
14. H. W. Leverenz, *J. Optical Soc. Am.*, **27**, 25 (1937).
15. A. H. Compton and S. K. Allison, "X-rays in Theory and Experiment," p. 69, D. Van Nostrand Co., Inc., New York (1935).
16. B. F. J. Schonland, *Proc. Roy. Soc. (London)*, **A54**, 235 (1923); **58**, 187 (1925).
17. F. J. Studer, D. A. Cusano, and A. H. Young, *J. Optical Soc. Am.*, **41**, 559 (1951); L. R. Koller and E. D. Alden, *Phys. Rev.*, **83**, 684 (1951).
18. F. A. Kröger and W. Hoogenstraaten, *Physica*, **14**, 425 (1948).
19. P. D. Johnson and F. E. Williams, *J. Chem. Phys.*, **18**, 1477 (1950).

Electrical Measurements on Electroluminescent Lamps with Zinc Sulfide Phosphors[1]

C. W. Jerome and W. C. Gungle

Sylvania Electric Products, Inc., Salem, Massachusetts

ABSTRACT

The electrical characteristics and light output of electroluminescent lamps made with zinc sulfide phosphors are described as affected by voltage and frequency. On the basis of these measurements, analogous circuits are derived which have electrical characteristics similar to those of the electroluminescent lamps.

Introduction

The present electroluminescent lamp has been described as a "luminous condenser." This is probably as descriptive a term from an electrical point of view as can be assigned to this lamp. Since the primary function of such a device is to give light, one of the purposes of measurements of the electrical characteristics of the lamp is to determine their effect on light output. Another, and equally important, purpose is to add to the over-all understanding of the phenomenon of electroluminescence and thereby assist in the development of a reasonable explanation of its operation.

The measurements described herein are applicable to lamps containing zinc sulfide phosphors activated by copper and lead. The phosphors occupy approximately 50 per cent by volume of a wide variety of film-forming dielectric media such as nitro- and ethylcellulose, synthetic plastics, oils, and resins. Changes in the type and percentage of the constituents of the light-producing film will change the magnitude of either or both of the parameters of the various relationships described, without seriously affecting the type of behavior shown.

A partial list of references to other articles pertaining to the phenomenon of electroluminescence is given in the References.

Lamp Operation

Electroluminescence is excited by placing the phosphor, embedded in a suitable dielectric medium, between the two plates of a condenser and impressing a varying field. One plate of the condenser of the electroluminescent lamp is transparent to allow the escape of the generated light. The varying field is necessary. When a d-c field is applied, there is a momentary flash of light while the condenser is being charged. Another flash of light is obtained if the lamp is subsequently discharged through an external resistance. Therefore, it appears that light is generated only when the field across the phosphor-dielectric layer is changing. This can be illustrated by oscilloscope traces of light, voltage, and current of the lamp when a square wave voltage is impressed as shown in Fig. 1.

It will be noted that the light emission occurs chiefly during the period when the voltage is changing. Presumably, if the voltage source used for these traces imparted a more perfect square wave voltage, the light curve would be narrower and would decrease more nearly to zero between flashes. However, the peak would have a finite width because there is a certain decay time involved which will be mentioned later.

Light Output and Maintenance

With a sinusoidal voltage, the light output varies approximately exponentially with the rms value of the voltage as shown for one type of lamp in Fig. 2. This figure should not necessarily be construed as indicating a threshold voltage for light output. Measurable light output on this lamp has been measured down to very low voltages. However, on the scale of Fig. 2, the values below 150 v are insignificant. The maintenance of light output during life for the same type of lamp is shown in Fig. 3. This lamp is one of the poorer types as far as maintenance and efficiency are concerned, but has been chosen for most of the measurements described herein since it illustrates the relationships between the several variables better than some of the other types. The interesting point shown in Fig. 3 is that most of the light deterioration occurs in the first thousand hours of life. After two or three thousand hours of life, a static situation seems to be reached after which any variation in light output is extremely small. This last statement is based on a large quantity of maintenance data on several different types of lamp over ranges up to 13,000 hours of burning time.

[1] Manuscript received April 29, 1952. This paper prepared for presentation before the Philadelphia Meeting, May 4 to 8, 1952.

all of which show essentially the same type of behavior.

Light-Power Relationship

It is to be expected that the brightness of these lamps depends on the power they absorb. The relationship between these two variables for the sample lamp is shown in Fig. 4. The two curves are the

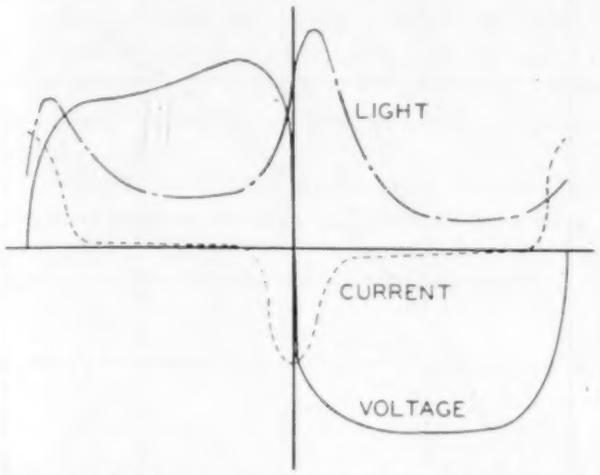

Fig. 1. Light and current wave forms with square-wave voltage.

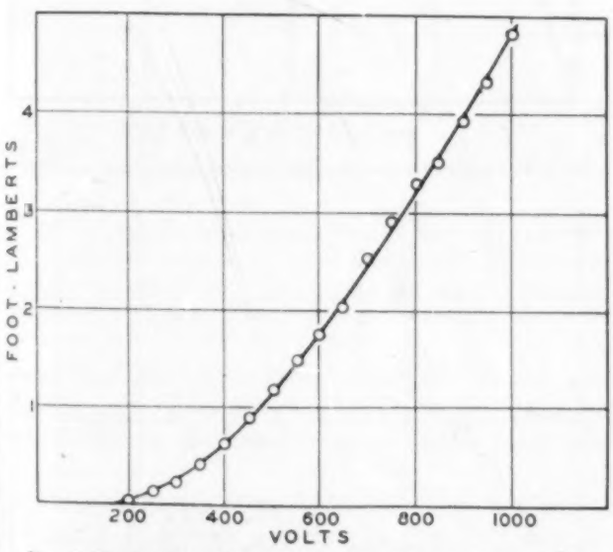

Fig. 2. Variation of light intensity with applied voltage

initial and 2500-hour values of the life test shown in Fig. 3. The interesting point of this figure is the intercept on the power axis. This is attributed to power lost in the dielectric, and its increase with life indicates an increasing loss of power in the dielectric as the lamp burns.

This raises the question of how this picture looks when the power absorbed by the phosphor is the abscissa instead of the total power absorbed by the phosphor plus dielectric. The electroluminescent lamps have been likened to a condenser and the power dissipated in a condenser is given by the square of the voltage divided by the resistive component of the impedance, provided that the equivalent resistance is considered as being in parallel with the capacitance. The equivalent shunt-resistance can be computed from the capacity and phase angle of the condenser. The capacity of electroluminescent lamps can be measured on a suitable bridge, and the phase angle can be computed from the ratio of power

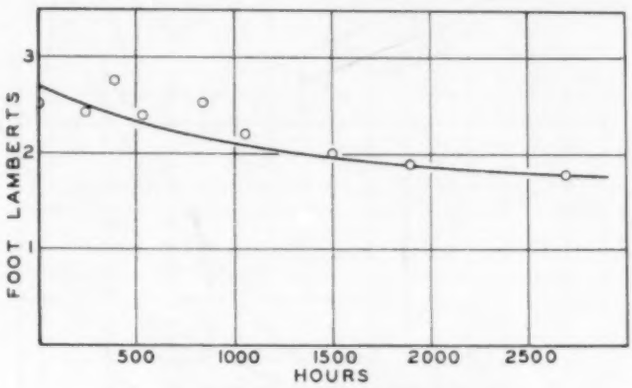

Fig. 3. Brightness maintenance curve

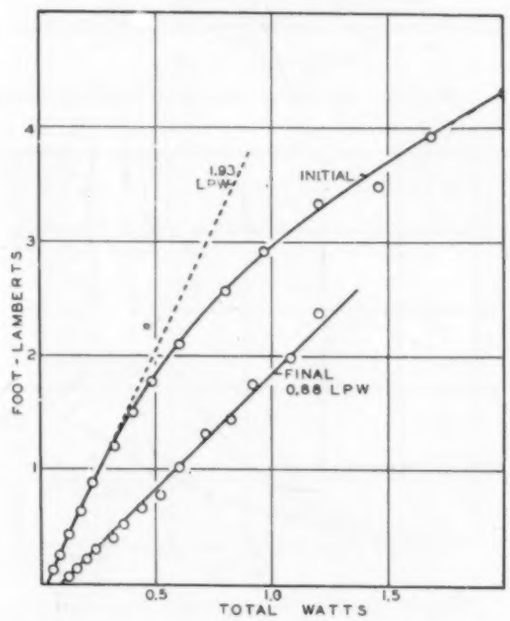

Fig. 4. Dependency of brightness on power absorbed

consumed (measured on a wattmeter) to the product of voltage and current. Therefore, an equivalent resistance for these lamps can be computed.

Dielectric Power Factor

However, it has been found that the power factor of any of these lamps is not a constant for all voltages as it would be for a true condenser. This behavior can be accounted for most simply by the assumption of nonohmic characteristics for a part of the resistive component of the lamp impedance. In view

of its other characteristics, the nonohmic property is assigned to the phosphor.

The variation of power factor with voltage for three lamps of different shapes and sizes is shown in Fig. 5. As can be seen, the shape of these curves is a function of the dimensions of the lamp.

To eliminate the variable imparted by the phosphor, the power factor curve is extrapolated back to zero volts. At this point there is no current flowing and, therefore, the discrepancy caused by

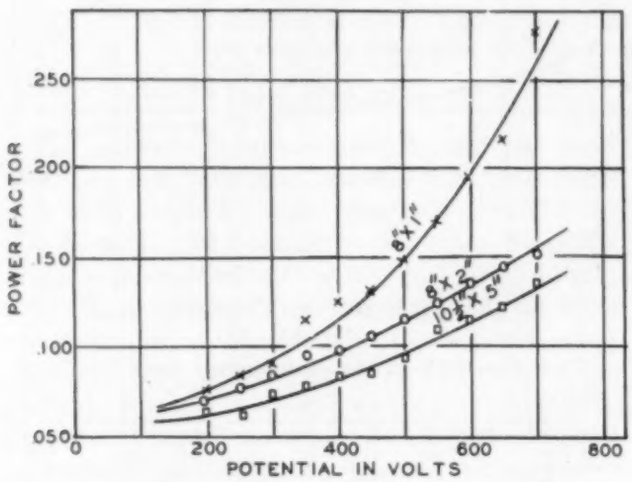

FIG. 5. Variation of power factor with applied voltage

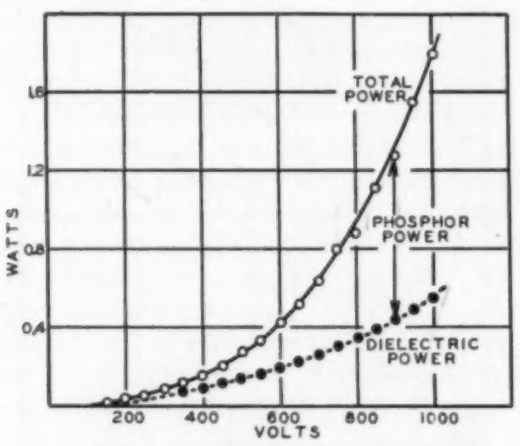

FIG. 6. Derivation of phosphor power

the phosphor will be eliminated and the resulting power factor, ϕ_0, will be that of the dielectric alone. That this is a valid assumption is supported by an experiment in which a lamp without phosphor is compared to a similar lamp with phosphor. The former has a power factor independent of voltage, of a magnitude the same as obtained for the latter by extrapolating its power factor curve back to zero volts. This is the value of the power factor that has been used in computing the resistance of the lamp for purposes of deriving the power absorbed by the dielectric. Subtracting the dielectric power loss from the total power input gives a measure of the power absorbed by the phosphor. This is shown in Fig. 6.

LIGHT VS. PHOSPHOR POWER

When light output is plotted as a function of phosphor power, the results shown in Fig. 7 are

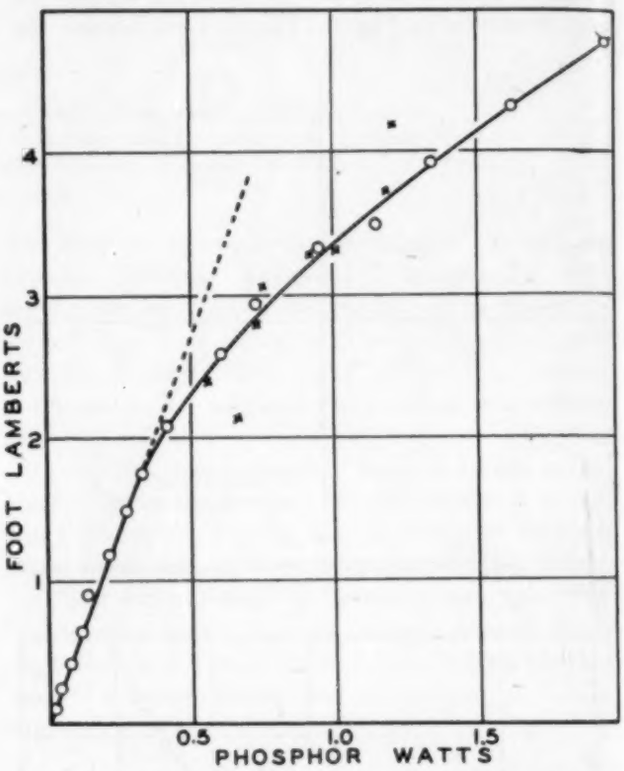

FIG. 7. Dependency of brightness on phosphor power

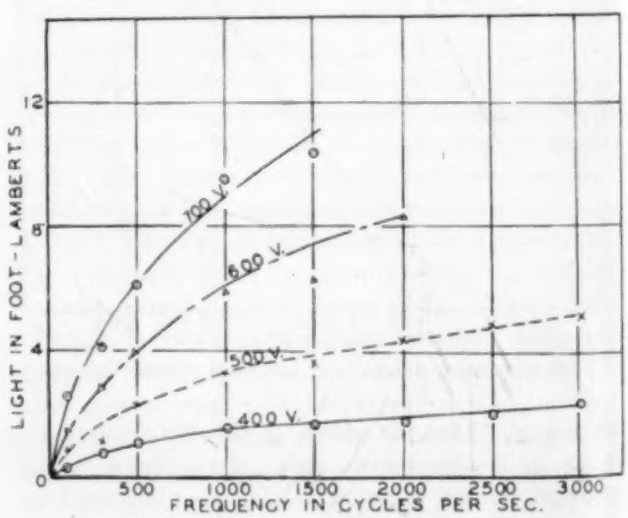

FIG. 8. Variation of brightness with frequency

obtained. This curve, it will be noted, passes through the origin, that is, no light is produced unless power is absorbed.

In Fig. 7, the curve and open circles are for the initial readings on the life test shown in Fig. 3. The crosses are the terminal points for the corresponding curves for the readings at the various points during

that life test. It is apparent that the crosses fall in a gun-shot pattern that is reasonably well represented by the initial line. This is taken as evidence that the efficiency of the phosphor does not depreciate with time. Consequently, the decay of light output observed is almost wholly due to the increase in power loss in the dielectric.

Effect of Frequency

Up to this point, the discussion has been confined largely to measurements at 60 cycles per second. Some of the results shown will apply equally well to higher frequencies; others will vary with frequency.

The variation of light output with frequency for the lamp used in the previous discussions is shown in Fig. 8. Brightness increases rapidly with frequency at low frequencies, but then appears to

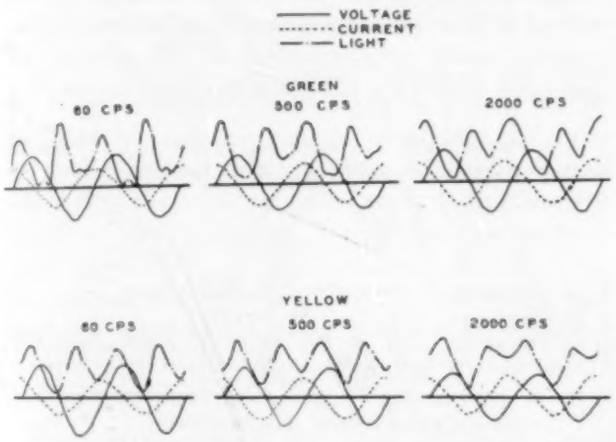

Fig. 9. Oscilloscope traces of voltage, current, and light. (These curves were traced from oscilloscope photographs on each of which only two traces appeared. Therefore, the phase relationships shown are not necessarily exact.)

saturate. There is in addition a shift toward blue in the color of green lamps as the frequency increases, which will be discussed in more detail in a later paper.

The explanation of the behavior shown here might be made clearer by reference to Fig. 9. These are oscilloscope traces of voltage, current, and light intensity in their approximate phase. Only curves for green and yellow lamps are shown. Those of blue lamps are, for all intents and purposes, identical with those of the green.

The leading phase angle of the current can be seen. The light intensity repeats itself every half cycle. The inequality of adjacent half cycles is probably due to lack of symmetry in the phosphor crystals. In the green lamp, the light in each half cycle consists of a major and a minor peak. It was thought that each of these peaks might be related to one of the energy bands of which these emissions are composed and which will be discussed in a later paper. However, as nearly as could be determined with filters over the pickup tube, the spectral composition of each of these peaks is the same. Another explanation of these peaks is in regard to the instantaneous power. It will be noticed that the major

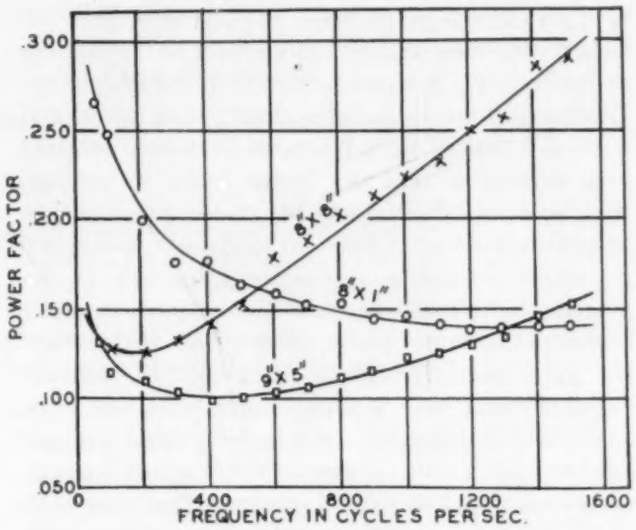

Fig. 10. Variation of power factor with frequency

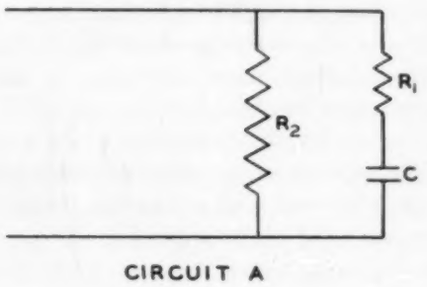

CIRCUIT A

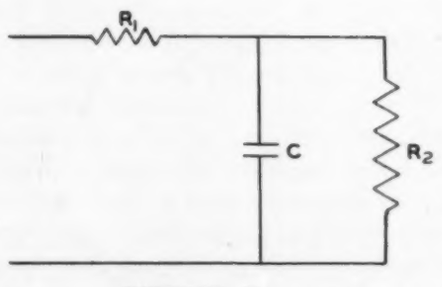

CIRCUIT B

Fig. 11. Equivalent circuit of electroluminescent lamp

peak occurs when the voltage and current are in the same direction, that is, when power is being absorbed by the lamp. The minor peak occurs when the voltage and current are in opposite directions, that is, when power is being released by the lamp back into the circuit.

As the frequency increases, two changes take place: (*a*) the number of flashes of light per second increases,

and (*b*) the power consumed by the lamp increases. The second of these changes induces an increase in the light intensity in keeping with the discussion on power earlier in this paper.

The eye, or a photocell, is an averaging instrument. At frequencies low enough so that each flash of light decreases to zero, the average light intensity will vary in direct proportion to the number of flashes, i.e., it is proportional to the frequency. However, there is a finite decay time associated with each flash of light. When the frequency becomes high enough so that the flashes begin to overlap, that is, a new flash starts before the previous one has entirely decayed, then an increase in frequency no longer imparts a proportional increase in the average light intensity and the saturation effect begins to show up. Finally, at very high frequencies, the light intensity will be essentially of constant value showing only a slight ripple from one peak to the next. In this range, any increase in the average light intensity will be due to the increased power associated with the higher frequency. The beginnings of this behavior are shown in the green curves where at 2000 cycles the decay of each peak is not quite completed when the next one begins.

The absence of a minor peak in the yellow emission at 60 cycles per second is taken to indicate a longer decay time for this phosphor. It will be noted that the curves for this phosphor at 60 cycles are very similar to those of the green at 2000 cycles and the changes observed with increasing frequency are in keeping with the above remarks.

The derivation of the power factor for the dielectric alone, ϕ_0, has been described above. It has been found that this power factor is also a function of frequency, as is shown in Fig. 10, in which data for several different shapes of lamps are plotted. In general, it can be seen that the power factor first decreases with increasing frequency, passes through a minimum, and then increases. This type of behavior can be duplicated by either of the circuits shown in Fig. 11, where R_1 is of the order of 1000 ohms, C is of the order of 0.01 μf, and R_2 is of the order of 10^5 ohms.

R_1 can be likened to the series resistance of the conducting coating of the glass, while R_2 is analogous to leakage resistance of the dielectric, "resistance" of the phosphor, and leakage around the ends of the lamp, if any. The variation of power factor with voltage can be accounted for by the assumption that R_2 is a decreasing function of the voltage.

In summary, the electrical characteristics of electroluminescent lamps have been sufficiently described to give an indication of the behavior to be expected under various conditions. In addition, an analogous circuit for the lamp has been shown.

Any discussion of this paper will appear in a Discussion Section, to be published in the December 1953 issue of the JOURNAL.

REFERENCES

1. G. DESTRIAU, *J. Chim. Phys.*, **33**, 620 (1936).
2. G. DESTRIAU, *Phil. Mag.*, **38**, 700 (1947).
3. G. DESTRIAU, *Bull. de Soc. Belge des Electriciens*, Vol. 68, No. 1, p. 21 (1952).
4. G. F. J. GARLICK, "Luminescent Materials," p. 145, Oxford University Press, London (1949).
5. E. C. PAYNE, E. L. MAGER, AND C. W. JEROME, *Ill. Eng.*, **45**, 688 (1950).

Influence of Impurities in the Electrolyte in Chlorine-Caustic Electrolysis by the Mercury Cell Process

III. Investigation of the Influence of Anions upon the Decomposition Rate of Sodium Amalgam[1]

GÖSTA ANGEL, TAGE LUNDÉN, AND ROLF BRÄNNLAND

Division of Applied Electrochemistry, Royal Institute of Technology, Stockholm, Sweden

ABSTRACT

Further investigation of the influence of foreign negative ions on the decomposition rate of sodium amalgam by shaking with buffered solutions of NaCl has shown that in the absence of other impurities SO_4^{2-}, Br^-, I^-, F^-, and ClO_3^- in concentrations up to 0.1 g/l have no effect on the decomposition rate, and also that certain substances, viz., silicate, borate, pyrophosphate, and stannate, are able to deactivate vanadium, which has previously (1) been demonstrated to promote the amalgam decomposition rate to a very high degree.

INTRODUCTION

In the previously published papers in this series (1, 2) the influence of metallic impurities on the decomposition rate of sodium amalgam has been treated. As it also seems possible that negative ions, which may occur in the brine, are able to affect the amalgam decomposition, the investigations have been extended to a number of anions. However, the experiments were not limited to anions which may normally occur in the brine, but also include other anions which may be expected to influence the effect of heavy metals.

EXPERIMENTAL

The experiments were carried out in exactly the same way as the previously described experiments with metal salts. Thus, at room temperature, an amalgam with 0.14 per cent sodium was shaken with concentrated NaCl solutions to which the ions to be investigated were added in various quantities. As a rule, the brine was buffered with acetic acid/acetate to a *p*H value of 6.5. The decomposition rate of the amalgam was estimated by measuring the volume of hydrogen evolved per minute.

Experiments with Anions Which May Normally Occur in the Brine

The following ions which are more or less common as contaminations in the brine were investigated: sulfate, bromide, iodide, chlorate, and nitrate. The ions were added as sodium salts.

Sulfate.—8 g/l SO_4^{2-} caused no hydrogen evolution beyond that of the blank.

Bromide.—0.1 g/l Br^-. No influence.

Iodide.—0.1 g/l I^-. No influence.

Chlorate.—0.1 g/l ClO_3^-. No influence.

Nitrate.—When the experiments with Ca, described in the first paper (1), were performed, the metal was added as $Ca(NO_3)_2$. Then the unusual observation was made that the hydrogen evolution decreased to a value far below the blank. If, on the other hand, the experiment was made with $CaCl_2$ instead of $Ca(NO_3)_2$, no decrease of the hydrogen evolution occurred. Evidently the decreased evolution of hydrogen was caused by the nitrate ions.

In order to investigate the phenomenon further, a number of experiments were performed, in which the nitrate was added as $NaNO_3$. Fig. 1 shows that the gas evolution rate decreased with increasing nitrate concentration, until at a value of about 20 mg/l NO_3^- the gas evolution ceased. If the concentration of nitrate ions is further increased, the evolution of hydrogen will increase again, and at high nitrate concentrations the evolution was several times that of a blank.

From the curve in Fig. 1 it can be concluded that the nitrate ion affects the hydrogen evolution in two opposite directions; it partly increases the amalgam decomposition catalytically, and partly oxidizes the hydrogen, thus decreasing the gas evolution. In the latter case it is likely that NO_3^- oxidizes the hydrogen formed by the amalgam decomposition to H_2O or oxidizes Na to Na^+ directly. In both cases no gas is liberated. The fact that the amalgam is really decomposed without gas evolution was shown in an experiment with 0.3 g/l NO_3^-, when the shaking was interrupted after 8 minutes, and the amalgam was then analyzed. The analysis showed that only 17.5 per cent of the original sodium content

[1] Manuscript received May 12, 1952. This paper prepared for delivery before the Montreal Meeting, October 26 to 30, 1952.

remained in the amalgam, while 4.4 per cent had reacted with water giving gas evolution, and 78.1 per cent had been decomposed without evolution of hydrogen. The oxidizing effect of the nitrate ions is represented by the following equation:

$$\frac{\partial H_2}{\partial t} = -k_1 \cdot C^m_{NO_3^-} \qquad (I)$$

in which t = time, $C_{NO_3^-}$ = nitrate concentration, and k_1 and m are constants. The catalytic effect is represented by the equation:

$$\frac{\partial H_2}{\partial t} = +k_2 \cdot C^n_{NO_3^-} \qquad (II)$$

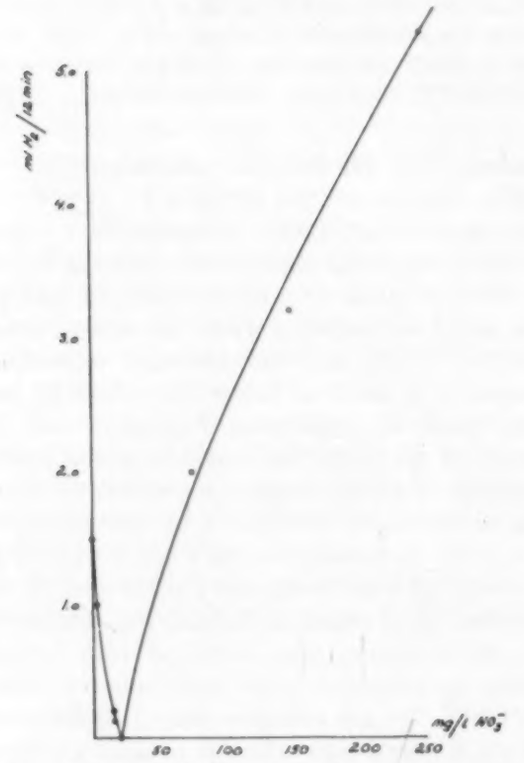

FIG. 1. Influence of NO_3^- in various concentrations

in which k_2 and n are constants. The hydrogen evolution is zero, if the following equation is satisfied by $C_{NO_3^-}$:

$$k_2 \cdot C^n_{NO_3^-} + b = k_1 \cdot C^m_{NO_3^-} \qquad (III)$$

in which b is the gas quantity in a blank.

If n is greater than m, the curve will have the same appearance as that in Fig. 1.

In Fig. 2 curves have been drawn representing the catalytic and the oxidizing effect, with the assumption that $n = 2$ and $m = 1$, which are probable values. This diagram also shows the two curves superimposed giving a curve of the same type as that in Fig. 1.

In short, the nitrate ion experiments show that this ion increases the amalgam decomposition rate to a considerable extent. The effect is, however, rather complicated, since the nitrate not only increases the amalgam decomposition, but also reacts without evolution of hydrogen; the latter effect probably being caused by oxidation of the hydrogen to water or direct oxidation of Na to Na^+. This explains why the gas evolution ceases entirely at a certain nitrate concentration.

Experiments with Anions Which May Act as Inhibitors

In addition to the negative ions mentioned above, which may occur in the circulating brine, a number of

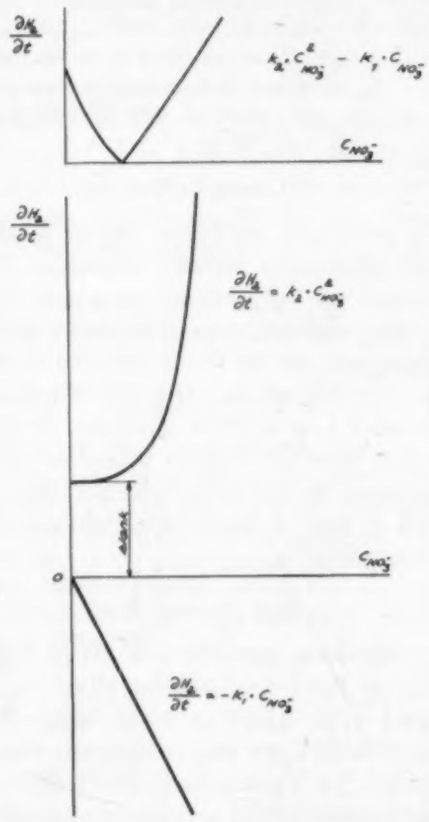

FIG. 2. $\frac{\partial H_2}{\partial t}$ curves, alone and superimposed

other ions were investigated, viz., SiO_3^{2-}, BO_3^{3-}, $P_2O_7^{4-}$, SnO_3^{2-}, and F^-. The experiments with these ions were performed in order to investigate a possible negative effect on the amalgam decomposition, i.e., lowering of the hydrogen evolution rate. However, the additions were not expected to increase the hydrogen overpotential on mercury, but to deactivate the metals previously found to be harmful, e.g., by forming complex compounds with these metals.

The order of magnitude of the additions was also in this case 1–25 mg/l. The ions were added before the amalgam, because in a number of special experiments it was shown that these ions had a very slight or no effect if they were added after the amalgam

decomposition had started and active spots had formed.

A patented method (3) of purifying the brine by the addition of colloidal silicic acid is said to improve the current efficiency of the mercury cell process. An experiment was performed here by adding colloidal silicic acid to a salt solution containing vanadium. This solution was then electrolyzed, and it was found that the influence of the vanadium salt disappeared entirely. This led to a separate investigation in which silicate was added to salt solutions containing vanadium or molybdenum in order to show the combined effect of these salts in shaking experiments.

The investigation was also extended to other ions, which might have the same properties as silicic acid, e.g., the borate ion.

In hydrogen peroxide manufacture a similar problem has caused much trouble, viz., the decomposition of hydrogen peroxide catalyzed by a number of heavy metals, e.g., iron, copper, and chromium. The stability of the hydrogen peroxide was considerably improved by the addition of certain substances, inhibitors, forming complexes with the harmful metal ions. According to Schumb (4) the most active substances are sodium pyrophosphate, sodium stannate, and 8-hydroxyquinoline.

Hence, in the shaking experiments with sodium amalgam in presence of vanadium the effect of sodium pyrophosphate was studied. As the pyrophosphate undergoes a slow hydrolysis to orthophosphate, the influence of the latter ion was also studied. Furthermore, the stannate ion, which is said to be strongly active in the conservation of hydrogen peroxide, was investigated thoroughly. On the other hand, the common analytical reagent 8-hydroxyquinoline was considered too unstable in brine saturated with chlorine, and therefore of no interest as an inhibitor in the chlorine-caustic process.

Finally the effect of addition of fluoride ions was studied, as in some electrolytic processes these ions are said to have a favorable influence.

The influence of each ion alone was first studied, and in no case did the hydrogen volume of the amalgam decomposition exceed that of a blank. Then the ion in question was added together with vanadium or molybdenum, and the gas evolution was recorded.

Silicate.—The shaking experiments showed that even small quantities of silicate in the brine decreased the hydrogen evolution considerably; thus, if sodium amalgam was shaken for 16 minutes with NaCl solution containing 10 mg/l Si (as sodium silicate), no gas evolution was observed.

Also in the presence of vanadium the effect was very strong, and the harmful metal was more or less deactivated. In Fig. 3 the hydrogen evolution is plotted against time, showing the results in a number of experiments with constant vanadium concentration (2.5–25 mg/l V) but increasing silicate

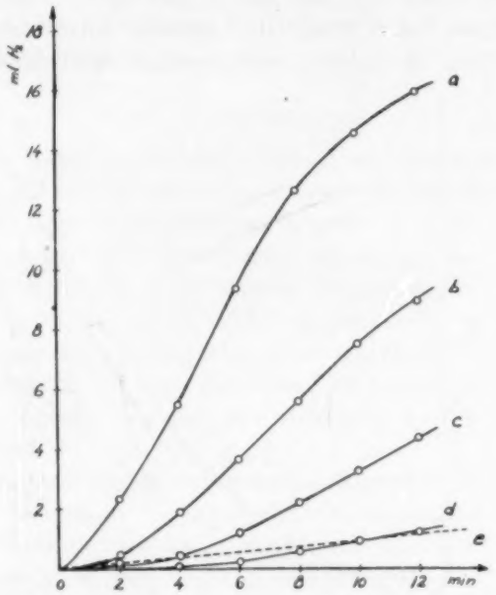

FIG. 3. Influence of V in presence of Si (as silicate), constant vanadium and increasing silicate concentration. *a*—2.5 mg/l V; *b*—2.5 mg/l V + 2.5 mg/l Si; *c*—2.5 mg/l V + 10 mg/l Si; *d*—2.5 mg/l V + 25 mg/l Si; *e*—blank.

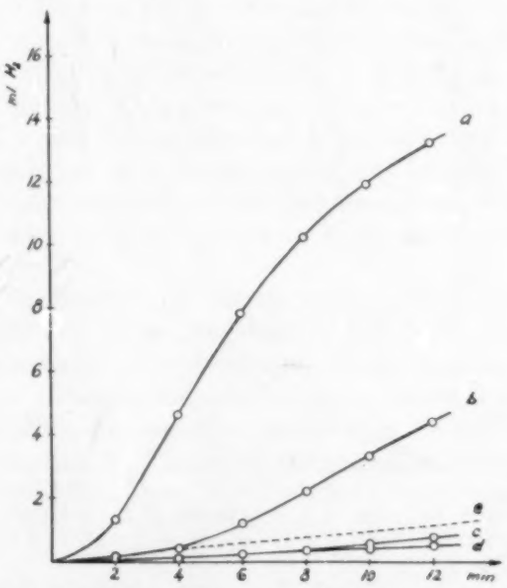

FIG. 4. Influence of V in presence of Si (as silicate), increasing vanadium and constant silicate concentration. *a*—5 mg/l V + 10 mg/l Si; *b*—2.5 mg/l V + 10 mg/l Si; *c*—1.0 mg/l V + 10 mg/l Si; *d*—0.5 mg/l V + 10 mg/l Si; *e*—blank.

concentration (2.5–25 mg/l Si). The fact that the decomposition rate of the amalgam decreases strongly with increasing silicate addition is obvious.

Fig. 4 shows the hydrogen evolution when the silicate concentration was constant (10 mg/l Si) but

the vanadium concentration steadily increased (0.5–5 mg/l V). This shows that with the two lowest concentrations of vanadium the gas volume is still below the blank value owing to the presence of silicate.

From Fig. 3 and 4 it is possible to estimate the quantity of silicate which is required for deactivating a certain amount of vanadium; the concentration of silicate must be approximately 10 times that of vanadium, if the gas evolution shall remain at the blank value.

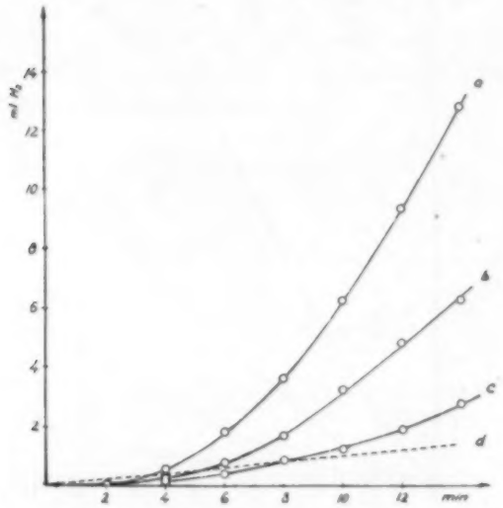

FIG. 5. Influence of Mo in presence of Si (as silicate) *a*—1 mg/l Mo; *b*—1 mg/l Mo + 10 mg/l Si; *c*—1 mg/l Mo + 25 mg/l Si; *d*—blank.

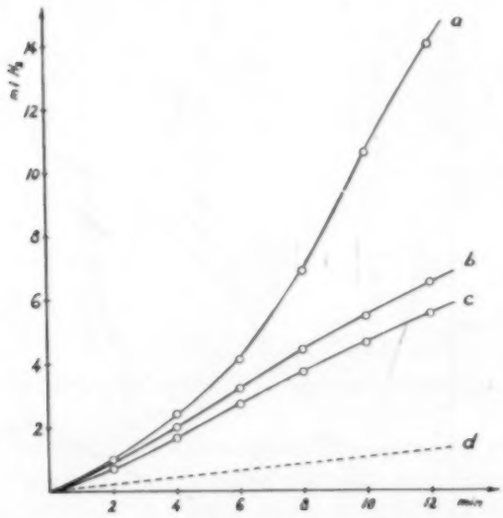

FIG. 6. Influence of V in presence of B (as borate). *a*—1 mg/l V; *b*—1 mg/l V + 10 mg/l B; *c*—1 mg/l V + 25 mg/l B; *d*—blank.

The influence of silicate on molybdenum is shown in Fig. 5. At first glance, molybdenum seems to be less harmful than vanadium, but in fact the long induction period of molybdenum is compensated by the high decomposition rate after a few minutes. Thus, molybdenum has a stronger effect than vanadium, and even when 25 times as much silicate as molybdenum is present in the brine, the gas evolution of the blank is exceeded.

Borate.—With borate alone no gas evolution was observed in a period of 12 minutes. Attention should be directed to the fact that the slight addition of borate and silicate respectively is able to cause only a very slight *p*H change (<0.5 *p*H units), so the decreasing decomposition rate cannot be caused by this *p*H change, but must depend on a purification of the brine, i.e., reaction with the harmful substances in the brine.

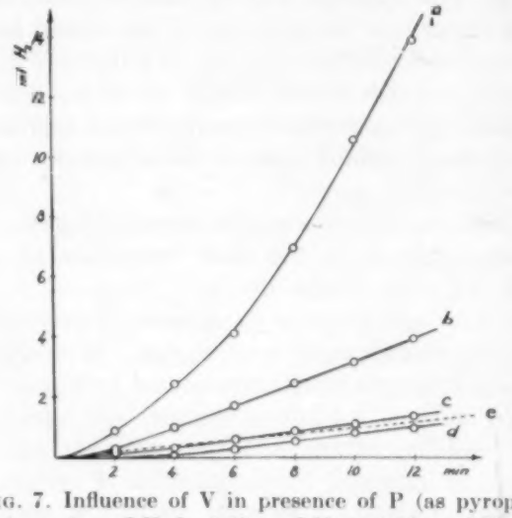

FIG. 7. Influence of V in presence of P (as pyrophosphate). *a*—1 mg/l V; *b*—0.25 mg/l V; *c*—0.25 mg/l V + 10 mg/l P, 1 mg/l V + 10 mg/l P; *d*—1 mg/l V + 25 mg/l P; *e*—blank.

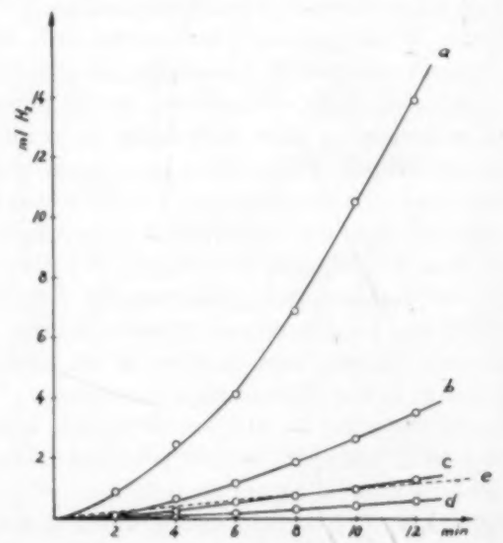

FIG. 8. Influence of V in presence of Sn (as stannate). *a*—1 mg/l V; *b*—1 mg/l V + 1 mg/l Sn; *c*—1 mg/l V + 5 mg/l Sn; *d*—1 mg/l V + 10 mg/l Sn; *e*—blank.

Later experiments showed, however, that the borate ion has only slight effect on vanadium, as illustrated in Fig. 6. If the borate addition was increased,

no stronger effect on the vanadium ion could be observed. Hence, sodium borate seems to be of little interest as inhibitor.

Pyro- and orthophosphate.—The ability of pyrophosphates to form complex compounds with a number of heavy metals is discussed by Schumb (4). When pyrophosphate was added to a pure salt solution, no distinct decrease of the decomposition rate below the blank value was observed as with silicate or borate additions: with 10 mg/l P (as pyrophosphate) 0.7 ml hydrogen was obtained in 10 minutes (in a blank the gas volume in 10 minutes is 1.0 ml), and about the same effect was obtained with the same quantity of orthophosphate.

However, pyrophosphate reacts readily with vanadium and, to a considerable extent prevents the metal from affecting the amalgam decomposition. Fig. 7 illustrates that the hydrogen evolution is reduced to about the blank value in a concentration of 10 mg/l P as pyrophosphate. Evidently, there is no possibility of lowering the gas evolution very much below the blank value, even if the concentration is increased to 25 mg/l P. In order to confirm this observation some experiments were made with 0.25 mg/l V and 10 mg/l P, and also in this case the blank value was reached. The investigation shows that pyrophosphate is useful as inhibitor, but unfortunately the pyrophosphate is gradually hydrolyzed to orthophosphate, a compound which turned out to be inactive in presence of vanadium. This observation agrees well with Schumb's results.

Stannate.—Stannate ions often occur in neutral and acid solutions in a colloidal state, and therefore it may be expected to have the same inhibitor properties as silicate.

With the addition of stannate alone only 0.2 ml hydrogen was obtained in 12 minutes with 5 mg/l Sn, while the corresponding blank value is 1.2 ml H_2.

The results in the simultaneous presence of vanadium and stannate are shown in Fig. 8. It is evident that the stannate ion is extremely active as inhibitor even in relatively small concentrations. Thus, 1 mg Sn per mg V reduces the gas evolution to one-fourth of the maximum value (i.e., with vanadium alone), while a tenfold addition of Sn gives hydrogen volumes considerably smaller than the blank value.

It is seen that sodium stannate is an exceedingly active inhibitor in the amalgam decomposition reaction, even more active than silicate.

Fluoride.—Addition of fluoride to a pure NaCl solution gave about 0.6 ml hydrogen in 12 minutes (blank value is as previously mentioned, 1.2 ml in the same time). A slight decrease in the effect of vanadium was observed, when the fluoride concentration was ten times the vanadium concentration. However, in reality the fluoride ions caused only a prolongation of the induction period which is characteristic for vanadium, etc., so fluoride cannot be regarded as a real inhibitor like silicate and stannate. On the other hand the experiments show that the presence of fluoride ions in low concentrations is harmless.

Summary

This work is the third part of an investigation of the influence of impurities in the brine in chlorine-caustic electrolysis in mercury cells. A number of negative ions were investigated which may be present in the brine under various conditions, viz., sulfate, bromide, iodide, chlorate, and nitrate, and moreover some anions were investigated which were expected to prevent the effect of vanadium and other harmful metals. The following results were obtained:

1. Sulfate ions in concentrations up to 8 g/l have no influence on the amalgam decomposition rate.

2. Bromide, iodide, and chlorate are harmless, at least in concentrations up to 0.1 g/l.

3. Nitrate ions increase the amalgam decomposition rate. The effect increases as the nitrate concentration increases. However, when the nitrate concentration has reached a certain value, the gas evolution ceases. The ion promotes the decomposition rate catalytically and also decomposes the amalgam without gas evolution or oxidizes the hydrogen already formed. At a given nitrate concentration the reaction rate has the same value in both reactions, and then no gas evolution occurs, but in higher nitrate concentrations the catalytic decomposition predominates, and a strong increase of the gas evolution is observed.

4. The addition of sodium silicate (which forms colloidal silicic acid) prevents the harmful influence of vanadium and molybdenum. If the quantity of silicate added to the solution is ten times that of vanadium, the vanadium influence is totally prevented. In the presence of molybdenum, however, a concentration about 40 times that of molybdenum is required in order to deactivate the metal.

5. The effect of borate on vanadium is similar to that of silicate, but much weaker.

6. Pyrophosphate is able to deactivate vanadium effectively by forming complexes with the metal, but is gradually hydrolyzed to orthophosphate, which is inactive as an inhibitor.

7. Colloidal stannic acid (added as sodium stannate) has properties similar to silicic acid and is able to adsorb vanadium effectively.

8. The addition of fluoride ions has very slight effect on the influence of vanadium.

Acknowledgment

This investigation was promoted by a grant from the State Council of Technical Research, for which the authors wish to express their deep appreciation.

Any discussion of this paper will appear in a Discussion Section, to be published in the June 1953 issue of the Journal.

REFERENCES

1. G. Angel and T. Lundén, *J. Electrochem. Soc.*, **99**, 435 (1952).
2. G. Angel and R. Brännland, *J. Electrochem. Soc.*, **99**, 442 (1952).
3. N. V. Koninklijke Nederlandsche Zoutindustrie, Dutch Pat. 68,706, Sept. 15, 1951.
4. W. C. Schumb, *Ind. Eng. Chem.*, **41**, 992 (1949).

Some Properties of Tin-II Sulfate Solutions and Their Role in Electrodeposition of Tin

I. Solutions with only Tin-II Sulfate Present[1]

C. A. Discher

Rutgers University, The State University of New Jersey, College of Pharmacy, Newark, New Jersey

ABSTRACT

Density, refractive index, surface tension, viscosity, freezing point depression, conductivity, transference number, electrode potential to pure tin and hydrogen, respectively, have been measured for various aqueous tin-II sulfate solutions. The relationship between concentration and the magnitude of these properties, and various derived properties, are discussed. When possible, inferences are drawn with respect to the structure of species in solution.

Introduction

During the years the author was engaged in the search for addition agents for the tin-II sulfate electrolyte in Dr. Mathers' laboratory,[2] and later in his own, three points stood out: (*a*) the wide range of deposits obtainable at will from the electrolyte, i.e., bright, matte, crystalline, powdered, treed, gray, silvery; (*b*) the lack of available information about the physical properties of solutions of this electrolyte; and (*c*) the lack of information as to whether the deposits are affected or controlled by one or more of the physical properties of the electrolyte, as modified by the addition agent.

This paper is the first study of a series on physical properties of aqueous tin-II sulfate systems. In it the properties and the nature of solutions of pure tin-II sulfate are presented and discussed. The second paper will be concerned with the modification of these properties by the presence of comparable quantities of sulfuric acid. In a final paper, the effects of addition agents capable of producing a variety of deposits will be studied. In this way it may be possible to determine whether one or more of the properties studied affects or controls the manner in which the metal is laid down on the cathode.

Experimental Procedures

Preparation, handling, and analysis of solutions.— The preparation of aqueous solutions of tin-II sulfate presents two difficulties: hydrolysis, and ease of oxidation to the tin-IV state by atmospheric oxygen. It was decided to allow hydrolysis to proceed to equilibrium rather than to work at a constant *p*H or a constant free-acid level. This proved satisfactory since later analysis of results with respect to acid, total sulfate, and tin-II sulfate showed that, with two exceptions to be pointed out in the discussion, the properties measured were apparently a function of the tin-II sulfate and were unaffected by the relatively small concentration of free acid present. Air oxidation was overcome experimentally by using an atmosphere of nitrogen throughout this work.

The tin-II sulfate used in this part of the work was prepared by precipitation with ethanol (95%) from saturated aqueous solutions of the commercial salt. The crystals formed were filtered with suction, washed several times with ethanol and ethanol-diethyl ether mixture, and finally dried under reduced pressure over sulfuric acid.

The solutions were prepared and handled in a closed glass system so constructed that an atmosphere of nitrogen could be maintained at all times. The preparation of a given solution proceeded as follows. Distilled water was introduced into the first of three interconnected glass vessels, boiled to remove dissolved gases, and cooled under nitrogen. This water was then transferred by nitrogen pressure to a nitrogen filled calibrated flask in which the required salt had been placed. The resulting solution was agitated with nitrogen and allowed to stand at least twenty-four hours to permit traces of insolubles to settle out. The clear supernatant was then transferred by nitrogen pressure to a third nitrogen-filled flask and again allowed to stand over night. This flask was so arranged that samples could be withdrawn from the center of the solution. It had auxiliary equipment for taking samples or filling apparatus under nitrogen. The success of this setup in the control of oxidation to the tetravalent state was shown by the fact that solutions were kept as

[1] Manuscript received June 25, 1952. This paper prepared for delivery before the Philadelphia Meeting, May 4 to 8, 1952.

[2] Indiana University, Bloomington, Indiana.

long as two weeks in the apparatus with little or no evidence of tin-IV.

Solutions were prepared to approximate concentration. The exact concentrations were determined using the methods given by Pine (1). Tin-II, hydrogen, and tin-IV ions were determined. Tin-IV concentrations were negligible.

Measurement of physical properties.—All measurements except conductivity were made at 25.000 ± 0.005°C using water as the thermostating fluid. The conductivity measurement was made at 25.00 ± 0.01°C using a kerosene bath.

Density measurements were made with a calibrated 25 ml pycnometer. Refractive index measurements were made with the Abbe instrument. Viscosity measurements were made with an Ostwald type glass viscometer having a water drainage time of about 80 seconds. Surface tension was determined using approximately 0.1 mm bore glass capillary tubing; the radius was determined by calibration with water. The freezing point of each solution was determined by the Beckman method using a differential thermometer.

Conductivity measurements were made with a bridge based on the Jones and Josephs' circuit (2, 3) using a Wagner ground. The conductivity cell had 1.5-cm diameter platinum electrodes placed 6.75 cm apart. The electrodes were coated with platinum black. The cell was standardized with 1.0*N* KCl. One thousand cycles per second a.c. was used.

Transference measurements were made using pure tin electrodes in a cell patterned after that described by MacInnes and Dole (4). A copper coulometer was used.

Electrode potentials against pure tin were made using a Leeds and Northrup type K potentiometer, calibrated with a standard Weston cell. The *n*-calomel reference electrode was used. Electrode potentials using the hydrogen electrode also were made with the same apparatus, electrodes being freshly platinized for each measurement. From time to time parallel measurements were made using a glass electrode.

Results

Measurements were made on a series of tin-II sulfate solutions ranging from 0.015 to 0.686 molar. (Unless otherwise noted molar concentrations will be used throughout this paper.) The concentrations of the solutions studied are given in Table I. The free acid present is also noted in this table. At the lowest concentration the mole fraction calculated as sulfuric acid is 0.15 while at the highest concentration the mole fraction approaches 0.01.

The variation of density (g/cc) with concentration is shown in Table I. A plot of this property vs. molarity is shown in Fig. 1. It will be noted that the density varies linearly and directly with concentration. However, it is further noted that this variation

TABLE I. *Variation of some physical properties with concentration of tin-II sulfate*

Moles Tin-II/l	Moles H_2SO_4/l	Density grams/cc	Refractive index	Surface tension	Freezing point	Absolute viscosity
0.015	0.004	0.9999	1.3331	73.2	−0.03	0.00888
0.031	0.005	1.002	1.3340	—	−0.08	—
0.052	0.004	1.006	1.3340	72.1	−0.10	0.00892
0.098	0.017	1.016	1.3362	73.8	−0.24	0.00911
0.133	0.015	1.022	1.3376	—	−0.22	0.00928
0.197	0.011	1.035	1.3398	73.6	−0.20	0.00960
0.225	0.035	1.038	1.3396	73.8	−0.38	0.00983
0.248	0.010	1.042	1.3410	73.0	−0.47	0.00993
0.299	0.015	1.053	1.3429	73.3	−0.43	0.00987
0.348	0.020	1.059	1.3440	72.3	−0.36	0.01001
0.430	0.026	1.072	1.3477	72.2	−0.72	0.01035
0.523	0.047	1.099	1.3511	73.7	−0.93	0.01097
0.590	0.012	1.108	1.3527	73.0	−0.89	0.01119
0.686	0.012	1.125	1.3553	74.2	−1.02	0.01157

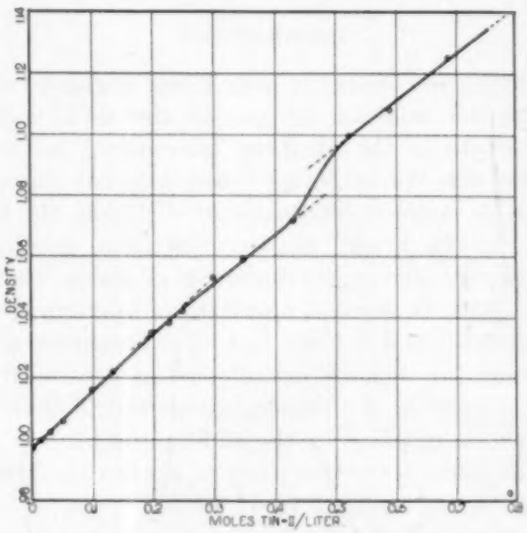

Fig. 1

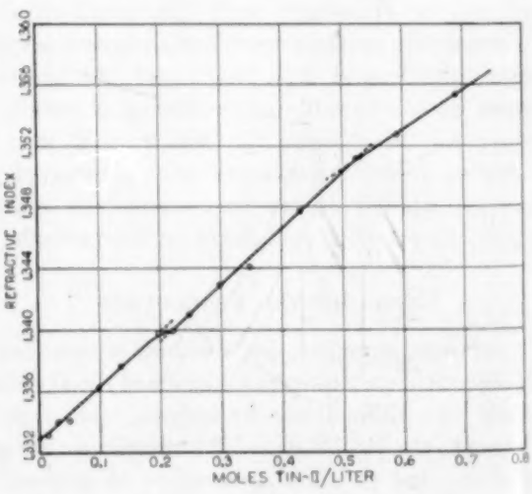

Fig. 2

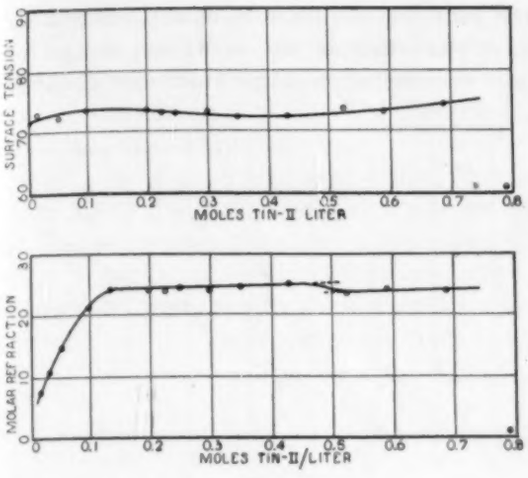

FIG. 3

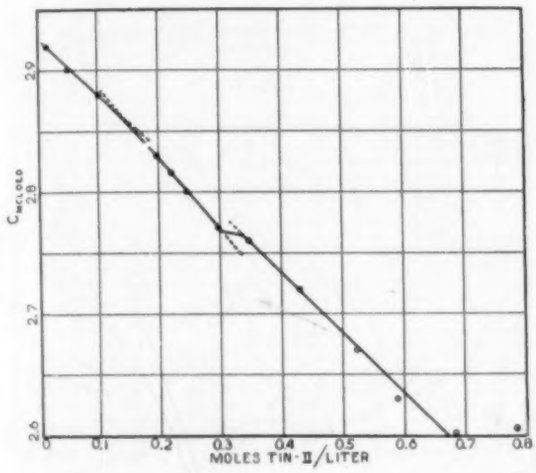

FIG. 4

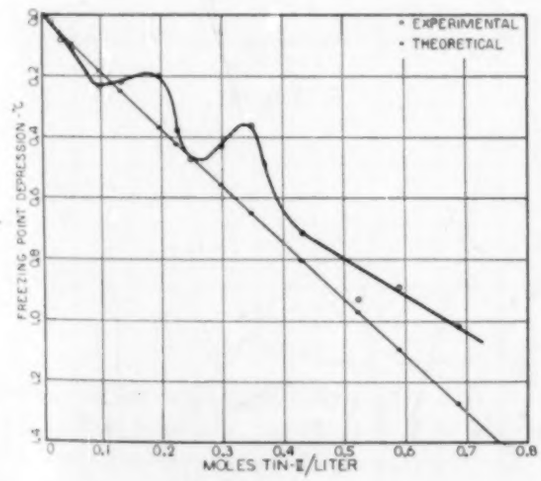

FIG. 5

falls into three distinct ranges depending on concentration.

Refractive index values are given in Table I, and plotted in Fig. 2. The similarity of this curve to the density curve is noteworthy. Molar refraction was calculated at each concentration and plotted in the lower curve of Fig. 3. While this plot shows the three ranges of variation the first is no longer linear. The molecule, $SnSO_4$, was assumed in this calculation, as in all parts of this paper unless otherwise noted.

The values for surface tension (dynes/cm) are given in Table I and plotted in Fig. 3. The surface tension of tin-II sulfate solutions is slightly higher than that of pure water. However, the variation is generally slight. Assuming that MacLoed's equation

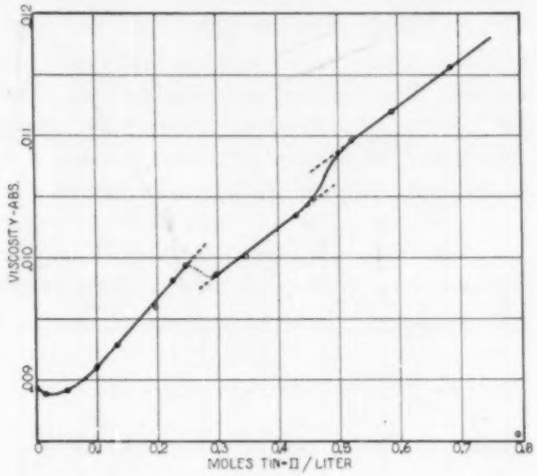

FIG. 6

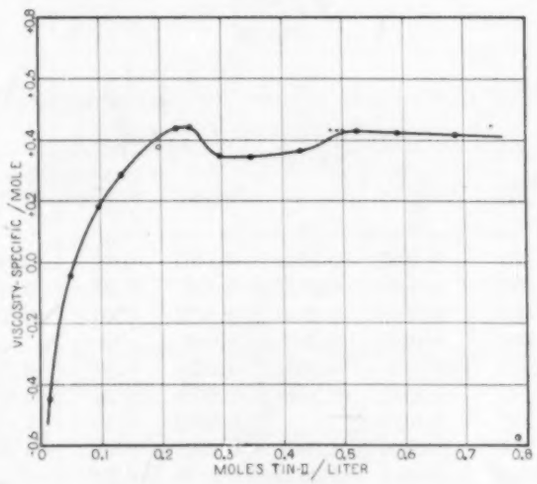

FIG. 7

applies and the vapor density of the solution is negligible, MacLoed's constant was calculated for each solution. The values of the constant are plotted in Fig. 4.

The freezing point of each solution is given in Table I and plotted in Fig. 5.

Viscosity data are given in Table I. The absolute viscosity (poise) is plotted vs. molarity in Fig. 6. A plot for specific viscosity is not shown since it duplicates the absolute viscosity curve. It is to be noted that the viscosity of the most dilute solutions is slightly less than that of water. The plot of specific viscosity/$M_{Sn^{++}}$ vs. $M_{Sn^{++}}$ (Fig. 7) does not

show a straight line relationship except at higher concentrations.

The values for specific conductivity are shown in Table II and plotted in Fig. 8. This property of tin-II sulfate electrolyte while dependent on the concentration of the salt is modified by the hydrogen-ion activity. There is a leveling off of the curve in the middle concentration range. If this is borne in mind when the hydrogen-ion activity plot is studied, it

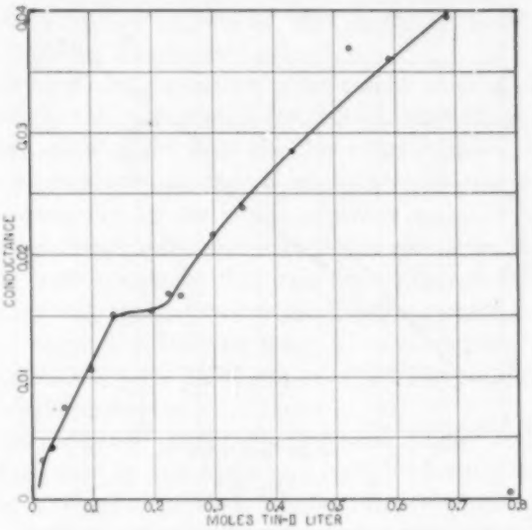

FIG. 8

TABLE II. *Variation of some electrical properties with concentration of tin-II sulfate*

Moles Tin-II/l	Specific conductivity	$E_{Sn,Sn^{++}}$	E_{H_2,H^+}	Transference No. $-Sn^{++}$	Transference No. $-H^+$
0.015	0.0032	0.2234	0.1182	0.72	−0.05
0.031	0.0042	0.2137	0.1117	0.65	0.03
0.052	0.0070	0.2109	0.1052	0.53	0.29
0.098	0.0106	0.2087	0.0987	—	—
0.133	0.0151	0.2054	0.0730	0.38	0.33
0.197	0.0153	0.2046	0.0704	0.34	0.22
0.225	0.0168	—	0.0993	0.49	0.09
0.248	0.0166	0.2003	0.1008	0.66	−0.06
0.299	0.0217	0.2000	0.0973	0.52	0.12
0.348	0.0238	0.2019	0.0975	0.42	0.18
0.430	0.0285	—	0.0851	—	—
0.523	0.0370	0.1979	0.0727	−0.12	0.34
0.590	0.0360	0.1959	0.0709	0.14	0.45
0.686	0.0394	0.1932	0.0741	0.27	0.52

will be seen that this leveling off corresponds to a point of minimum activity of hydrogen ion. The Onsager equation was used to calculate values for equivalent conductance at infinite dilution. These values are plotted in Fig. 9.

The electrode potentials $E_{Sn,Sn^{++}}$ and E_{H_2,H^+} are given in Table II and plotted in Fig. 10 and 11. The activities of these ions are plotted in Fig. 12. While the comparative concentration of hydrogen ion is very low the activity of this ion generally is greater than that of the tin-II ion except for the middle concentration range. However, at the beginning of the middle region, despite a minimum in molar concentration of hydrogen ion the activity of this ion becomes extremely high only to fall to a low

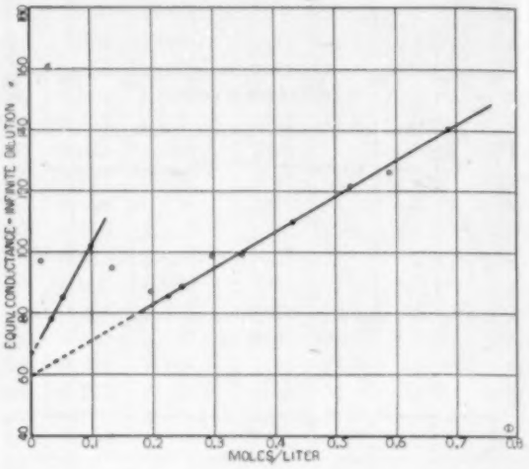

FIG. 9

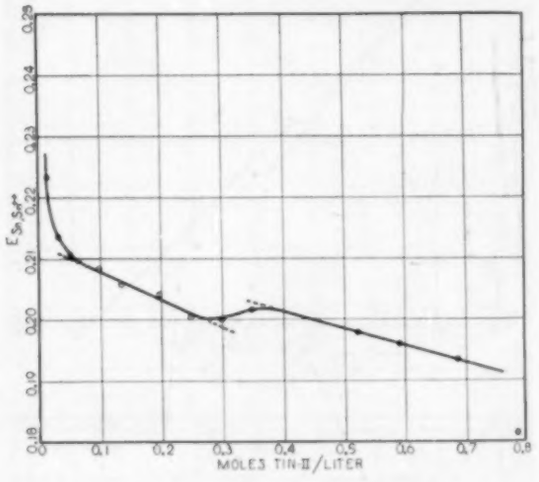

FIG. 10

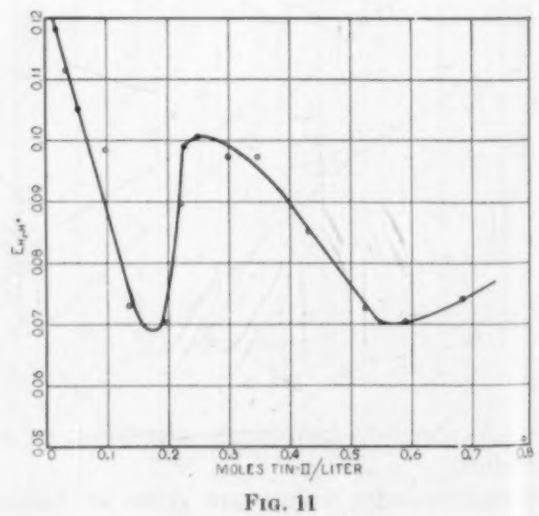

FIG. 11

value, despite no relative change in molar concentration. At the same time the activity of the tin-II ion reaches a maximum value. In fact it is in this region alone that the activity of the tin-II ion exceeds that of the hydrogen ion.

Table II and Fig. 13 and 14 give the transference number data. The data presented are probably the least reliable because of numerous experimental difficulties encountered. The values reported at a given concentration represent average values, based on determinations of both anode and cathode compartments. In a few cases these values differed by as much as 0.3 units. However, the averages give, as can be seen from the graphs, a consistent variation. Furthermore, the validity of these data is indicated by comparison with activity data, conductivity data, etc.

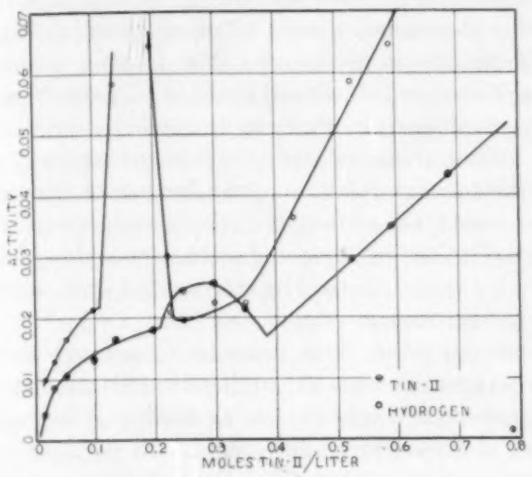

FIG. 12

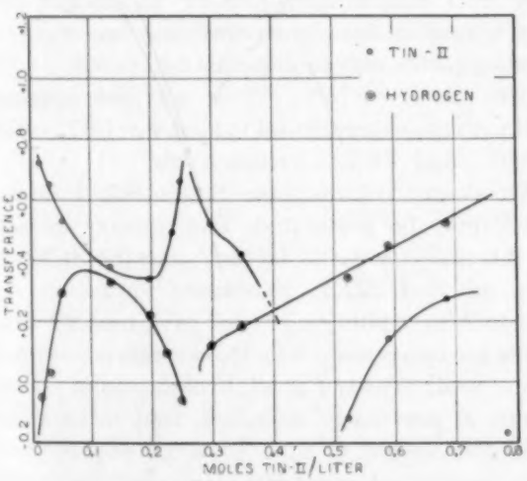

FIG. 13

As expected, electrodeposition from these solutions was unsatisfactory. Plating samples were made at 0.025, 0.15, and 0.50 amp/in.^{2}, in the still and the agitated bath, using 1 in. x 1 in. strip steel cathodes. The following generalizations may be made about the appearance of the samples:

(*a*) The deposited metal was consistently gray in appearance. There was a tendency toward increasingly lighter shades with increasing concentration.

(*b*) The surface areas generally showed a uniform growth rate and crystal distribution. The crystals were very small and closely placed, giving the surface a relatively smooth, powdery appearance. Individual crystal size, and the tendency for single crystals to outstrip neighboring crystals and destroy the uniform surface increased with decreasing current density and decreasing concentration.

(*c*) The rate of growth of crystals on the edges and corners of the samples, compared to that on the surface, increased with increasing current density and increasing concentration; short-circuiting to the anode was very rapid at higher current densities and higher concentrations.

(*d*) At the lowest concentrations there was increasing gassing with decreasing concentration and increasing current density. Otherwise gassing was not a problem.

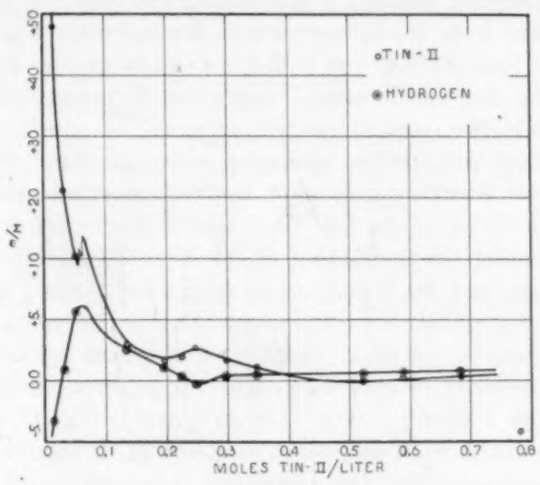

FIG. 14

DISCUSSION

Examination of the experimental data indicates that there are three general areas of behavior in the solutions studied: 0.00–0.12, 0.12–0.35, and 0.35–0.70 molar (tin-II). Generally there is a sharp break in going from one range to the other. Since the variation of a given property, or derived property, is consistent within these three ranges, the evident conclusion is that there are changes in particle species, and that within a given concentration range certain species of ions or molecules predominate.

Species in concentration range 0.0–0.12 molar.—It would seem safe to postulate that in this concentration range the tin-II is present partially as the molecular tin-II sulfate, and partially as the free ion. With increasing concentration, within this range, the concentration of the molecular form increases at the

expense of the free ions. At the upper concentration range named, the relative amount of free tin-II ion becomes small.

This is consistent with the following experimental observations. Within this concentration range the mole fraction of free acid by hydrolysis is comparatively higher than in other concentration ranges. The transference by hydrogen ion is comparatively low, being negative in the beginning of the range, and increasing steadily, inversely to the mole fraction. This indicates that the hydrogen must be present as bisulfate ion, which necessitates high relative concentration of free sulfate. The increasing activity and transference of hydrogen ion indicates the gradual binding of the sulfate ion with tin-II ion in the molecular form. The gradual leveling off of the activity of tin-II with the increasing molar concentration in this range also indicates the disappearance of this free ion from the solution.

Freezing points for these solutions also are consistent with this interpretation. Assuming the molecular form $SnSO_4$, van't Hoff's i can be greater than unity only with simple ionization. Experimentally this is the only concentration range in which i is greater than unity, becoming unity at about 0.12 molar. Furthermore, using the experimental values for activity of the tin-II ion and hydrogen ion, and assuming the remaining tin-II as molecular tin-II sulfate and the remaining hydrogen as bisulfate ion, one can calculate the freezing points for the solutions studied as $-0.04°$, $-0.09°$, $-0.14°$, and $-0.24°$C respectively. Comparing these with experimental values $-0.02°$, $-0.08°$, $-0.11°$, and $-0.24°$C, respectively, good agreement is observed. It should be remembered that the calculated values are based on measurements at 25°C.

A gradual change in the ratio of competing species is indicated by the changing slope of the curves obtained on plotting all measurements in this range. The appearance of a new structural form beyond 0.12 molar is indicated by the breaks in all of the curves presented, except conductivity.

These conclusions are consistent with those of O'Connor (5). Working with 0.00005–0.001N tin-II sulfate, he concluded that complete dissociation was indicated.

Concentrations greater than 0.35 molar.—On referring to the graphs of the various properties presented it may be noted that in general, at approximately 0.35M, the variation of the properties measured becomes linear with increasing concentration of tin-II. The additional interesting fact is that if a molar property, or the ratio of the magnitude of a given property to molar concentration, is plotted against molar concentration of tin-II, the variation is linear and the curve becomes parallel, or approximately so, to the concentration axis. The latter plot was made for molar refraction, activity of tin-II, activity of hydrogen ion, transference number for tin-II, transference number for hydrogen ion, and specific viscosity. This would seem to indicate that the species of particles present above 0.35 molar have reached a constant ratio toward each other, increasing concentration resulting in an increase of each species in approximately the same ratio.

Interpretation of individual properties gives some clues as to the nature of these particles. Transference number data indicate that tin-II, while contributing to this phenomenon, must be present to some extent as molecules or as heavy, slow moving, negative ions. This may be deduced from: (*a*) the transference is accomplished largely by hydrogen ion, even though the mole fraction of free acid is extremely low, and (*b*) the low net values for transference of the tin-II ions would be expected if the simple metal ions migrate to the cathode and at the same time slower complex ions, with tin-II as the central unit, migrate toward the anode.

Freezing point data indicate an average molecular weight of about 275 in this concentration range, the molecular weight increasing slightly in the range. Using this value one can calculate 35 per cent ionization; assuming the molecule $Sn[Sn(SO_4)_2]$ and the ions Sn^{++} and $[Sn(SO_4)_2]^{=}$. Using this percentage and known molar concentrations, the theoretical freezing points may be calculated as $-1.09°$, $-0.95°$, $-0.98°$, and $-0.75°$C. These compare reasonably well with the experimental values of $-1.02°$, $-0.89°$, $-0.93°$, and $-0.72°$C, respectively.

An alternative molecule $Sn_2[Sn(SO_4)_3]$ (mol. wt 644.3) may be postulated. The primary ionization for this molecule would be Sn^{++} plus $[Sn(Sn(SO_4)_3)]^{=}$ (avg mol. wt 322.2). Secondary ionization would lead to 2 Sn^{++} plus $[Sn(SO_4)_3]^{=}$ (avg mol. wt 214.8). There are two reasons why this system is not present to any great extent, if at all. Freezing point measurements, as previously indicated, lead to an average molecular weight of 275. To achieve this value a large amount of secondary ionization is required, since only secondary ionization leads to an average molecular weight less than 275. That the secondary ionization takes place to any extent seems highly improbable, the charge of minus four on the negative ion being achieved with great difficulty.

Concentration range 0.125 to 0.35 molar.—On the basis of the conclusions already made a dual system must be assumed in this region. Tin-II sulfate molecules[3] probably predominate in the lower part of the range. Gradually, as concentration increases, the $Sn[Sn(SO_4)_2]$ system and its concomitant ions appear

[3] There is some evidence that these molecules may be dimeric.

and increase at the expense of the molecular tin-II sulfate. This is supported by the following experimental evidence.

The plots of property vs. molar concentration with the primary exceptions of density and molar refraction are not linear in this range. In most cases there is a pronounced maximum, e.g., E_{H_2,H^+} transference number for tin-II, or a minimum, e.g., ηspec/M, transference number for hydrogen ion, in each of the plots at about 0.25M. Without a change in species generally a linear relationship should exist.

In addition to the over-all picture, several specific pieces of evidence support the coexistence of both species, for example the behavior of tin-II ion. Its activity increases but slightly with concentration up to 0.20 molar while transference continues to drop; in other words, the molecular tin-II sulfate is predominant. Beyond this concentration the activity and transference number of this ion increase to a maximum, which would indicate that the complex molecule is highly ionized at low concentrations of the new species, and then again drops somewhat with its increased concentration. The behavior of hydrogen ion is in keeping with these observations. In the lower regions of this concentration range, with the negative sulfate ion sequestered in the molecules of tin-II sulfate, the activity of the hydrogen ion is high. At the mid-range both it and the transference number for hydrogen ion drop rapidly, negative sulfatostannite ions being available to hold the hydrogen ion.

Conductivity behavior is consistent with these observations. It is nearly constant in the lower part of the range under discussion since increasing concentration does not increase the actual free ion necessary to conduct current. In calculating the equivalent conductance at infinite dilution, a straight line relationship exists below 0.12 molar and above 0.35 molar. Between these concentrations, in the range under discussion, a second degree relationship exists.

Acknowledgment

The author is indebted to the Research Council of Rutgers University for providing funds for the employment of Mr. Stanley Bauer as laboratory technician to assist in routine laboratory work necessary for this project.

Any discussion of this paper will appear in a Discussion Section, to be published in the December 1953 issue of the Journal.

References

1. P. R. Pine, *Trans. Electrochem. Soc.*, **80**, 640 (1941).
2. H. J. Creighton, "Principles and Applications of Electrochemistry," Vol. I, 4th ed., p. 73. John Wiley & Sons, Inc., New York (1947).
3. G. Jones and R. C. Josephs, *J. Am. Chem. Soc.*, **50**, 1049 (1928).
4. D. A. MacInnes and M. Dole, *J. Am. Chem. Soc.*, **53**, 1357 (1931).
5. E. A. O'Connor, *Nature*, **139**, 151 (1937).

THE ELECTROCHEMICAL SOCIETY, INC.

The Electrochemical Society is an international organization of individuals and companies concerned with or interested in Electrochemistry and allied subjects.

The Society is dedicated to the advancement of the theory and practice of Electrochemistry and related subjects, as shown in the foilowing divisions:

Battery	Electro-Organic
Corrosion	Electrothermic
Electric Insulation	Industrial Electrolytic
Electrodeposition	Theoretical Electrochemistry
Electronics	

Among the means to this end are the holding of meetings for the reading and discussion of professional and scientific papers on these subjects, the publication of such papers, discussions, and communications as may seem appropriate, and cooperation with chemical, electrical, and other scientific and technical societies.

It is an incorporated society without capital stock. The affairs of the Society are managed by a Board of Directors under a Constitution and By-Laws. Officers are nominated by a nominating committee appointed by the Board of Directors and elected by the members.

Direct all general correspondence and inquiries regarding membership to Society headquarters at 235 West 102nd Street, New York 25, N. Y., c/o Mr. W. J. Holian, Assistant Secretary.

Officers of the Society

President ..... J. C. Warner
Past President ..... Ralph M. Hunter
Vice-President ..... Robert J. McKay
Vice-President ..... Marvin J. Udy
Vice-President ..... H. H. Uhlig
Treasurer ..... E. Gideon Widell
Secretary ..... Henry B. Linford